



**HAL**  
open science

# Elaboration of microgel protein particles by controlled selfassembling of heat-denatured beta-lactoglobulin

Minh-Tuan Phan-Xuan

► **To cite this version:**

Minh-Tuan Phan-Xuan. Elaboration of microgel protein particles by controlled selfassembling of heat-denatured beta-lactoglobulin. Other. Le Mans Université, 2012. English. NNT : 2012LEMA1018 . tel-00770331

**HAL Id: tel-00770331**

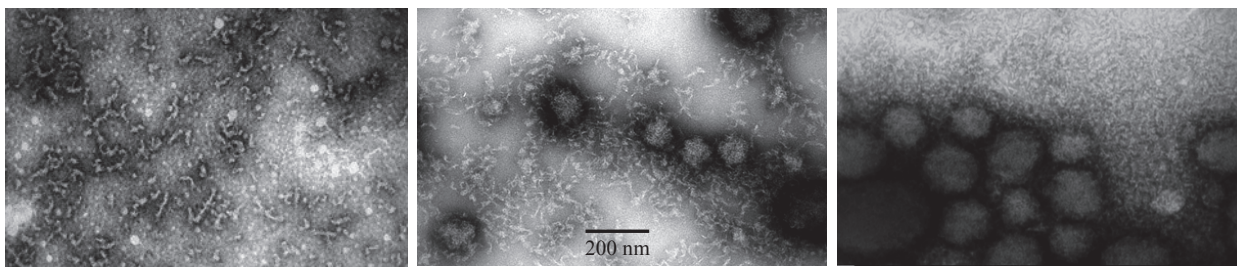
**<https://theses.hal.science/tel-00770331>**

Submitted on 4 Jan 2013

**HAL** is a multi-disciplinary open access archive for the deposit and dissemination of scientific research documents, whether they are published or not. The documents may come from teaching and research institutions in France or abroad, or from public or private research centers.

L'archive ouverte pluridisciplinaire **HAL**, est destinée au dépôt et à la diffusion de documents scientifiques de niveau recherche, publiés ou non, émanant des établissements d'enseignement et de recherche français ou étrangers, des laboratoires publics ou privés.

# Elaboration of microgel protein particles by controlled self-assembly of heat-denatured beta-lactoglobulin



Par **PHAN XUAN Minh Tuan**

Thèse de doctorat en Chimie et Physico-chimie des polymères

Université du Maine  
Faculté des Sciences et des Techniques  
Institut des Molécules et des Matériaux du Mans  
Département Polymères Colloïdes Interfaces

Le Mans, France, Novembre 2012

*Présentée le 22 Octobre 2012 devant le jury composé de:*

M. Saïd BOUHALLAB	Directeur de Recherche - INRA Rennes	Rapporteur
M. Christian SANCHEZ	Professeur - Université de Montpellier II	Rapporteur
M. Rémi SAUREL	Professeur - AgroSup Dijon	Examineur
Mme Laurence DONATO – CAPEL	Research Scientist - Nestlé Research Center, Lausanne, Switzerland	Examineur
M. Dominique DURAND	Directeur de Recherche - CNRS Université du Maine	Directeur de thèse
M. Taco NICOLAI	Directeur de Recherche - CNRS Université du Maine	Directeur de thèse

## ACKNOWLEDGMENT

I am grateful to my thesis advisor, Dr. Taco Nicolai, for his guidance and support. He was always available to all issues and questions during my PhD time. His expertise in protein aggregation and scattering techniques improved my research skills and prepared me for future challenges. I also give thanks to my co-advisor, Dr. Dominique Durand for his support, encouragement and enthusiasm.

My gratitude goes next to my collaboration in Nestlé Research Centre in Lausanne, Dr. Laurence Donato-Capel, Christophe Schmitt and Lionel Bovetto, for their helpful suggestions and comments during this research. A special thank to Laurence, who has taken care of me throughout of the project with many insightful questions, comments and advice on my work. I believe that her input has helped me improving my skills in scientific writing and presentation.

Acknowledgements are also made to the Nestec Ltd. for financial support for this study.

I would like to thank to my jury members, Professor Christian Sanchez, Professor Rémi Saurel and Dr. Said Bouhallab for accepting to judge my work and giving me valuable comments and discussions for a better understanding of the aggregation process.

A big thank to Magali Martin (PCI, Le Mans) and Bertrand Schmitt (Nestec, Lausanne) for providing the analysis of SEC and TEM images. My appreciation also extends to all friends and colleagues at PCI, who created a positive atmosphere in which to leave and to do science.

Above ground, I am indebted to my family for their unceasing love, encouragement and support despite the long distance between us; to anh Tien and his family who always consider me part of the family. And finally, I acknowledge my love, Nga, who shared with me a life of joy in the hours when the lab lights were off.

## Abstract

Beta lactoglobulin ( $\beta$ lg) is a major whey protein in the bovine milk. Upon heating above its denaturation temperature (which is pH-dependent), this globular protein undergoes molecular changes leading to the irreversible aggregation. Depending on the pH and ionic strength, either protein aggregates or gels exhibiting various structures and morphologies have been described. Very recently, it was found that in a narrow range of the pH close to iso-electric point, stable suspensions of rather monodisperse spherical particles with a radius of about a hundred nanometers were formed. These spherical particles which were called microgels might be of special interest for the production of liquid dispersions of  $\beta$ -lactoglobulin aggregates exhibiting various functionalities for food applications. The project on which I report here was a collaboration with the Nestlé Research Center (Lausanne, Switzerland) and its objective was to study the formation and structural properties of the microgels in different environmental conditions.

The first part of the project is to study the influence of the pH on the formation of microgels. Stable suspensions of protein microgels are formed by heating salt free  $\beta$ lg solutions at concentrations up to about  $C = 50 \text{ g.L}^{-1}$  if the pH is set within a narrow range between 5.75 and 6.1. The internal protein concentration of these spherical particles is about  $150 \text{ g.L}^{-1}$  and the average hydrodynamic radius decreases with increasing pH from 200 nm to 75 nm. The formation of the microgels leads to an increase of the pH, which is a necessary condition to obtain stable suspensions. The spontaneous increase of the pH during microgel formation leads to an increase of their surface charge density and inhibits secondary aggregation. This self-stabilization mechanism is not sufficient if the initial pH is below 5.75 in which case secondary aggregation leads to precipitation. Microgels are no longer formed above a critical initial pH, but instead short curved protein strands are obtained with a hydrodynamic radius of about 15-20 nm.

The second part of the work is about the formation of microgels driven by the addition of calcium ions. We found that stable suspensions of spherical protein particles (microgels) can be formed by heating  $\beta$ lg solutions in the presence of calcium ions. The conditions for the calcium induced microgel formation were studied at different pH between 5.8 and 7.5 and different protein concentrations between 5 – 100  $\text{g.L}^{-1}$ . The results showed that a critical molar ratio of calcium to proteins ( $R$ ) is needed to form microgels independent of the protein concentration.  $R$  decreases with decreasing pH. The microgels have a hydrodynamic radius ranging from 100 to 300 nm and their internal protein concentration ranges from 0.2 to 0.45  $\text{g.mL}^{-1}$ . The determination of calcium bound to the microgels suggests that the crucial parameter for microgel formation is the net charge density of the native proteins. The microgel suspensions are stable in a narrow range of  $R$  but aggregate at higher  $\text{Ca}^{2+}$  concentrations.

In the third part, we continued to investigate the formation of microgels at initial step and how it is growing in the presence of calcium ions. We have proposed a mechanism of formation of  $\beta$ lg microgels which follows a nucleation and growing process. The nucleus with define size are formed at the initial state and that is growing in size to reach final size of aggregates. At low calcium concentration it stabilizes and then we obtain a stable suspension of microgels. But at high concentrations, the microgels here can jump to form big aggregates and finally a gel. The structure of gel from microgels is heterogenous at the scale of confocal microscopy and similar to those formed in the presence of NaCl 0.3 M. However the process of formation of these gels is not the same.

To conclude, this work gives us a better understanding of the formation mechanism of different kind of aggregates from heat induced  $\beta$ lg solution (strands, microgels or fractal aggregates) and their structural properties under various environmental conditions. The knowledge of the structure of these aggregates will be useful for industrial food and nutraceutical applications.

# CONTENTS

<b>General Introduction .....</b>	<b>1</b>
<b>Chapter I. Background .....</b>	<b>3</b>
I.1. $\beta$ -lactoglobulin .....	3
I.1.1. Molecular structure.....	3
I.2. Native $\beta$ -lg in aqueous solution .....	6
I.2.1. Influence of the pH .....	6
I.2.2. Influence of salt .....	7
I.3. Heat induced denaturation and aggregation of $\beta$ -lg.....	8
I.3.1. Aggregation .....	9
I.3.2. Aggregation kinetics.....	10
I.3.3. Structure of the aggregates .....	11
I.3.3.1. Effect of the pH.....	11
I.3.3.2. Effect of salt .....	13
I.3.4. Stability of the aggregates .....	15
I.3.5. Structure of the gels.....	16
I.4. Aggregation mechanism .....	16
<b>Chapter II. Materials and Methods.....</b>	<b>19</b>
II.1. Materials.....	19
II.2. Methods.....	20
II.2.1. Light Scattering .....	20
II.2.2. Turbidity measurements .....	24
II.2.3. Centrifugation.....	24
II.2.4. Determination of the protein concentration in the supernatant .....	27
II.2.5. Size exclusion chromatography (SEC).....	29
II.2.6. Confocal laser scanning microscopy (CLSM).....	30
II.2.7. Pair correlation function of CLSM images .....	31
II.2.9. Gel point determination.....	34
II.2.10. Calcium binding measurements.....	34

<b>Chapter III. Results and discussion .....</b>	<b>35</b>
III.1. Structure of heat-induced $\beta$ -lg aggregates at steady state .....	35
III.1.1. Aggregation in pure water.....	35
<i>Influence of the protein concentration at pH 5.8 .....</i>	<i>36</i>
<i>Effect of the pH.....</i>	<i>36</i>
<i>Fraction, molar mass and size of the microgels as a function of the pH.....</i>	<i>37</i>
<i>Effect of the heating temperature .....</i>	<i>39</i>
III.1.2. Aggregation in the presence of calcium ions .....	40
<i>Effect of heating at 85°C at steady state .....</i>	<i>40</i>
<i>Effect of the pH.....</i>	<i>40</i>
<i>Dependence on the temperature.....</i>	<i>41</i>
III.2. Evolution of the system during heating.....	44
III.2.1. Aggregation kinetics .....	44
<i>At low pH in pure water .....</i>	<i>44</i>
<i>At neutral pH in the presence of calcium ions .....</i>	<i>45</i>
III.2.2. Evolution of the system during heating.....	45
<i>Evolution at low pH in pure water .....</i>	<i>45</i>
<i>Evolution at neutral pH in the presence of calcium ions .....</i>	<i>49</i>
<i>Calcium bound to the proteins before and after heating .....</i>	<i>50</i>
III.3. Mechanism of the formation and stabilization of strands and microgels. ....	51
III.4. Secondary aggregation and gelation .....	53
III.4.1. Secondary aggregation and gelation in pure water .....	53
III.4.2. Secondary aggregation and gelation at pH 7 in the presence of CaCl <sub>2</sub> .....	55
III.5. Comparison of aggregation and gelation at pH 7 in the presence of NaCl and CaCl <sub>2</sub> .....	56
<b>Chapter IV Conclusions and perspectives.....</b>	<b>61</b>
IV.1. Conclusions.....	61
IV.2. Perspectives.....	64
<b>References .....</b>	<b>67</b>
<b>PAPER I .....</b>	<b>75</b>
<b>PAPER II .....</b>	<b>101</b>
<b>PAPER III .....</b>	<b>123</b>

## General Introduction

Beta-lactoglobulin ( $\beta$ -lg) is the main component of whey proteins in bovine milk. This globular protein is widely used in food formulation for its nutritional and functional properties (emulsifier, texturing, foaming). Upon heating above its denaturation temperature (which is pH-dependent), the protein undergoes conformational changes leading to irreversible aggregation. Depending on the pH and ionic strength, either protein aggregates or gels exhibiting various structures and morphologies have been observed. At acidic pH and low ionic strength large rigid rod-like aggregates are formed. At neutral pH, small strands are formed at low concentrations and low ionic strength that associate at higher protein concentrations into larger randomly branched aggregates with a self similar structure. Recently, it was found that in a narrow range of the pH close to its iso-electric point of 5.2, stable suspensions of rather monodisperse spherical particles with a radius of about a hundred nanometers were formed. These spherical particles, which were called microgels, might be of special interest for the production of liquid dispersions of concentrated protein particles exhibiting various functionalities for food applications.

At higher concentrations, the denatured proteins form a system spanning network. The gels are transparent at low ionic strength when electrostatic repulsion is strong and highly turbid close to the iso-electric point or at high ionic strength. Microscopy showed that the turbid gels consisted of connected spherical particles with a radius of about a micrometer, so-called particulate gels, whereas the transparent gels were formed by cross linked protein strands, so-called finely stranded gels.

The project on which I report here was a collaboration with the Nestlé Research Center (Lausanne, Switzerland) and its objective was to study the formation and structural properties of the microgels in different environmental conditions. To do this, many parameters were tested: heating conditions (temperature and duration) and environmental conditions (protein concentration, pH and  $\text{CaCl}_2$  and  $\text{NaCl}$  concentrations). The relationship between the formation of microgels and small strands, on one hand, and particulate gels and finally stranded gels, on the other was also investigated.

This thesis consists of 3 chapters and a general conclusion and perspectives. In the first chapter we describe the background literature of heat-induced aggregation of  $\beta$ -lg and focusing on systems with pH above the iso-electric point. In the second chapter we discuss the materials and methods that have been used in this study. In the third chapter the main results of the investigation are presented and discussed. The influence of the pH close to pI in pure water and

that of adding calcium ions at higher pH will be presented together for comparison. More details can be found in the 3 publications included at the end of the thesis. Chapter III is divided into 5 sections.

The first section reports on the structure and the size distribution of aggregates formed in  $\beta$ -lg solutions after extensive heat treatment when steady state has been reached, i.e. when the system stops evolving. We will show that stable microgel suspensions can be formed in a narrow range of pH close to pI in pure water or by adding calcium at higher pH. Larger and denser microgels can be formed in the presence of calcium than in pure water.

In the second section, we will follow the evolution of the system during heating. After a short description of the aggregation kinetics, we will discuss in more detail the evolution of the formation of microgels at pH 5.8 in pure water and compare it to that of microgels at neutral pH in the presence of calcium ions. The most interesting results is the finding that the crucial parameter for the formation and self stabilization of the microgels is the net charge density of the native proteins that can be controlled either by the pH or by adding calcium ions.

Based on these results, we propose in the third section a mechanism for the formation of microgels, which involves a nucleation and growth process, and their stabilization, which involves an increase of their surface charge density.

In the fourth section, we discuss secondary aggregation and gelation of the strands and microgels at higher protein concentrations. The structures of large aggregates close to the gel point and that of the gels are shown as a function of pH and calcium concentration. It is shown that the transition between particulate gels and finely stranded gels at lower pH or higher calcium ions concentrations is related to the transition between the formation of microgels and strands.

The last section compares aggregation and gelation at neutral pH in the presence of  $\text{CaCl}_2$  and  $\text{NaCl}$ . Homogeneous finely stranded gels are formed at low  $\text{NaCl}$  concentrations, but their structure becomes more heterogeneous at high  $\text{NaCl}$  concentrations even though no microgels are formed. The structure at high  $\text{NaCl}$  concentrations appears similar to that of particulate gels formed in pure water at pH close to pI or in the presence of  $\text{CaCl}_2$ , but the mechanism of formation is different.

Chapter III is followed by general conclusions and perspectives. Three publications have been written based on the results of this thesis and are included. The first has already appeared in print, the second has been accepted for publication and the last has been submitted.

## Chapter I.

## Background

### *I.1. $\beta$ -lactoglobulin*

$\beta$ -lactoglobulin ( $\beta$ -lg) is the major whey protein in the milk of ruminants and many other mammals. It is a member of lipocalin family of proteins (Oliveira, Valente-Mesquita et al. 2001) which carry small hydrophobic molecules into their hydrophobic cavity and therefore may provide a transport for bioactive ingredient such as retinol (Papiz, Sawyer et al. 1986). Ten different genetic variants of  $\beta$ -lg have been identified (Farrell, Jimenez-Flores et al. 2004), among these two are most abundant: variants A and B that differ at two amino acid substitutions 64 (Asp/Gly) and 118 (Val/Ala).  $\beta$ -lg has been the subject of a wide range of biophysical studies because of its abundance and ease of isolation from milk.

#### **I.1.1. Molecular structure**

There are four different levels in protein molecular structure.

**The primary structure** composed of a chain of amino acids linked together by peptide bonds and, in rare cases di-sulfide bridges. The  $\beta$ -lg primary structure consists of 162 amino acids with a molecular weight around 18.60 Kg/mol. In both variants A and B,  $\beta$ -lg contains two disulphide bridges and one free cysteine group (Hambling, Mc Alpine et al. 1992).

**The secondary structure** attributes to certain patterns of polypeptide chain torsion angles within adjacent amino acid residues, which are maintained via hydrogen bonds in a regular and well defined position. There are two major elements of secondary structure which depends on the arrangement of the polypeptide chain: helicoidally ( $\alpha$  helix) and pleated sheet structure (mainly  $\beta$  sheet). In the  $\alpha$  helix, the polypeptide main chain is folded into a right handed spiral, which about 3.6 residues per turn. The  $\beta$  sheet structure is formed by laterally assembly of many linearly elongated  $\beta$  strands. The proportion of these structural elements in the secondary structure of  $\beta$ -lg can be estimated by calculation using sequence data and structural probabilities (Creamer, Parry et al. 1983) or experimentally by different techniques such as crystallography (Papiz, Sawyer et al. 1986), IR spectroscopy and Circular Dichroism (Timasheff, Townend et al. 1966). For  $\beta$ -lg it consists of about 10-15 % of  $\alpha$  helix, 43-50 % of  $\beta$  sheet and 15-20% of  $\beta$  strands.

**Tertiary structure** refers to the three-dimensional folding of a polypeptide chain. The secondary and tertiary structure is maintained by a range of interactions between the amino acids:

**Covalent bonds.** The covalent bonds besides the peptide link are disulphide bridges. The disulfide bond is strong, with a typical bond dissociation energy of  $251 \text{ kJ}\cdot\text{mol}^{-1}$  and thus its position can imply a geometry restriction and increase the stability of the structure.

**Hydrogen bonds** are a weak links with bond strengths between about 10 and 40  $\text{kJ}\cdot\text{mol}^{-1}$  and a length of about 0.18 nm (Bryant and McClements 1998). However, because there are a large number, hydrogen bonding is the most important interaction for maintaining the secondary and tertiary structures.

**Electrostatic interactions** act between charged side chains of amino acids and also with ions in the solvent. They can be either repulsive when the charges have the same sign or attractive when their signs are different. Because the proteins are composed of both acidic and alkaline units, they are amphoteric, and the number and distribution of charges vary as a function of the pH of the surrounding aqueous solution. Above the isoelectric point (pI), which is 5.2 for  $\beta$ -lg, the proteins are negatively charged, whereas at lower pH the net charge is positive. At pI the net charge is zero, but the protein still contain positive and negative charges (Bryant and McClements 1998). Electrostatic interaction can be reduced by charge screening with electrolytes. Electrostatic interactions play a very important role in the intermolecular interactions between different protein molecules in solution that we will discuss later, but they participate relatively little in the stabilization of the protein conformation.

**Van der Waals interactions** are linked to the polarizability of certain molecules or atoms. This is a weak interaction of about 1 to 3  $\text{kJ}\cdot\text{mol}^{-1}$  but it can play a significant role in conformation stabilization because of the large number of contacts (Kinsella and Whitehead 1989 ).

**Hydrophobic interactions** appear between apolar groups of amino acids. When a apolar group is in contact with water, it leads to a disruption of hydrogen bonds between water molecules. These changes are not thermodynamically favorable and the system tends to minimize the area of contact between  $\text{H}_2\text{O}$  and apolar groups. As consequence it ends up by associating apolar groups together. In many cases this results in the apolar side chains

of amino acids being concentrated within the core of a globular protein, while the outside of the protein contains mainly polar groups.

It is not easy to estimate the contribution of each interaction to the stability of the protein, but most authors agree that the major stabilizing forces are hydrophobic interactions and hydrogen bonds (Pace, Shirley et al. 1996). In a given thermodynamic condition, many proteins adopt a well-defined conformation which tends to minimize the exposure of apolar groups to the solvent. These apolar groups bury inside the protein structures to form a hydrophobic core from which the solvent tends to be excluded. This very ordered and compact folded conformation allows the protein to minimize its free energy in aqueous solutions (Kinsella and Whitehead 1989 ).

The 3D chain conformation of  $\beta$ -lg was determined by X ray crystallography at 3.0 Å resolution and is shown in figure 1.1 (Brownlow, Morais Cabral et al. 1997 ). It is made up of an 8 stranded antiparallel  $\beta$ -barrel, A to H, with a 3 turn  $\alpha$  helix on the outer surface and a ninth  $\beta$ -strand, I, which is in antiparallel position of the first strand A. It is this strand that is involved in the formation of dimers. The  $\beta$ -barrel contains a central cavity or calyx and has a conical form. It consists of  $\beta$ -strands A-D forming 1 sheet and strands E-H forming a second. It is known that this calyx offers the ligand-binding site. The capacity to binding small molecules is reviewed in some detail in (Sawyer, Brownlow et al. 1998);(Creamer, Blair et al. 2000); (Kontopidis, Holt et al. 2004)

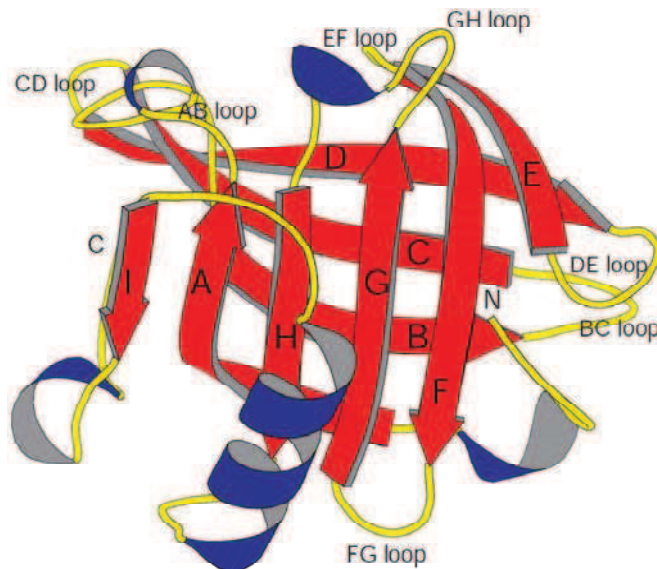


*Figure 1.1: Schematic drawing of the structure of  $\beta$ -lactoglobulin (Brownlow, Morais Cabral et al. 1997 )*

In an aqueous surrounding, protein molecules often interact with each other. They tend to assembly and form a **quaternary structure** that is stabilized by the same type of weak non-covalent forces as described above for the folding of individual protein chains. The number of subunits which assemble varies as a function of environmental conditions. In the next part, we will discuss the effect of pH and ionic strength, which are considered to be the most important factors that control the behavior of native  $\beta$ -lg in aqueous solution (Iametti, Scaglioni et al. 1998).

## ***1.2. Native $\beta$ -lg in aqueous solution***

### **1.2.1. Influence of the pH**

The dependence of the charge of proteins on the pH can be determined by an acid - base titration. With increasing pH from 2 to 10, the net charge decreases from +20 to -15 by passing through zero at the iso-electric point  $pI \approx 5.2$  (Figure I.2).

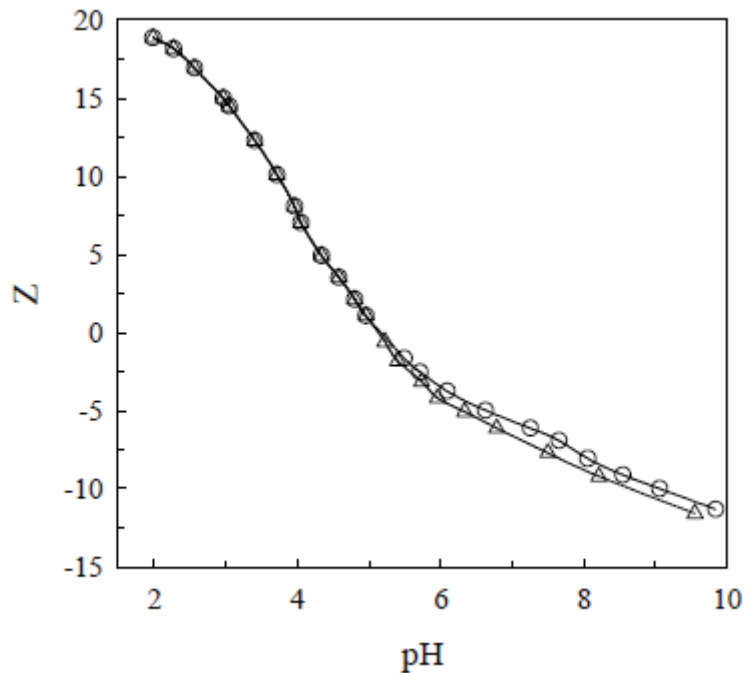


*Figure 1.2: Titration curve of the  $\beta$ -lactoglobulin for 2 variants A (○) et B (Δ) in the presence of 0.25M of KCl at 25°C. Z represents the net charge per monomer (Basch and Timasheff 1967).*

At pH close to the pI, the proteins are ambivalent and interaction between opposite charges can lead to aggregation through hydrophobic interaction and hydrogen bonds (Majhi, Ganta et al. 2006); (Mehalebi, Nicolai et al. 2008); (Schmitt, Bovay et al. 2009); (Stading and Hermansson 1990). The rate of aggregation is very slow at room temperature and may be imperceptible at low protein concentrations. However, it increases with increasing temperature and can lead to precipitation of a significant fraction of the proteins at high concentrations (Mehalebi, Nicolai et al. 2008). The rate of aggregation is maximum at about pH 4.6 (Majhi, Ganta et al. 2006) and is negligibly slow for pH 5.5 even at 50°C and C=100g/L (Mehalebi, Nicolai et al. 2008).

Outside this pH zone close to pI, native  $\beta$ -lg exists in an equilibrium state of monomers and dimers. At neutral pH and room temperature, the main element in the equilibrium is a dimer with a radius of gyration 1.8 nm (Aschaffenburg 1959) held together by association of the strands I of each molecule (Papiz, Sawyer et al. 1986). The equilibrium shifts towards the monomer with increasing temperature, increasing charge density and decreasing ionic strength ((Apenten and Galani 2000); (Aymard, Gimel et al. 1996); (Renard, Lefebvre et al. 1998); (Verheul, Pedersen et al. 1999)). At pH above 8.5-9,  $\beta$ -lg denatures irreversibly by so-called alkali induced denaturation and tends to aggregate (Hambling, Mc Alpine et al. 1992).

### **I.2.2. Influence of salt**

Salts have a significant effect on water absorption, swelling and solubility of  $\beta$ -lg. At physiological conditions,  $\beta$ -lg has many charges on its surface and is stable in water due to electrostatic repulsion. Opposite charges in the surrounding will be condensed and form an electric double layer. There is an equilibrium between repulsive electrostatic interactions caused by the double layers and attractive van der Waals forces. At high salt concentrations, the thickness of the layer decreases and as consequence it favors the attractive interactions. This behavior is called salting out. However, closer to pI adding a small amount of salt actually increases the solubility of  $\beta$ -lg, which is called salting in (Arakawa and Timasheff 1984).

Divalent cations, such as  $\text{Ca}^{2+}$  may induce aggregation by their ability to act as bridges between negatively charge carboxylic groups on neighboring protein molecules (Bryant and McClements 1998). However, (Xiong, Dawson et al. 1993) showed that the

role of  $\text{Ca}^{2+}$  in the formation of intermolecular bridges was unlikely, which was confirmed by Simons et al. (2003). (Jeyarajah and Allen 1994) observed larger changes by adding Ca ions compared to Na ions on intrinsic and extrinsic fluorescence and supposed that divalent cations must be participating in a specific interaction other than charge neutralization. (Simons, Kusters et al. 2002) suggested that calcium needs to be bound specifically to carboxylates with a threshold affinity. This binding is weak, not covalent or via coordination complexes (Jeyarajah and Allen 1994). (Zittle, Monica et al. 1957) found that the binding of calcium to  $\beta$ -lg is analogue of the pI in terms of the net charge and can make the protein isoelectric without adjusting the pH to pI.

### ***1.3. Heat induced denaturation and aggregation of $\beta$ -lg***

The effect of heat on the milk proteins is important for the dairy industry, because heating is involved in the manufacture of almost all milk products. Upon heating,  $\beta$ -lg undergoes intramolecular and intermolecular changes. Raising the temperature shifts the equilibrium toward monomers ((Aymard, Gimel et al. 1996); (Verheul, Roefs et al. 1998); (Renard, Lefebvre et al. 1998). Upon heating the molecule undergoes conformational changes and partially unfolds, called denaturation, leading to a more mobile, but still compact structure, which is often referred to as molten globule. Apolar groups and the thiol that in native state are buried inside become exposed and may interact with other proteins. As a consequence, bonds may be formed between proteins leading to aggregation and even to gelation at high enough protein concentrations.

The structure of aggregates is strongly influenced by pH and ionic strength (Nicolai, Britten et al. 2011). Far below the pI, the protein has a large net positive charge. This leads to repulsion between the protein molecules and a lower tendency for aggregation. At pH 2.0 without added salt, the large elongated rod like aggregates are formed. This kind of aggregates have attracted much attention in part because they resemble so-called amyloid fibrils that are responsible for a number of neurodegenerative diseases (Aymard, Gimel et al. 1996); (Aymard, Nicolai et al. 1999); (Arnaudov, De Vries et al. 2003); (Veerman, Ruis et al. 2002); (Adamcik, Jung et al. 2010); (Gosal, Clark et al. 2004); (Krebs, Devlin et al. 2009). In the following, we will focus on the pH zone close to and above pI.

### **I.3.1. Aggregation**

For  $\beta$ -lg, aggregation is an exothermic process which follows directly the denaturation. Many interactions are involved during this process such as hydrogen bonds, Van der Waals and hydrophobic interactions. The aggregation process and the structure of the aggregates depend strongly on the temperature, the pH, the ionic force and the protein concentration.

During the early stages of the aggregation process the formation of non-native monomers has been observed between pH 6.0 and 8.7 (Bauer, Hansen et al. 1998); (Cairoli, Iametti et al. 1994); (Carrotta, Arleth et al. 2003); (Croguennec, O'Kennedy et al. 2004); (Croguennec, Bouhallab et al. 2003); (Hoffmann and van Mil 1997); (Mehalebi, Nicolai et al. 2008); (Schokker, Singh et al. 1999). These authors suggested that reshuffling of intramolecular disulfide bonds may be responsible. The non-native monomers undergo intermolecular sulfhydryl/disulphide-bond exchange reactions to give non-native dimers. The dimers undergo further sulfhydryl-catalyzed disulphide-bond interchange to give larger oligomer species. The proteins that form these oligomers still have a large amount of secondary structure, but the structure is thought to be more mobile (Bauer, Hansen et al. 1998); (Carrotta, Arleth et al. 2003); (Croguennec, Bouhallab et al. 2003). Disulfide bonds are exchanged within the proteins and are formed between proteins at pH>5.7. (Surroca, Haverkamp et al. 2002) did not observe covalently crosslinked aggregates at pH 4.9, but (Otte, Zakora et al. 2000) reported that  $\beta$ -lg gels formed at pH 5.0 were cross-linked with disulfide bonds.

At low proteins concentrations, the oligomers persist, but at higher concentrations they associate into larger aggregates. Both covalent bonds and non-covalent bonds are involved in the formation of the aggregates. The rate at which the aggregates are formed increased with decreasing pH between 8.0 and 6.0 even at temperatures where the depletion rate of native  $\beta$ -lg decreased with decreasing pH (Bauer, Hansen et al. 1998); (Verheul, Roefs et al. 1998).

(Mehalebi, Nicolai et al. 2008) suggested the existence of a critical association concentration (CAC) of proteins below which they did not form large aggregates. When  $\beta$ -lg solutions were heated at 80°C for different pH (6.0, 6.5, 7.0, 8.0), size exclusion chromatography (SEC) showed that the solutions contained monomers and small oligomers, mainly dimers and trimers, and a distinct population of larger aggregates. With increasing concentration the fraction of large aggregates increased until more than 95%

had formed large aggregates. In pure water the CAC increased from 1.2g/L at pH 6.0 to 10 g/L at pH 8.0. It decreased when NaCl was added.

### **I.3.2. Aggregation kinetics**

The aggregation rate of  $\beta$ -lg can be determined by measuring the decrease of the native protein concentration as a function of time. The depletion rate of native proteins can be well described by the general rate equation:  $-dC/dt = k_n C^n$  and after integration for  $n \neq 1$ :  $(C_0/C)^{(n-1)} = 1 + (n-1)k_n C_0^{(n-1)}t$ , where  $C_0$  and  $C$  are the concentrations of native protein at time  $t = 0$  and time  $t$ , respectively,  $n$  is the order of the reaction and  $k_n$  is the rate constant.

In the literature, a reaction order of about 1.5 was often reported at least close to neutral pH (Anema and McKenna 1996); (Roefs and De Kruif 1994); (Dannenberg and Kessler 1988); (Verheul, Roefs et al. 1998) but lower and higher values were found at higher and lower pH, respectively (Croguennec, O'Kennedy et al. 2004); (Hoffmann and van Mil 1999); (Law and Leaver 2000); (Tolkach, Steinle et al. 2005); (Le Bon, Nicolai et al. 1999); (Schokker, Singh et al. 2000); (Unterhaslberger, Schmitt et al. 2007); (Zuniga, Tolkach et al. 2010).

The temperature dependence of the depletion rate of native proteins could be described in terms of an activated process ((Anema and McKenna 1996); (Dannenberg and Kessler 1988); (De Wit 2009); (Galani and Apenten 1999); (Mounsey and O'Kennedy 2007)). This means that there is no critical so-called denaturation temperature, but that the rate varies rapidly with the temperature. Nevertheless, an apparent denaturation temperature will be observed during a temperature ramp depending on the rate of the temperature variation. Different behaviors were observed above and below about 90°C:

- In the temperature range below 90°C the activation energy is high and denaturation of proteins is the rate-limiting steps.

- Above 90°C, considerably lower activation energies were observed indicated that all  $\beta$ -lg is rapidly denatured and the aggregation process is the rate-limiting step.

The rate of the denaturation of the native proteins depends on the pH. It was reported to increase with increasing pH from 6 to 8 when heated at 65°C – 68.5°C ((Hoffmann and van Mil 1999); (Verheul, Roefs et al. 1998)) but to stay constant in this pH range when heated at 75°C (Verheul, Roefs et al. 1998). (O'Kennedy and Mounsey 2009) also reported that the fraction of denatured protein increased with increasing pH from 6.4

to 8 at 78°C. However, (Zuniga, Tolkach et al. 2010) found a small increase of the depletion rate with decreasing pH between pH 6.8 and 6.0 at 80°C. (Donato, Schmitt et al. 2009) observed that the depletion of native proteins was faster at pH 5.7 and 5.9 than at pH 7.0 at 85°C, but it was slower at 70°C.

Adding a small amount NaCl leads to an increase of the depletion rate of native  $\beta$ -lg (Baussay, Le Bon et al. 2004); (Croguennec, O'Kennedy et al. 2004); (O'Kennedy and Mounsey 2009); (Verheul, Roefs et al. 1998). When more than about 0.1M NaCl is added the depletion rate decreases with increasing salt concentration (Verheul, Roefs et al. 1998). The effect is much stronger for CaCl<sub>2</sub> than for NaCl ((Croguennec, O'Kennedy et al. 2004); (Roefs and Peppelman 2001)).

From this overview, it is clear that the aggregation rate depends on the temperature, the concentration, the pH, and the ionic strength. In addition, their influence is not independent, which can be explained in part by the fact that unfolding and aggregation are not influenced in the same way.

### **I.3.3. Structure of the aggregates**

As mentioned above, the structure of the aggregates depends strongly on the pH and the ionic strength. Different scattering and microscopy techniques have been used to study the effect of these parameters on the size, mass, density and form of the aggregates.

#### **I.3.3.1. Effect of the pH**

As a function of the pH, aggregates with different structures were obtained. Electron microscopy showed small curved strands at pH 7.0 and low ionic strength, spheres at pH 5.8 and long rigid strands at pH 2.0 (Figure 1.3). (Schmitt, Bovay et al. 2007) characterized the aggregates that were formed after heating during 15 min at 85°C at C=10g/L between pH 6.0 and 7.0. The results showed that the hydrodynamic radius ( $R_h$ ) decreased from 60 nm at pH 6.0 to 27 nm at pH 7.0.

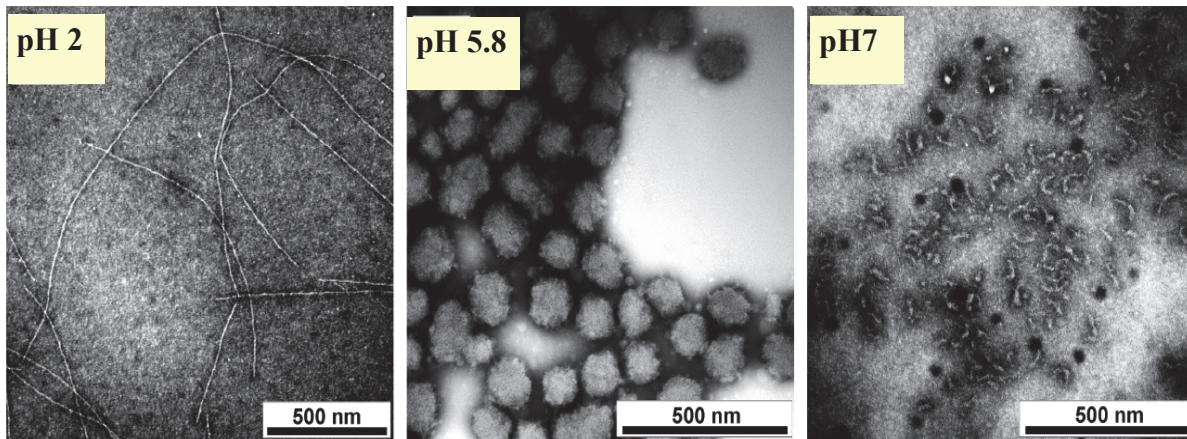


Figure 1.3: Negative staining TEM images of  $\beta$ -lg aggregates formed at different pH mentioned in the figure. Scale bars are 500 nm. Reproduced from (Jung, Savin et al. 2008).

(Mehalebi, Nicolai et al. 2008) studied the effect of the pH on the aggregation in pure water in the range between 6.0 and 8.0 at different protein concentrations. They found that the hydrodynamic radius of the aggregates was approximately independent of the protein concentration until it increased rapidly close to the gelation concentration ( $C_g$ ).  $C_g$  increased with increasing pH from about 60g/L to about 95 g/L. At lower concentrations,  $R_h$  was found to increase with decreasing pH from about 12nm at pH 8.0 to about 20 nm at pH 6.0. Values of about 15nm at pH close to neutral had already been reported in earlier studies (Aymard, Gimel et al. 1996); (Baussay, Le Bon et al. 2004); (Jung, Savin et al. 2008); (Verheul, Roefs et al. 1998). The form of these aggregates was investigated by Cryo-TEM. The images showed curved strands with a diameter of about 10nm and a length of about 50nm (Durand, Gimel et al. 2002). Similar images were obtained using ordinary TEM (Donato, Schmitt et al. 2009); (Schmitt, Bovay et al. 2009); (Jung, Savin et al. 2008).

The structure factor ( $S(q)$ ) of large aggregates that formed close to  $C_g$  was determined by light scattering as a function of the scattering wave vector ( $q$ ) after infinite dilution (Mehalebi, Nicolai et al. 2008).  $S(q)$  obtained for aggregates with different radii of gyration ( $R_g$ ) was found to be universal of a function of  $q.R_g$  and showed that the structure of the aggregates was self similar. At large  $q.R_g$  where the light probed the internal structure of aggregates,  $S(q)$  decreased with increasing  $q$  following a power law. The exponent of this power law is equal to the so-called fractal dimension ( $d_f$ ) that characterizes self similar particles, see e.g. in (Nicolai, Durand et al. 1996). The structure factor was the same for values of the pH between 5.8 and 8.0 with  $d_f=1.7$ . Self similar

structure of the particles was also clearly observed when the molar mass ( $M$ ) was plotted as a function of  $R_g$  which followed a power law:  $M \propto R_g^{\text{df}}$ . However, the authors found that the prefactor was larger at pH 5.8 implying that the aggregates were denser at this pH. A combination of light scattering and small angle X-ray scattering (SAXS) on aggregates formed at pH 7 showed that the power law extended to  $q \approx 0.15 \text{ nm}^{-1}$  (Pouzot, Nicolai et al. 2005). Cryo-TEM images showed that the large aggregates were formed by cross-linking of the short curved strands (Durand, Gimel et al. 2002); (Pouzot, Nicolai et al. 2005).

(Donato, Schmitt et al. 2009) studied in more detail  $\beta$ -lg aggregation at pH 5.7 and 5.9 during heating at  $70^\circ\text{C}$  up to 24h and at  $85^\circ\text{C}$  up to 8h. The concentration was fixed at 10g/L. Transmission electron microscopy showed that spherical particles were formed. At pH 5.7 they observed that the particles agglomerated into large clusters and slowly precipitated. The hydrodynamic radius of the particles formed at pH 5.9 increased with increasing heating time from 62 to 87nm at  $70^\circ\text{C}$  and from 105 to 130nm at  $85^\circ\text{C}$ . These particles could be removed by centrifugation and the supernatant was found to contain besides residual native  $\beta$ -lg, small oligomers and aggregates similar to those observed at higher pH.

(Schmitt, Bovay et al. 2009) studied the aggregation of  $\beta$ -lg as a function of the pH between pH 3.0 and 7.0 keeping the concentration (10g/L) and the heating protocol ( $85^\circ\text{C}$ , 15min) fixed. TEM showed spherical particles with a radius of 100-150 nm at pH 4.6 and about 50nm at pH 5.8. At pH 5.0 and 5.6 they observed somewhat larger spherical particles, but these particles agglomerated into clusters that slowly precipitated. The hydrodynamic radius of the aggregates determined with DLS was 110nm at pH 5.6 and 80nm at pH 5.8. The size of the aggregates decreased if the pH was set further above or below the isoelectric point.

### **1.3.3.2. Effect of salt**

At pH 7, the fraction of denatured monomers and small oligomers at steady state decreases with increasing NaCl concentration ( $[\text{NaCl}]$ ) (Baussay, Le Bon et al. 2004). The CAC decreased with increasing NaCl concentration from about 3 g/L without salt to about 0.2g/L at  $[\text{NaCl}] = 0.4\text{M}$ . Others have also observed fewer oligomers in the presence of added NaCl (Bauer, Hansen et al. 1998); (Croguennec, O'Kennedy et al. 2004). Isolated

stable oligomers that were formed at low ionic strength aggregated rapidly when salt was added.

The effect of added NaCl on the structure of the aggregates formed at pH 7.0 has been studied in some detail (Baussay, Le Bon et al. 2004); (Pouzot, Nicolai et al. 2005). In some sense, adding salt at a fixed pH is equivalent to lowering or raising the pH towards pI at a fixed ionic strength. In both cases the electrostatic interactions are reduced either by increasing screening or by decreasing the charge density. In addition, a similar transition between finely stranded gels and particulate gels can be induced in either way (Ako, Nicolai et al. 2009).  $C_g$  decreases with NaCl concentration from about 95 g/L without salt to less than 10 g/L if more than 0.1M is added (Baussay, Le Bon et al. 2004); (Renard and Lefebvre 1992). We note that if  $C_g$  is less than about 10 g/L the gels are no longer self supporting and the proteins precipitate in the form of large flocs.

For  $pH > 6.0$  and  $[NaCl] < 50mM$  the size of aggregates was found to depend little on the protein concentration for  $C < C_g$  and to increase weakly with increasing NaCl concentration (Pouzot, Durand et al. 2004); (Baussay, Le Bon et al. 2004). Close to  $C_g$  the size of the aggregates increases sharply. At higher ionic strengths the increase of the aggregate size with increasing protein concentration is more progressive. Large aggregates are self similar at all NaCl concentrations at least up to 0.4M and  $d_f$  increases from 1.7 to 2.0 when salt is added (Baussay, Le Bon et al. 2004). SAXS showed that the local structure ( $q > 0.15nm$ ) is the same up to about 0.1M, but differs significantly at  $[NaCl] = 0.2M$  (Pouzot, Nicolai et al. 2005). The local density of the aggregates increases progressively with increasing ionic strength.

Cryo-TEM images showed that at each ionic strength the large aggregates are formed by cross-linking of the short curved strands (Durand, Gimel et al. 2002); (Pouzot, Nicolai et al. 2005), but the structure is more densely branched at higher ionic strengths. The internal dynamics of large aggregates were probed with DLS. They showed that the rigidity of the aggregates increases with increasing salt concentration probably because the branching density increases (Baussay, Le Bon et al. 2004). A more detailed investigation of the system at pH 7 in 0.1M  $CH_3COONH_4$  showed that first native  $\beta$ -lg ( $C = 19g/L$ ) is transformed into relatively monodisperse aggregates with a radius of about 15nm (Le Bon, Nicolai et al. 1999). With increasing heating time these so-called primary aggregates crosslink to form larger and more polydisperse aggregates with a self-similar structure (Aymard, Gimel et al. 1996); (Le Bon, Nicolai et al. 1999). The aggregation process was

found to be the same at all temperatures tested between 67 and 87°C, but the rate of aggregation increases with increasing temperature.

The effect of adding salt on aggregation at other pH values above pI has not yet been studied in much detail. (Schmitt, Bovay et al. 2007) found that the turbidity of a  $\beta$ -lg solution (10g/L) after 15 min heating at 85°C increased more quickly with increasing NaCl concentration if the pH was lowered between pH 7.0 and 6.0. It is reasonable to suppose that the effect of adding salt in this pH range is similar to that at pH 7, but that it occurs at lower salt concentrations when the pH is lower.

The aggregation process in 0.1M  $\text{CH}_3\text{COONH}_4$  is the same as in 0.1M NaCl, but  $C_g$  is smaller at  $\text{CH}_3\text{COONH}_4$  (~7g/L) than in 0.1M NaCl (~15g/L), which means that  $\text{CH}_3\text{COONH}_4$  screens electrostatic interaction more efficiently. A much bigger effect is found when  $\text{CaCl}_2$  is used. (Baussay, Le Bon et al. 2004) mentioned that at pH 7.0  $C_g < 1\text{g/L}$  in 1mM  $\text{CaCl}_2$ . (Croguennec, O'Kennedy et al. 2004) observed at this pH much faster depletion of native  $\beta$ -lg in 1mM  $\text{CaCl}_2$  than in 15mM NaCl. No oligomers and a smaller amount of non-native monomers were formed in the presence of  $\text{CaCl}_2$ . Oligomers that were formed without salt aggregated rapidly when 1 mM  $\text{CaCl}_2$  was added. O'Kennedy observed in the pH range 5.0-7.0 that more proteins were denatured after 10 min at 78°C in 5mM  $\text{CaCl}_2$  than in 100mM NaCl (O'Kennedy and Mounsey 2009).

#### **I.3.4. Stability of the aggregates**

After steady state is reached the aggregates can be cooled, diluted and reheated without break-up or further aggregation. They only partially break-up after addition of SDS or urea indicating that they are partially held together by disulfide bonds. (Schmitt, Moitzi et al. 2010) studied the formation and stability of WPI particles formed at pH 5.9. These particles were stable between pH 2 and 9 except in a narrow range around pI and only about 6% of the proteins was released at pH 2 or 8. The radius increased by 15% when the pH was reduced to pH 2, but remained the same when it was raised to pH 8. However, when salt was added or the pH was decreased towards pI further association of aggregates was invariably observed. Because it may lead to gelation and happens even at room temperature, this process is called cold gelation (Bryant and McClements 1998).

### **I.3.5. Structure of the gels**

Above a critical gelation concentration  $C_g$  that depends on the pH and type and amount of added salt, the proteins form a system spanning network. The gels are transparent when electrostatic interaction is strong, i.e. at low ionic strength away from the iso-electric point and highly turbid at pH close to pI or at high NaCl concentrations (Ako, Nicolai et al. 2009). Microscopy showed that the turbid gels consisted of connected spherical particles with a radius of about a micrometer, so-called particulate gels, whereas the transparent gels were formed by cross linked protein strands, so-called finely stranded gels.

### ***I.4. Aggregation mechanism***

We may resume the heat induced aggregation process of  $\beta$ -lg in aqueous solution at  $\text{pH} > 5.7$  as follows, see figure 1.4. Before heating, proteins represent in aqueous solution in a native form with an equilibrium of monomers or dimers. When heated the equilibrium is shifted towards the monomers. The protein structure changes and they become more mobile. Buried hydrophobic groups and thiols become exposed and interact with other molecules. Initially, small oligomers (mainly dimers and trimers) are formed that are covalently linked through disulfide bonds. When the concentration of oligomers exceeds a critical amount they associate into relatively monodisperse so-called primary aggregates. The critical association concentration decreases with increasing ionic strength and decreasing pH, while the size of the primary aggregates increases. The primary aggregates are curved strands at pH 7 with a length of about 50nm and a diameter of about 10nm, and approximately spherical with radii up to 200nm at pH 5.8. At higher protein concentrations the primary aggregates associate further into polydisperse self similar aggregates. Above a critical gel concentration which decreases with increasing salt concentration and decreasing pH, a system spanning network is formed.

The range of protein concentrations over which stable aggregate solutions are formed decreases with decreasing pH and increasing ionic strength. Close to the iso-electric point or at high ionic strength, dense particles are formed with radii of several hundred nanometers that associate into large clusters that precipitate or form a system spanning network.

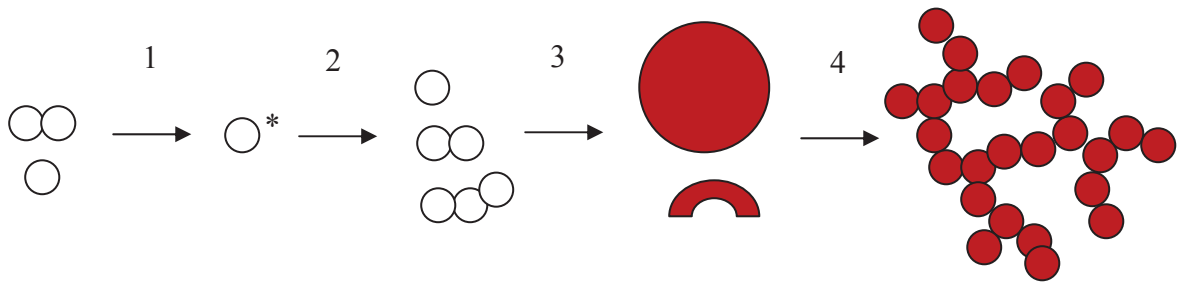


Figure 1.4: Schematic representation of the aggregation process of  $\beta$ -lg at pH > 5.7, which composed of 4 steps:

- Step 1: Loss of monomers and dimers equilibrium of native  $\beta$ -lg and the denaturation proceeds when heated.
- Step 2: Formation of denatured monomers and small oligomers.
- Step 3: Formation of larger primary aggregates above a critical association concentration with different shapes and sizes ( $15 < R_h < 200 \text{nm}$ ) depending on the pH and the salt concentration.
- Step 4: Formation of large self-similar aggregates from the primary aggregates at higher protein concentrations. These large aggregates gel or precipitate above a critical gel concentration.







## Chapter II. Materials and Methods

### *II.1. Materials*

#### **$\beta$ -lactoglobulin**

The  $\beta$ -lactoglobulin (Biopure, lot JE 001-8-415) used in this study was purchased from Davisco Foods International, Inc. (Le Sueur, MN, USA) and contained about equal fractions of the variants A and B and less than 2% of other whey proteins. The powder was dissolved in salt free Mili-Q water with 200ppm  $\text{NaN}_3$  added to avoid bacterial growth. The solutions were dialysed against the solvent for a period of 8 hours with four exchanges of the solvent. The pH was set to the desired value by drop wise addition of 0.1M HCl or 0.1M NaOH under vigorous stirring. The salt concentration was set by adding concentrated concentrations of  $\text{CaCl}_2$  or NaCl. Because addition of  $\text{CaCl}_2$  reduces slightly the pH of the solution, we used small amounts of 0.1 M NaOH to bring the pH back to the initial value. The amount of NaOH used to readjust the pH was noted for the calculation of the net charge of the proteins. The solutions were filtered through 0.2 $\mu\text{m}$  pore size Anotop filters before heating. The protein concentration was measured after filtration by UV absorption at 278nm using extinction coefficient 0.96  $\text{Lg}^{-1}\text{cm}^{-1}$ . Solutions were heated in air tight cylindrical glass vials with a radius of 10mm using a thermostated water bath. The heating rate was fast as the set temperature was reached within 4 min. The samples were cooled rapidly by holding the vial under running tap water.

As will be discussed below, the pH changed during heating. In a few cases the pH was maintained at an approximately constant value. This was done by quickly cooling the sample at regular intervals, which arrests the aggregation process. The pH was subsequently measured and adjusted at room temperature by drop wise addition of 0.1M HCl under vigorous stirring after which the sample was heated again in a water bath and the aggregation process was continued.

## II.2. Methods

### II.2.1. Light Scattering

Light Scattering is a non-invasive method that is well suited for studying protein systems. Proteins are usually sufficiently large to be strong scatterers at low concentrations, and their diffusion constants are generally appropriate to give rise to intensity autocorrelation functions that can be accurately measured.

Dynamic light scattering (DLS) reveals information on the hydrodynamic radius ( $R_{hz}$ ) (through the diffusion coefficient at infinite dilution). Static light scattering (SLS) gives information on the weight-averaged molecular weight and the second virial coefficient. If the aggregates are large compared with the wavelength, then the radius of gyration, and the structure factor may also be determined.

Furthermore, light scattering is a very suitable technique to study aggregation processes, because the signal is very sensitive to the small amount of aggregates, even though their fraction is very low. In this study, we used DLS to observe the initial state of aggregation process in different condition of added salts and pH.

Below is a brief discussion on how to determine the various physical parameters from light scattering experiments. More information is to be found in textbooks (Brown 1996); (Berne and Pecora 1993).

#### Static light scattering

In a static light scattering the time – average intensity is measured. We define the relative scattered intensity,  $I_r$ , as the intensity measured  $I_{measured}$  after subtraction of the intensity scattered by the solvent,  $I_{sol}$ , divided by that of a reference  $I_{ref}$  (toluene) with a known Rayleigh ratio:

$$I_r = \frac{I_{measured} - I_{sol}}{I_{ref}} \quad 2.1$$

The relative intensity  $I_r$  is related directly to concentration fluctuations and given by the following relation:

$$I_r = KCRT \left( \frac{\partial \pi}{\partial c} \right)^{-1} S(q) \quad 2.2$$

with  $C$  the concentration of the particles,  $(\partial\pi/\partial C)^{-1}$  the osmotic compressibility,  $S(q)$  the structure factor of the particle and  $K$  an optical constant which is given by:

$$K = \frac{4\pi^2 n_s^2}{\lambda^4 N_a} \left( \frac{\partial n}{\partial C} \right)^2 \left( \frac{n_{tol}}{n_s} \right)^2 \frac{1}{R_{tol}} \quad 2.3$$

Here  $N_a$  is Avogadro's number,  $(\partial n/\partial C)$  is the refractive index increment,  $\lambda$  the wavelength of the incident light and  $R_{tol}$  is the Rayleigh constant of toluene at 20°C.  $n_{tol}$  and  $n_s$  are the refractive indices of toluene and the solvent, respectively.  $(n_{tol}/n_s)^2$  corrects for the difference in the scattering volume of the solution and the solvent. We have used  $(\partial n/\partial C)=0.189\text{mL/g}$  and  $R_{tol}=1.35\times 10^{-5}\text{cm}^{-1}$ .

At low concentrations, we can express the osmotic compressibility as follow:

$$\left( \frac{\partial\pi}{\partial c} \right)^{-1} = RT \frac{1}{M} (1 + 2A_2 MC + \dots) \quad 2.4$$

where  $M$  is the molar mass of the particle and  $A_2$  is the second virial coefficient. If there is no interaction between particles, i.e.  $A_2 = 0$ , then  $I_r$  is related to the weight average molar mass ( $M_w$ ) and the structure factor ( $S(q)$ ) of the solute:

$$I_r / KC = M_w S(q) \quad 2.5$$

$$M_w \text{ is given by: } M_w = \frac{\sum_i M_i C(M_i)}{\sum_i C(M_i)} \quad 2.6$$

The structure factor describes the dependence of the intensity on the scattering wave vector ( $q = \frac{4\pi n_s}{\lambda} \sin(\frac{\theta}{2})$ ), with  $\theta$  the angle of observation) and depends on the structure and the size of the solute. The z-average radius of gyration ( $R_{gz}$ ) can be determined from the initial  $q$ -dependence of  $S(q)$ :

$$S(q) = \left[ 1 + \frac{q^2 R_{gz}^2}{3} \right]^{-1} \quad qR_{gz} \leq 1 \quad 2.7$$

$R_{gz}$  is calculated by the equation:

$$R_{gz}^2(q) = \frac{\sum_i R_{gi}^2 M_i C(M_i)}{\sum_i M_i C(M_i)} \quad 2.8$$

## Dynamic Light Scattering

In DLS experiment, the time – averaged intensity autocorrelation function  $g_2(t)$  is measured ( $g_2(t)=\langle I(0).I(t)\rangle/\langle I\rangle^2$ ), which is related to the normalized electric field correlation function,  $g_1(t)$ , by the Siegert relation.  $g_1(t)$  was analysed in terms of a distribution of relaxation times:

$$g_1(t) = \int A(\log \tau) \exp(-t / \tau) d \log \tau \quad 2.9$$

In most cases the scattering intensity was dominated by that of the protein aggregates and  $g_1(t)$  could be analyzed in terms of a monomodal distribution of relaxation times and we used the so-called generalized exponential (GEX) distribution:  $A(\tau)=k.\tau^p \exp[-(\tau/\tau^*)^s]$ . The GEX distribution contains two parameters ( $p,s$ ) to describe the shape of a wide range of single peaked distributions such as the Schultz-Zimm and the Pearson distribution.  $\tau^*$  is the characteristic relaxation time and  $k$  is a normalisation constant. In some cases we could observe in addition a distinct contribution of the residual native proteins. In that case,  $g_1(t)$  was fitted to the sum of a GEX distribution to describe the aggregates and a log-normal distribution to describe the native proteins. For the latter the average relaxation time and the width of the distribution, but not the relative amplitude, were fixed at the values obtained on unheated solutions.

In dilute solutions the relaxation is caused by self diffusion of the particles and  $\tau$  is related to the diffusion coefficient ( $D$ ):  $\tau=(q^2.D)^{-1}$ . The hydrodynamic radius ( $R_h$ ) may be calculated using the Stokes-Einstein equation:

$$D = \frac{k.T}{6.\pi.\eta.R_h} \quad 2.10$$

with  $\eta$  the viscosity,  $k$  Boltzman's constant and  $T$  the absolute temperature. The z-average hydrodynamic radius ( $R_{hz}$ ) was calculated from the average diffusion coefficient and is

defined by the equation: 
$$R_{hz} = \frac{\sum_i \left(\frac{1}{R_{hi}}\right)^{-1} M_i C(M_i)}{\sum_i M_i C(M_i)} \quad 2.11$$

## Apparatus

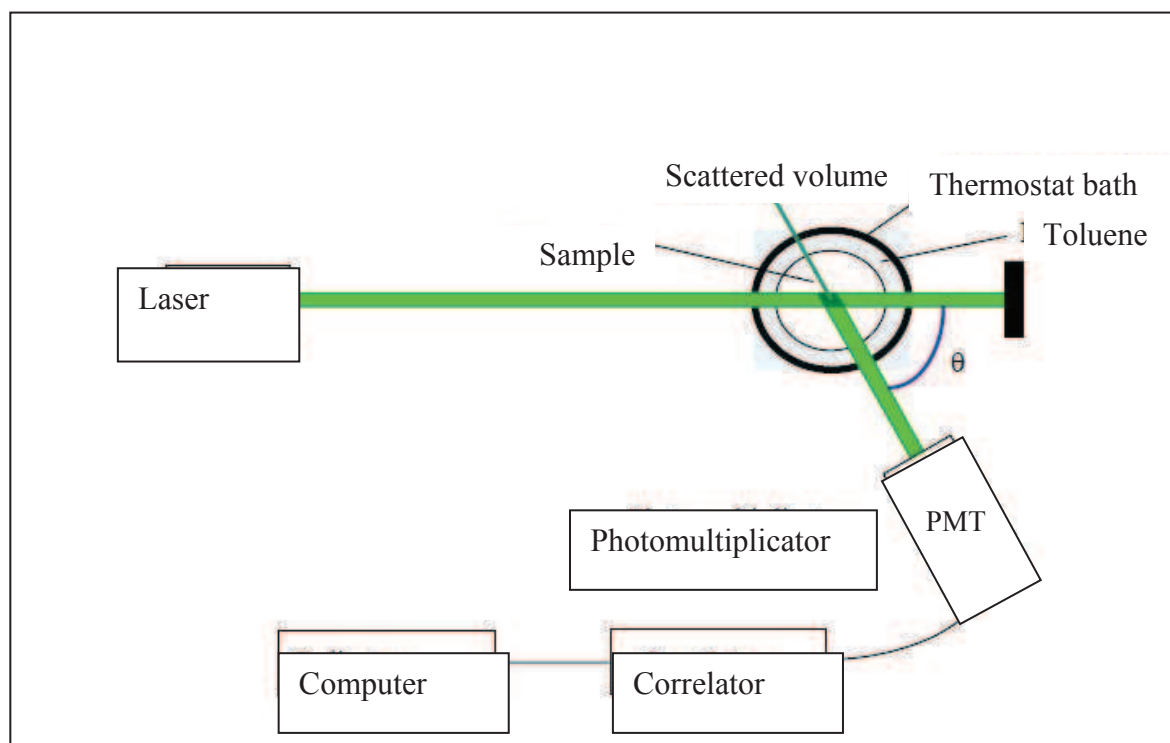


Figure 2.1: Light scattering apparatus

Figure 2.1 shows a schematic representation of the light scattering apparatus. In this work, dynamic and static light scattering measurements were done using a commercial apparatus (ALV-Langen). The light source was a He-Ne laser with wavelength  $\lambda=632\text{nm}$ . Measurements were made at angles of observation ( $\theta$ ) between 12 and 150 degrees, which corresponds to a spatial scale of ( $q^{-1}$ ) ranging from 30 à 365 nm. The temperature was controlled by a thermostat bath to within  $\pm 0.2$  °C.

The laser beam is focused at the center of the scattering cell by an optic system (pinhole + lens). The scattered light intensity is measured by a photomultiplier (PMT). The PMT amplifies the small single-photon signal; the incoming photon is converted into an electron, which is accelerated by an electric field onto a metal sheet. The PMT converts these electrons into an electric pulse of a proper amplitude and duration that can be used directly for the analysis. The photon correlation is made by a digital correlator (ALV-5000/E). We obtain a normalized time – average intensity autocorrelation function  $g_2(t)$  and deduce the normalized electric field autocorrelation function  $g_1(t)$  by using the Siegert relation (Berne and Percora, 1996):

$$g_2(t) = 1 + a \cdot [g_1(t)]^2 \quad 2.12$$

where  $a$  is a constant and depends on characteristic of the instrument.

## II.2.2. Turbidity measurements

This technique is very similar to those that we used in light scattering because it is based on the measurement of non transmitted photons following a scattering or absorption phenomenon in contact with particles.

In our case, the turbidity was determined in a range of wave lengths far from the absorption zone. Thus only scattering of incident photons causes the turbidity of the solution. The value of the turbidity,  $\tau$ , of the solution corresponds to the quantity of loss photons per unit of path length of an incident beam through the solution, L. For an isotropic system, the turbidity is directly given by:

$$\tau = \ln\left(\frac{I_0}{I_{tr}}\right) \frac{1}{L} \quad 2.13$$

with  $I_0$  the intensity of the incident light and  $I_{tr}$  the intensity of the transmitted light

Experimentally, the turbidity is deduced from the value absorbance (A) given by the spectrophotometer as  $\tau = A \cdot \ln(10) / d$  where d is path length or the transmittance ( $\%T = 10^{2-A}$ ).

Turbidity measurements were done as a function of the wavelength in rectangular air tight cells using a UV-Visible spectrometer Varian Cary-50 Bio (Les Ulis, France). Different pathlengths (1 or 10mm) were used depending on the turbidity of the samples in order to avoid saturation. Measurements were done at different temperatures that were controlled within 0.2°C using a thermostat bath.

## II.2.3. Centrifugation

With the light scattering technique, we measure the average value of protein aggregate size and mass. In order to determine size distributions of aggregates and to be able to calculate accurately their mass, size and density, we have used sedimentation by centrifugation at different speeds and analyzed the supernatant. Some basic concepts of sedimentation by centrifugation will be described below.

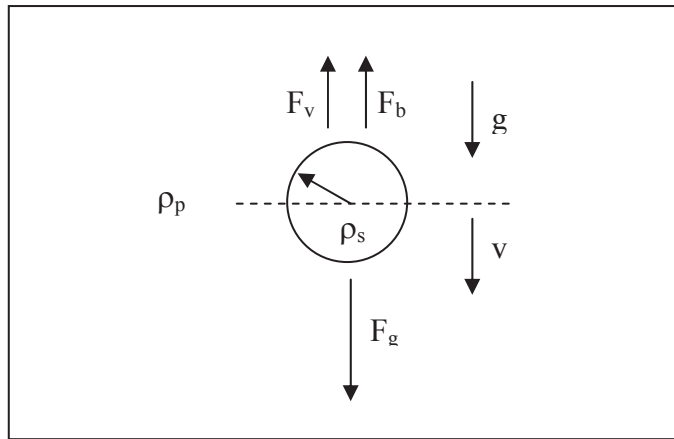


Figure 2.2: Force acting on a spherical particle due to gravity and viscosity of the medium.

A particle in a centrifugal field will experience 3 major forces:

- Centrifugal force ( $F_c$ ) =  $m g = m \omega r$
- Buoyant force ( $F_b$ ) =  $-m_0 g = -m_0 \omega r$
- Frictional force ( $F_f$ ) =  $-fv$

where

$m$  = mass of the particle,

$g$  = the ratio of the centrifugal force to the gravitational force,

$\omega$  = angular velocity,

$r$  = distance from the axis,

$m_0$  = the mass of the displaced solution,

$f$  = frictional coefficient =  $6\pi\eta R_h$ , with  $\eta$  the viscosity of the solvent and  $R_h$  the hydrodynamic radius of the particle

$v$  = velocity of the particle.

The particle will move at a velocity such that the total force equals 0, therefore:

$$m\omega^2 r - m_0\omega^2 r - fv = 0$$

Substituting  $m\nu\rho_s = m_0$ , where  $\nu$  is the partial specific volume of the particle (i.e., the reciprocal of the density of the particle or  $\rho_p$ ) and  $\rho_s$  is the density of the solvent, and solving for  $v$  results in:

$$v = \omega^2 r m (1 - \nu\rho_s) / f = \omega^2 r m \nu (\rho_p - \rho_s) / f = g V \Delta\rho / f \quad 2.14$$

where  $V$  is the volume of the solution and  $\Delta\rho$  is the density difference between particle and solvent.

Equation 2.14 tells us several things about sedimentation:

- Increase of the centrifugal force ( $\omega^2 r$ ) results in a faster sedimentation of the particle.
- Increase of the particle mass ( $m$ ) and density ( $\rho_p$ ), it moves faster.
- Increase of the solution density ( $\rho_s$ ), the particle will move slower.
- Increase of the frictional coefficient (which related to viscosity, particle shape, etc...), the particle will move slower.
- When the solution density is greater than the particle density, the particle velocity is negative (creaming).

Example of the relation between  $R_h$  and g factor:

The velocity of the particle can be written in the form below:

$$R_h g \Delta \rho 2 R_h^2 / (9 \eta) = v \quad 2.15$$

In water, the viscosity  $\eta = 0.001$  Pa.s, so that

$$v = 2178. N_g \cdot \Delta \rho \cdot R_h^2 \text{ (m/s)} \quad 2.16$$

For proteins,  $\Delta \rho = 0.35 * \rho_p$  ( $\text{Kg/m}^3$ ) when  $\rho_p$  is the density of protein particle and expressed in g/l.

If  $R_h$  is in nm and  $\rho_p$  in g/ml, eq. 2.12 becomes:

$$v = 2.7 * 10^5 \cdot N_g \cdot \rho_p \cdot R_h^2 \quad 2.17$$

The sedimentation trajectory of a particle is  $t * v$  where  $t$  is the sedimentation time.

If we choose for the trajectory 1 cm in 1h, we have the following relation between  $R_h$ ,  $\rho_p$  and g:

$$R_h^2 = 3.6 * 10^6 / (N_g \cdot \rho_p) \text{ (nm}^2\text{)} \quad 2.18$$

Centrifugations were carried out at room temperature with an Allegra 64R centrifuge (Beckman Coulter, USA) at different rotor speeds (50-50 000 g) during 1 h. The heated  $\beta$ -lg solutions were diluted before centrifugation to  $10 \text{ gL}^{-1}$ . After each centrifugation, the supernatant was taken 1.5 cm from the top of the solution and analyzed.

## II.2.4. Determination of the protein concentration in the supernatant

The protein concentration of the supernatant was determined by measuring the optical absorbance (OA) of the solutions. After heating the solutions were turbid which contributed to the measured OA. The turbidity decreased with increasing wavelength following a power law, see fig. 2.3 and was subtracted from the data. The OA of the heated samples at pH 5.8 was larger than that of the native proteins and had a different wavelength dependence, see figure 2.4. Such a difference was not observed for samples heated at pH>6.0.

Figure 2.5 shows results for supernatants obtained at different rotor speeds after dilution by the same factor. As expected the OA decreased with increasing rotor speed, but also the wavelength dependence changed. This is better seen if the data are normalized by the peak value at  $\lambda=280\text{nm}$ , see fig. 2.6. Comparison with native proteins shows that for centrifugal forces larger than about 4000g, the absorption spectrum is the same as that of native proteins. Notice that at these rotor speeds the supernatant contains mainly small aggregates.

In order to derive the protein concentration at larger rotor speeds we have assumed that the supernatant consists of two populations of proteins with fractions  $F_1$  and  $F_2$ , respectively. Smaller aggregates that absorb like native proteins ( $OA_1$ ) and larger aggregates that absorb more strongly ( $OA_2$ ):  $OA=F_1.OA_1+F_2.OA_2$ .  $F_2$  was assumed to be negligible at 4000g and  $F_1$  was calculated using the extinction coefficient of native proteins.  $F_1$  is constant up to about 4000g and decreases weakly at higher rotor speeds. For lower rotor speeds the contribution of the larger aggregates was calculated as  $F_2.OA_2=OA-F_1.OA_1$ . The wavelength dependence of  $OA_2$  was found to be almost the same for all supernatants, which justifies our assumption of two distinct populations. Before centrifugation  $F_2 = (1-F_1)$ , which enabled us to deduce  $OA_2$ . The values of  $F_2$  at higher rotor speeds were obtained by fitting OA to  $F_1.OA_1+F_2.OA_2$ , see solid lines in fig. 2.5.

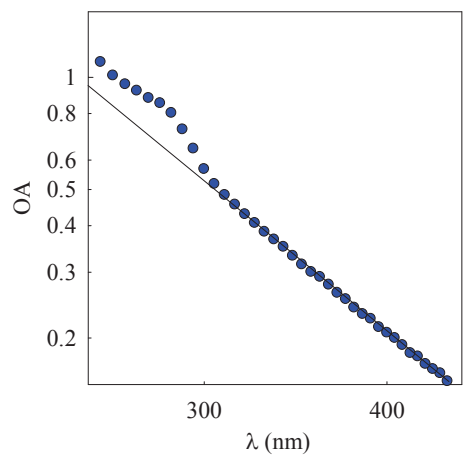


Figure 2.3: Double logarithmic representation of the optical absorption before correction for the turbidity. The solid line represents the power law dependence of the turbidity.

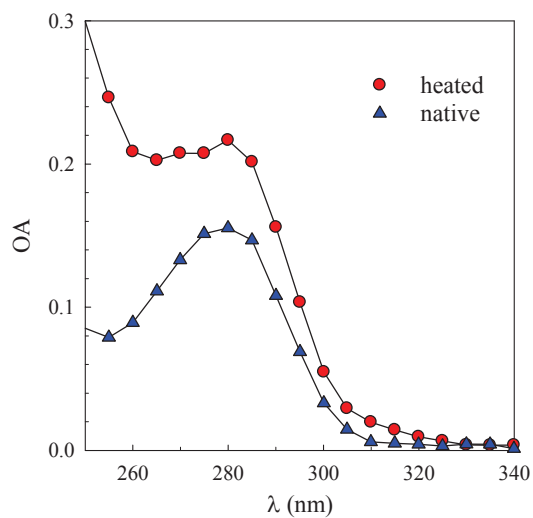


Figure 2.4: Optical absorption after correction for the turbidity before and after heating.

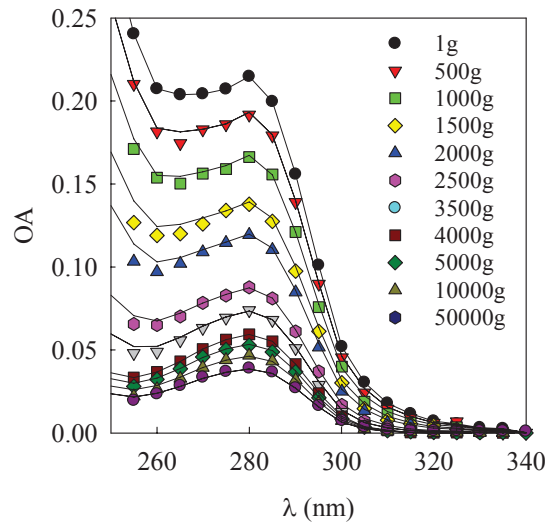


Figure 2.5: Optical absorption after correction for the turbidity of the supernatants of heated samples after centrifugation at different rotor speeds. The solid lines represent  $F_1.OA_1+F_2.OA_2$ , see text.

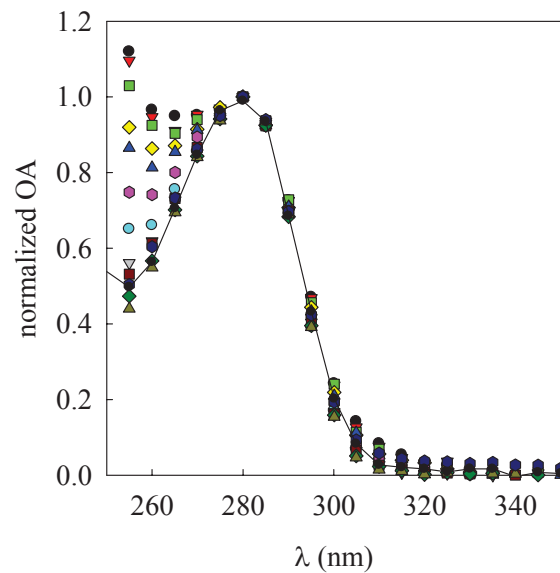


Figure 2.6: Normalized optical absorption after correction for the turbidity of the supernatants of heated samples after centrifugation at different rotor speeds. The filled symbols represent the results for native proteins. The open symbols are as in figure 2.5

## II.2.5. Size exclusion chromatography (SEC)

This technique is a good complement together with sedimentation technique for separating different protein populations when they cannot sediment by centrifugation. However, SEC cannot be applied to large aggregates ( $R_h > 50\text{nm}$ ), because these are all

fully excluded by the columns and thus not separated. SEC experiments were carried out at room temperature with a TSK PW 5000 + PW 6000 column set (30 cm + 60 cm) in series in addition to a Zorbax GF-450 pre-column (25 cm). The refractive index was measured at the exit of the columns using a differential refractive index detector (SHODEX RI 71). 300  $\mu$ l of the protein solution was injected using an automatic injection system (Autoinjector 234, Gilson) at a concentration of approximately 1 g.L<sup>-1</sup>. The system was eluted at 20°C with 0.1 M NaNO<sub>3</sub> at pH 7 with a flow rate of 1 ml.min<sup>-1</sup>.

## **II.2.6. Confocal laser scanning microscopy (CLSM)**

The conventional microscopy is a common technique to study the colloidal suspension (Elliot, Haddon et al. 2001). However, it suffers from low contrast and multiple scattering problems from objects that are out of focus within the illuminated region. Confocal microscopy may solve these problems. Figure 2.7 shows the working principle of a confocal laser scanning microscopy. In this method, the light from the laser source passes through a pinhole aperture that is situated in a conjugate plane (confocal) with a scanning point on the specimen. For scanning, the microscope uses a dichromatic mirror that reflects light shorter than a certain wavelength but transmits light of longer wavelength. Thus the light from the laser source is reflected and scanned across the specimen in a defined focal plane, by the dichromatic mirrors. The fluoresced (higher wave length) light from the sample passes back through the objective and is descanned by the same mirrors used to scan the sample. Before it reaches the detector, the fluoresced light passes through the pinhole which is placed in the conjugate focal (hence the term confocal) plane of the sample. The significant amount of fluorescence emission that occurs at points above and below the objective focal plane is not confocal with the pinhole and hence most of this out of focus light is not detected by the photomultiplier tube and does not contribute to the resulting image. In confocal microscopy, there is never a complete image of the specimen because at any instant only one point is observed. Thus, for visualization, the detector is attached to a computer, which builds up the image, one pixel at a time. The speed of most confocal microscopes is limited by the rate at which the mirrors can scan the entire sample plane. This particular type of fluorescence microscopy, in which the objective used by the illuminating light is also used by the fluorescence light in conjunction with a dichroic mirror, is called epifluorescence ((Prasad, Semwogerere et al. 2007)).

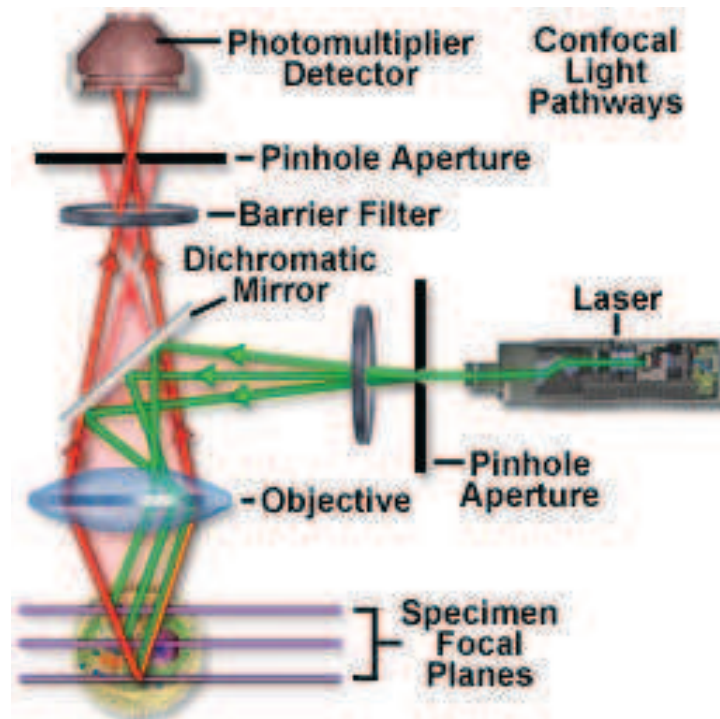


*Figure 2.7: Illustrating the basic configuration of a modern confocal laser scanning microscope*

In this study, confocal Laser Scanning Microscopy (CLSM) was used in the fluorescence mode. Observations were made with a Leica TCS-SP2 (Leica Microsystems Heidelberg, Germany). A water immersion objective lens was used HCxPL APO 63x NA=1.2 with theoretical resolution of  $0.3\mu\text{m}$  in the x-y plane. A small fraction of  $\beta\text{-Ig}$  was labelled with the fluorochrome rhodamine B isothiocyanate, by adding a small amount of a concentrated rhodamine solution (5ppm) to the  $\beta\text{-Ig}$  solutions before heat treatment. No effect of labelling on the aggregation process was observed.

### **II.2.7. Pair correlation function of CLSM images**

The images were analysed by calculating the pair correlation function ( $g(r)$ ) of the intensity fluctuations as a function of the distance ( $r$ ) between the pixels. We make sure that the intensity is proportional to the concentration of the fluorophores (and thus the proteins) in the system so that  $g(r)$  also represents the pair correlation function of the concentration fluctuations. The intensity  $A_i$  of a random pixel  $i$  of the image is chosen and is correlated with the intensity  $A_j$  of pixel  $j$ . The pair correlation function is defined as:

$$g(r) = \frac{\sum_{i=1}^n \sum_{j=1}^m A_i A_j}{\sum_{i=1}^n A_i \sum_{j=1}^m A_j} \text{ with } r = |i - j| \quad 2.19$$

for large  $r$  values  $A_i$  and  $A_j$  are no longer correlated and hence  $g(r)$  becomes unity. In order to avoid finite size effects, the pixel  $i$  is chosen in such a way that the distance from the edge to the  $i^{\text{th}}$  pixel is larger than the maximum value of  $r$  ( $r_{\text{max}}$ ).

$g(r) - 1 = \sigma^2$  for  $r$  smaller than the resolution of the microscope.  $\sigma$  characterizes the amplitude of the intensity fluctuations and is defined as:

$$\sigma = \langle A \rangle^{-1} \sqrt{n^{-1} \sum_{i=1}^n (A_i - \langle A \rangle)^2} \quad 2.20$$

where  $\langle A \rangle$  is the spatially averaged intensity. Random fluctuations of the fluorescence intensity of the marker in time do not have any influence on  $g(r)$ , but it does influence the value of  $\sigma$ . The effect of fluctuations of the fluorescence can be reduced by increasing the marker concentration or averaging over several images.

In practice the minimum useful value of  $r$  corresponds to the resolution of the microscope. It was found that the best resolution was obtained with a HCx PL APO 63x water immersion objective and is theoretically  $0.3 \mu\text{m}$  in the x-y plane, but in the z-direction (perpendicular to the objective) it is  $0.6 \mu\text{m}$ . Fortunately, for isotropic systems like protein gels it is sufficient to correlate the pixel intensities as a function of  $r$  in the x-y plane.

Figure 2.8 shows an example of  $g(r)$  for different zooms and objectives before (a) and after superposition (b). By analyzing images of the same system with different zooms and with two different lenses a broad range of  $r$  could be covered. For the protein gels studied here, the decay  $g(r)$  could be described by a stretched exponential:

$$g(r) - 1 = B_1 \exp \left[ \left( -\frac{r}{\xi} \right)^\beta \right] \quad 2.21$$

where  $B_1$  is the contrast,  $\xi$  is the correlation length and  $\beta$  is the stretching exponent. However, this function failed to describe the weak minimum of  $g(r)$  observed at larger  $r$  values.

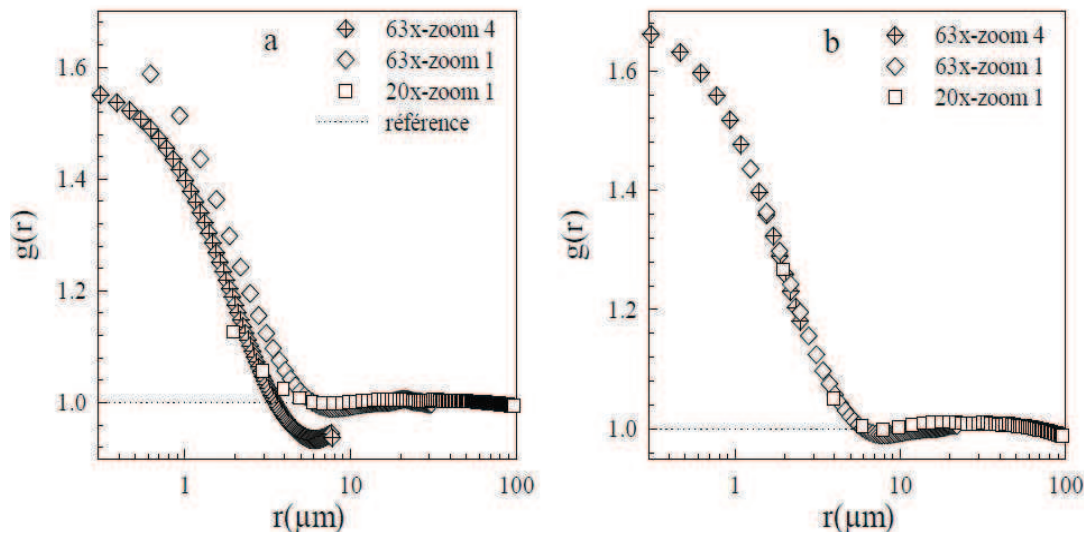


Figure 2.8:  $g(r)$  as a function of  $r$  for different zooms and objectives before (a) and after superposition (b).

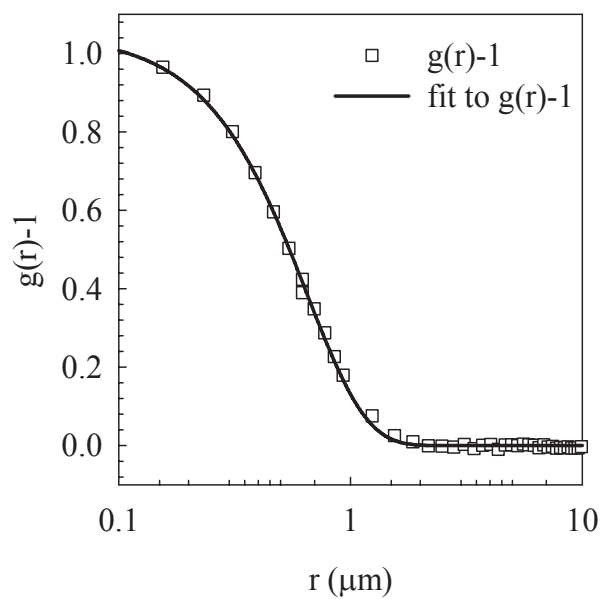


Figure 2.9:  $g(r)-1$  for a  $\beta$ -lg gel formed at  $C=20$  g/l,  $C_s=0.15$  M and at pH 7. The solid line represents a fit to Eq. 2.21

### **II.2.8. Transmission electron microscopy**

The microstructure of heated protein dispersions was investigated by transmission electron microscopy (TEM) using the negative staining method. A drop of the protein dispersion diluted to 0.1wt% in Millipore water was deposited onto a formvare-carbon coated copper grid. The excess product was removed after 30 s using a filter paper. A droplet of 1% phosphotungstic acid at pH7.0 was added for 15 s, removing any excess. After drying the grid at room temperature for 5 min, observations were made with a FEI Tecnai G2 Spirit Biotwin transmission electron microscope operating at 120 kV (FEI company, The Netherlands). Images were recorded using a Quemesa camera (Olympus soft imaging solutions, Germany).

### **II.2.9. Gel point determination**

The critical concentration of gelation ( $C_g$ ) was defined here as the lowest concentration where the system was visually homogeneous and did not flow when the vial was tilted after heating at 85°C for 15 hours. This definition led for the systems studied here to values that are close to those determined in other ways such as divergence of  $M_w$  or insolubility after dilution, except for pH<5.75 where we observed precipitation even at low concentrations. There is necessarily some ambiguity in the value of  $C_g$ , because close to the critical concentration the gels are very fragile and they easily break when tilted. In addition, it was found that close to but below  $C_g$  the solutions gel when kept in the refrigerator for a day or more. This, in addition to the sensitivity to the mineral content, may explain the slightly different values of  $C_g$  reported in the literature for  $\beta$ -lg at the same conditions.

### **II.2.10. Calcium binding measurements.**

The calcium ion activity in solution was determined using a calcium-specific electrode (Fisher Scientific, USA). A calibration curve was obtained by measuring  $\text{CaCl}_2$  solutions in water at concentrations ranging from 0 to 25 mM. We have calculated the concentration of free calcium ions by assuming that the activity of bound  $\text{Ca}^{2+}$  was zero and the activity of free  $\text{Ca}^{2+}$  was the same as in pure water.

## Chapter III. Results and discussion

This chapter is an overview of the most important findings presented in papers I-III. Not being restricted by the format of scientific articles, it is organized with a more systematic approach that shows better similarity of the mechanism of  $\beta$ -lg microgel formation by reducing the pH or by adding  $\text{CaCl}_2$  and the elucidation of which was the main objective of the thesis. The chapter consists of 5 sections.

The first section shows the conditions where microgels are formed in  $\beta$ -lg solutions that are heated until steady state is reached. We discuss the effect of lowering the pH to close to pI in pure water and adding  $\text{CaCl}_2$  at neutral pH. In the second section, we discuss the evolution of the system during heating. In the third section we propose a mechanism for the formation of stable microgel suspensions. The fourth section deals with secondary aggregation and gelation of the microgels. Finally, in the fifth section we compare aggregation and gelation in the presence of  $\text{NaCl}$  and  $\text{CaCl}_2$ .

### *III.1. Structure of heat-induced $\beta$ -lg aggregates at steady state*

In this section, conditions for the formation of different aggregated structures by heating  $\beta$ -lg solution (microgels and strands) will be presented. We show first how the protein concentration and pH influence the formation of different aggregates in pure water. In this study we focused on the influence of the pH above the isoelectric point. We will show that microgels are not formed for  $\text{pH} > 6.2$ . It was already shown in the literature that stable microgel suspensions at higher pH cannot be produced by adding  $\text{NaCl}$ , see chapter I. Therefore we tried successfully to add calcium ions in order to induce the formation of microgels at higher pH.  $\beta$ -lg solutions were heated at different temperatures until steady state was reached, i.e. the system stopped evolving. Various experimental techniques for determining aggregate size, mass, fraction and morphology were used (DLS, SLS, SEC, TEM, differential centrifugation), see chapter II.

#### **III.1.1. Aggregation in pure water**

At neutral pH,  $\beta$ -lg solutions in pure water remained transparent upon heating, but they became more turbid with decreasing pH below about 6.2. Close to the pI ( $< 5.75$ ), proteins precipitated in the form of large flocs. If the protein concentration was higher than

a critical gelation concentration ( $C_g$ ), the system gelled by the formation of a percolating network.

### ***Influence of the protein concentration at pH 5.8***

When  $\beta$ -lg solutions at pH 5.8 were heated at 85°C, aggregates were formed with the same size and independent of the protein concentration (C) up to 50 g/L, see figure 3.1. At higher concentrations, these primary aggregates stuck together to form bigger aggregates and finally a gel at  $C > C_g$ .

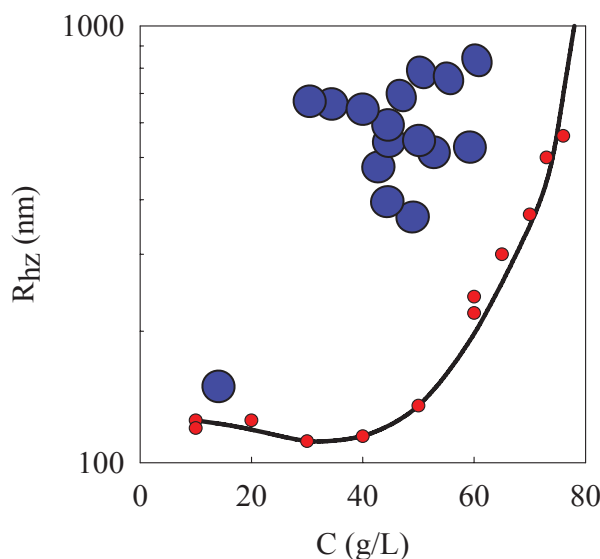


*Figure 3.1: Concentration dependence of the z-averaged hydrodynamic radius of aggregates formed by heating at 85°C  $\beta$ -lg solutions at pH 5.8 until steady state was reached.*

### ***Effect of the pH***

We have investigated systematically the concentration dependence of the aggregate size for different pH between 5.75 and 7.0. A similar behavior as at pH 5.8 was observed: formation of primary aggregates below 50 g/L and secondary aggregation at higher protein concentrations. The size of the primary aggregates was independent of the concentration except at intermediate pH (6.1 to 6.3) where we found an increase of  $R_{hz}$  with decreasing C below 30 g/L, see paper I. In the intermediate concentration range (30-50 g/L),  $R_{hz}$  was almost independent of the concentration in the whole pH range.

The dependence of  $R_{hz}$  as a function of pH is shown in figure 3.2. It decreases from around 200nm at pH 5.75 to 20nm at pH 6.3 and remains the same at higher pH. At low pH where the aggregates are big, TEM images showed that they are spherical. We call these primary aggregates microgels. At  $pH > 6.3$ , the aggregates have the form of small curved strands. Interestingly, at intermediate pH, both microgels and strands were present in the same sample.

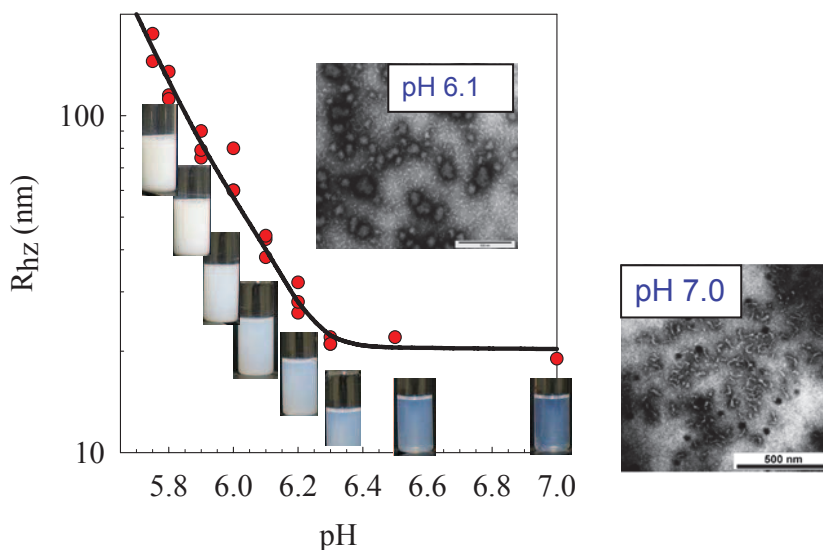


Figure 3.2: pH dependence of the z-averaged hydrodynamic radius of primary aggregates formed by heating  $\beta$ -Ig solutions in the concentration range between 30 – 50 g/L at 85°C until steady state was reached. Inserted pictures are TEM micrographs of aggregates obtained at different pH indicated in the figure.

### ***Fraction, molar mass and size of the microgels as a function of the pH***

By centrifugation, we can separate the microgels and the strands (see chapter II). The fraction of microgels is plotted as a function of the pH in figure 3.3. It drops strongly with increasing pH at a critical value that shifts to slightly higher values when the concentration is decreased. The weak concentration dependence of the critical pH explains the increase of  $R_{hz}$  with increasing protein concentration at intermediate pH mentioned above.

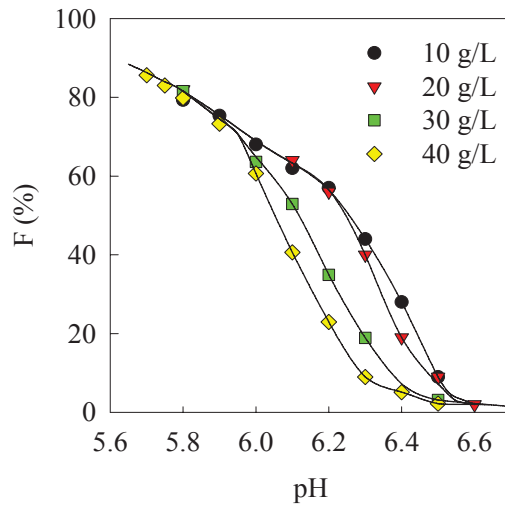


Figure 3.3: pH dependence of the fraction of proteins that sedimented in the form of microgels after centrifugation at 50.000 g during 1h for different protein solutions indicated in the figure. The protein solutions were heated at 85°C until steady state was reached.

The molar mass and size distributions of the microgels were determined using a differential centrifugation (paper I). Figure 3.4 shows the results at pH 5.8. The microgels are rather monodisperse with a molar mass of about  $2.10^9$  g/mol and a radius of about 110 nm. With increasing pH, we observed that the mass and size distributions of the microgels shifted to smaller values but the density of the microgels remained approximately constant at 0.15 g/ml.

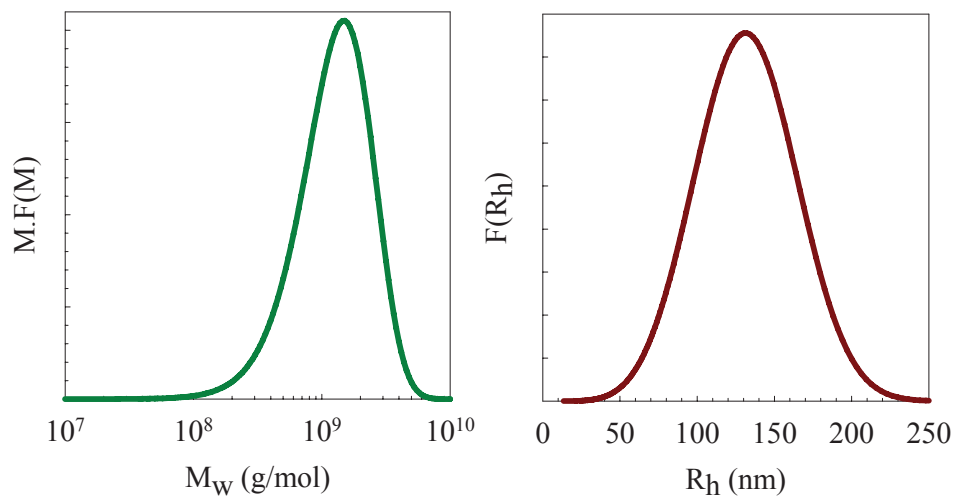


Figure 3.4: Distribution of the molar mass and the hydrodynamic radius of microgels formed by heating  $\beta$ -lg solutions at  $C=40$ g/L and pH 5.8 at 85°C until steady state was reached.

Aggregates in the supernatant were analyzed by Size Exclusion Chromatography (SEC), which showed that the supernatant contained mainly strands, but also a small fraction (5%) of denatured monomers, dimers and oligomers. Figure 3.5 shows an example of the composition of a  $\beta$ -lg solution at pH 5.8 after extensive heat treatment at 85°C. The size and the fraction of strands and microgels depend strongly on the pH and somewhat on the protein concentration, see paper I.

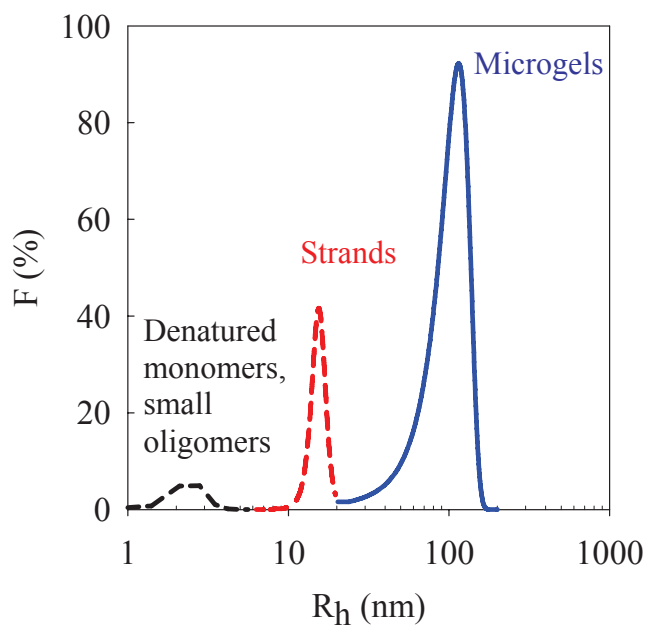


Figure 3.5: Size distribution of aggregates formed after extensive heat treatment at 85°C of a  $\beta$ -lg solution at pH 5.8 and  $C=40$  g/L.

### ***Effect of the heating temperature***

The heating temperature (T) has a strong effect on the aggregation kinetics, see paper I, but we found no effect of the heating temperature on the size and structure of microgels between 75°C to 85°C (see figure F1 of paper I). However, at 70°C where the aggregation became slow, larger microgels were formed. (Bromley, Krebs et al. 2006) reported that the spherical particles that constituted gels formed in pure water at pH 5.3 were also larger if the heating rate was slow. They suggested that larger particles were formed because the nucleation rate was slower compared to the growth rate at lower temperatures.

### III.1.2. Aggregation in the presence of calcium ions

#### *Effect of heating at 85°C at steady state*

Stable suspension of microgels can also be formed at neutral pH by adding calcium ions. For example, figure 6 shows the fraction of microgels after heating at 85°C a  $\beta$ -lg solution at pH 7.0 as a function of the molar ratio of calcium to protein (R). At low R (<1), aggregates have the form of small curved strands, while at high R microgels are formed. At intermediate values both strands and microgels were observed in the same sample. The transition between strands and microgels (placed at 50% of microgels) was rather narrow in between R = 1 – 2.

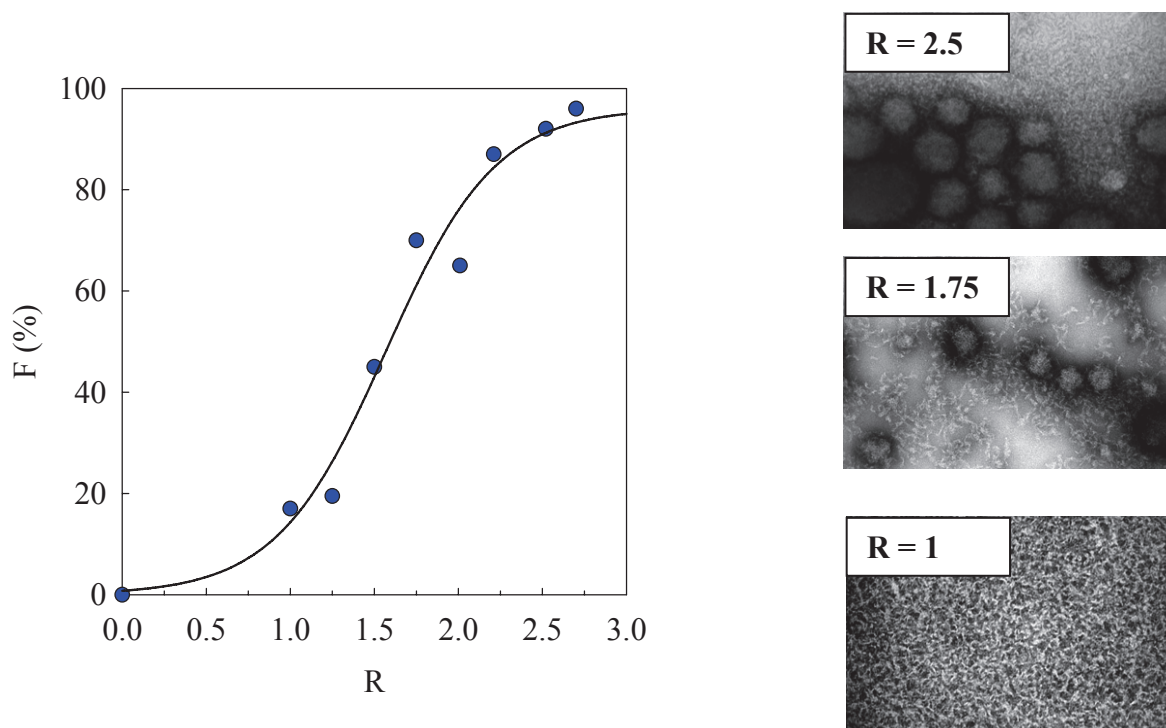


Figure 3.6: Fraction of proteins that form microgels at pH 7.0 as a function of the molar ratio of  $\text{CaCl}_2$  to  $\beta$ -lg in  $\beta$ -lg solutions at  $C=40$  g/L after heating at 85°C until steady state.

#### *Effect of the pH*

The transition between the formation of strands and microgels is shown in figure 3.7 as a function of the protein concentration at different pH. At high pH (6.9-7.5), the transition is almost independent of the protein concentrations. At lower pH, the critical value of R increases with increasing protein concentration. As was discussed above, at low protein concentrations, a significant amount of microgels can be formed without adding calcium ions for  $\text{pH}<6.4$ .

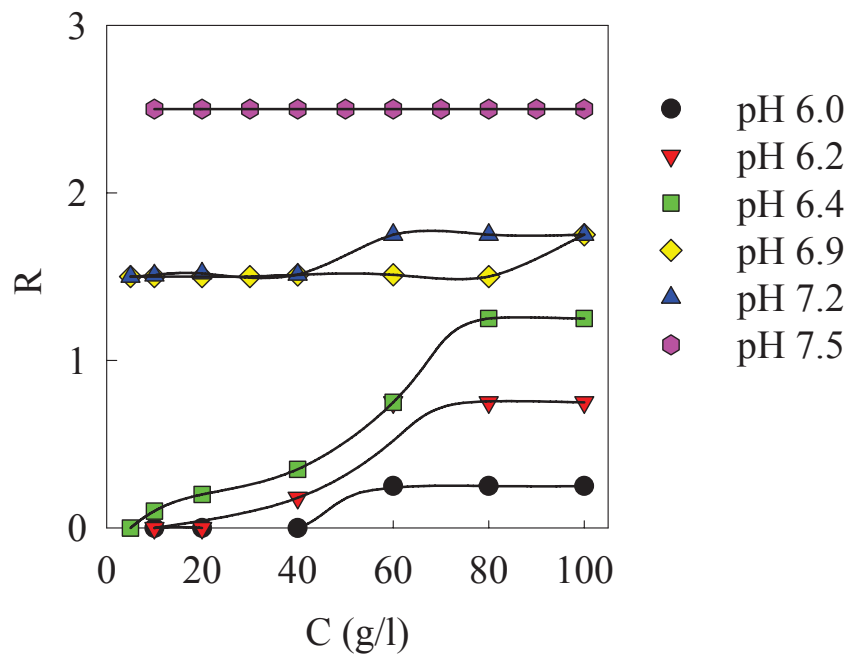


Figure 3.7: Transition between the formation of strands (small  $R$ ) and microgels (large  $R$ ) as a function of the protein concentrations at different pH after heating at  $85^{\circ}\text{C}$ .

The size and the density ( $\rho$ ) of the microgels were found to increase with increasing  $\text{CaCl}_2$  concentration, ranging from  $R_h=100$  to  $300$  nm and  $\rho=0.2$  to  $0.45$  g/mL. They can be larger and denser than the microgels formed in the absence of Ca. The addition of calcium ions is an easy way to modulate the size and structure of the microgels.

### ***Dependence on the temperature***

The influence of the heating temperature on the size and the structure of the aggregates at steady state is shown here for the  $\beta$ -lg solutions at  $C=40\text{g/L}$  and  $\text{pH } 7.0$ . The evolution of  $R_{hz}$  as a function of  $R$  is shown in figure 3.8 for different  $T$ . Notice that  $R_{hz}$  is the z-average of the total aggregate population that can contain both microgels and strands. However since this average gives a high weight to larger particles, the contribution of the microgels dominates even if its weight fraction is small.

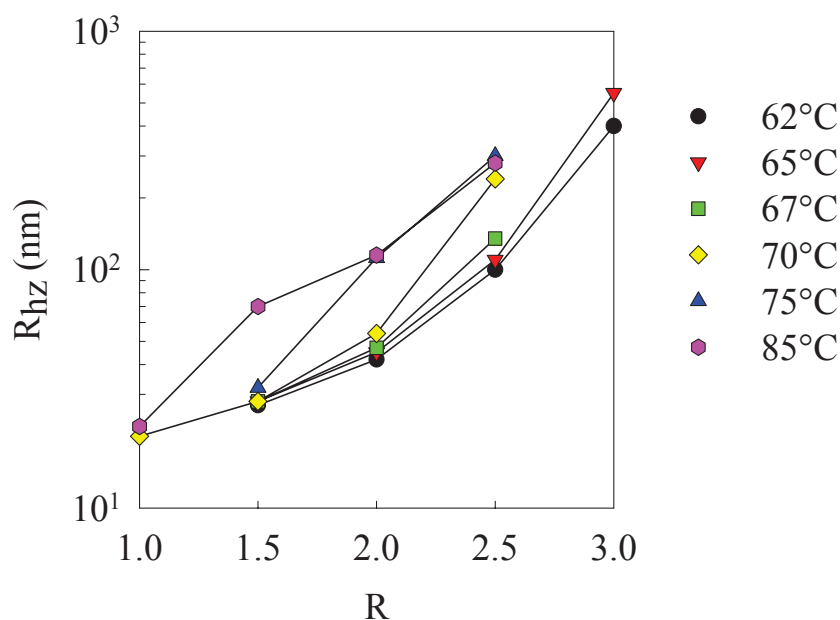


Figure 3.8: Evolution of  $R_{hz}$  as a function of  $R$  for  $\beta$ -lg aggregates formed by heating at different temperatures solutions at  $C=40$  g/L and at pH 7.0.

We observed a sharp increase of  $R_{hz}$  with increasing  $R$  between  $R = 1 - 1.5$  at  $85^\circ\text{C}$ , which corresponded to the transition between the formation of strands and microgels. Probably the sharp increase at  $75^\circ\text{C}$  and  $70^\circ\text{C}$  also caused by this transition. The values of  $R$  where this transition occurred increased with decreasing  $T$  ( $R = 1.5 - 2$  at  $75^\circ\text{C}$  and  $R = 2 - 2.5$  at  $70^\circ\text{C}$ ). The size of the microgels increased with increasing  $R$ , but appeared to be independent of the heating temperature (Figure 3.8). For  $T < 70^\circ\text{C}$ , the increase of  $R_{hz}$  was more gradual and microgels were not yet formed at  $R=2$ . Solutions heated at  $T \geq 70^\circ\text{C}$ , gelled at  $R \geq 3$ , but at lower heating temperatures, stable suspensions were still formed at  $R = 3$  and only at  $R = 4$  the system gelled. Possibly, the affinity between  $\text{Ca}^{2+}$  and proteins denatured at lower temperatures is less so that more  $\text{Ca}^{2+}$  per protein is needed to drive the formation of microgels.

TEM images of aggregates formed after heating at  $62^\circ\text{C}$  at different  $R$  are shown in figure 3.9. Up to  $R=2$  more or less strand-like aggregates were formed with a size that increased with increasing  $R$ . At  $R = 2.5$  and  $R = 3$ , the aggregates have a more spherical form with a radius of about 50 nm and may perhaps be considered as small microgels. Clearly, the transition between the formation of strands and microgels is much more gradual at  $T=62^\circ\text{C}$  than at  $T>70^\circ\text{C}$ . In addition, we did not observed two distinct populations at  $T=62^\circ\text{C}$ .

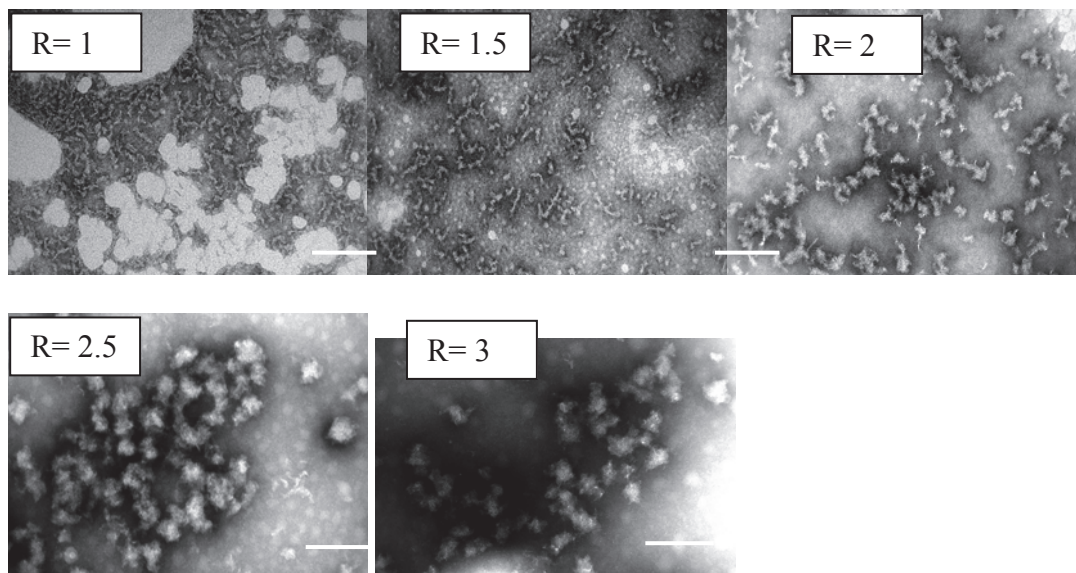


Figure 3.9: TEM images of stable microgel suspensions formed at different  $R$  after heating of  $\beta$ -lg solutions at  $62^{\circ}\text{C}$  until steady was reached ( $C=40\text{g/L}$ ,  $\text{pH}7.0$ ). The bars represent  $200\text{ nm}$ .

It appears that the microgels formed at  $T=62^{\circ}\text{C}$  are not stable in solution, because with DLS we found larger radii:  $R_{\text{hz}} \approx 100\text{nm}$  for  $R=2.5$  and  $R_{\text{hz}} \approx 400\text{nm}$  for  $R = 3.0$ . This means that at these conditions secondary aggregation of the microgels occurred. The size of the aggregates formed at  $R = 2.5$ ,  $62^{\circ}\text{C}$  and  $R = 2$ ,  $75^{\circ}\text{C}$  was found to be almost the same ( $R_{\text{h}} \approx 100\text{nm}$ ). However their form as seen in the TEM images was different. Large spherical microgels were formed at  $75^{\circ}\text{C}$  with a radius compatible with  $R_{\text{hz}}$  from DLS, whereas at  $62^{\circ}\text{C}$ , oligomers of smaller microgels were formed (Figure 3.10).

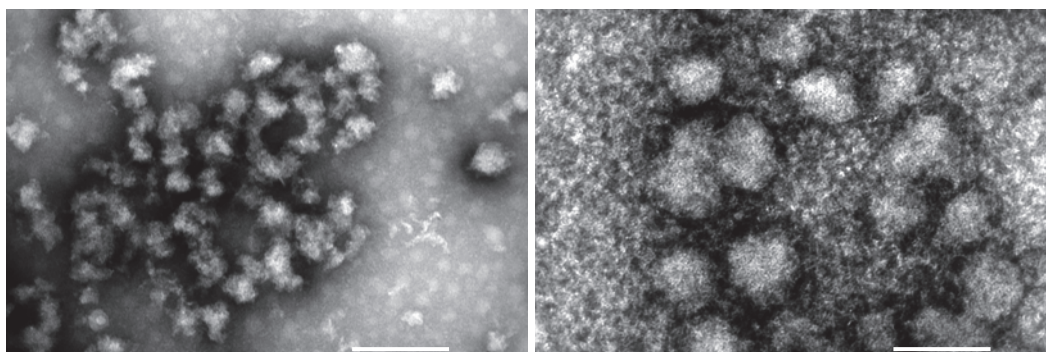


Figure 3.10: TEM images of stable suspensions of aggregates formed in  $\beta$ -lg solutions ( $C=40\text{g/L}$ ,  $\text{pH}7.0$ ) at  $R = 2.5$  heated at  $62^{\circ}\text{C}$  (left) and at  $R = 2$  heated at  $75^{\circ}\text{C}$  (right). The bars represent  $200\text{ nm}$ .

### III.2. Evolution of the system during heating

The system can be quenched at different stages of the aggregation process by rapid cooling to room temperature. In this way, the formation and growth of aggregates can be characterized as a function of heating time. In this section, we first discuss the aggregation kinetics and then the evolution of the aggregate size during heating.

#### III.2.1. Aggregation kinetics

##### *At low pH in pure water*

In order to determine the effect of the pH on the rate of microgel formation, we measured the turbidity ( $\tau$ ) of protein solutions during heating at different pH in the range where stable microgel suspensions were formed. The results obtained at  $T=77.5^\circ\text{C}$  are shown in figure 3.11.  $\tau$  increased until it reached a plateau after about 50 min. The time necessary to reach the plateau ( $t_p$ ) was the same at different pH, but the value of the turbidity at the plateau increased with decreasing pH, because larger microgels are formed at lower pH.

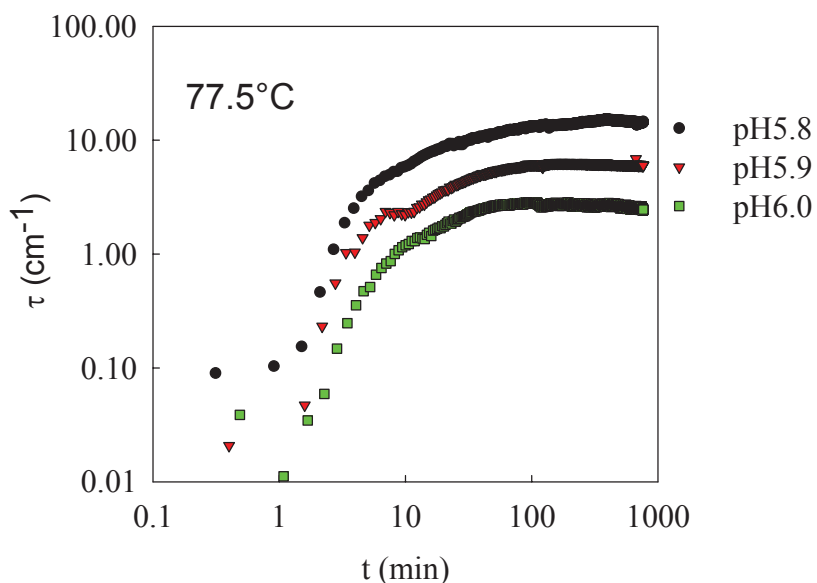


Figure 3.11: Time dependence of the turbidity at 750 nm during heating  $\beta$ -lg solutions ( $C = 10\text{g/L}$ ) at  $77.5^\circ\text{C}$  at different pH indicated in the figure.

When  $t_p$  determined at different temperatures is plotted in an Arrhenius representation (figure 3.12), one obtains a straight line and from the slope of the line one can deduce an apparent activation energy of about 300 kJ/mol. This value is very close to

that found at pH 7 (Le Bon, Nicolai et al. 1999) and 6.5 (Tolkach, Steinle et al. 2005). From this result, we may conclude that the rate limiting step of the formation of both microgels and strands is denaturation of the proteins.

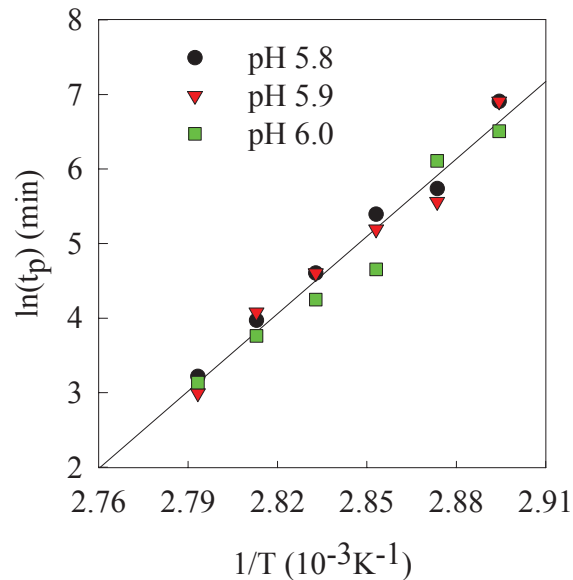


Figure 3.12: Arrhenius representation of the temperature dependence of the time needed to reach a plateau turbidity for  $\beta$ -lg solution ( $C = 10 \text{ g/L}$ ) at different pH values indicated in the figure.

#### ***At neutral pH in the presence of calcium ions***

The depletion of native proteins with heating time at  $62^\circ\text{C}$  was studied at different R for solutions at  $C=40 \text{ g/L}$  and pH 7.0. This evolution could be described by an apparent reaction order of 1.5 independent of R, but the depletion rate increased somewhat with increasing R. (see paper III). We note that the same reaction order was found for aggregation in the presence of NaCl (Le Bon, Nicolai et al. 1999).

### **III.2.2. Evolution of the system during heating**

#### ***Evolution at low pH in pure water***

We have studied the microgel formation during heating in pure water at pH 5.8 using dynamic light scattering. DLS is very sensitive to the presence of large aggregates, which allows us to measure the size of the aggregates even at the initial stage of the process where its fraction is still very small. Of course, the initial stage can only be characterized if the aggregation rate is small that is at lower heating temperatures. Figure 3.13 shows the size distributions at different times after heating at  $60^\circ\text{C}$ ,  $65^\circ\text{C}$  and  $70^\circ\text{C}$ .

At 60°C we find 2 distinct picks: at  $R_h=2$  nm representing the residual native proteins and at  $R_h=40$ nm representing the microgels. This means that the very first step of the aggregation process is the formation of distinct microgels. With time, more native proteins are converted into microgels with the same size. When the fraction of aggregated proteins attains a few percent, the microgels start to grow until steady state is reached. The growth is better seen at higher temperatures where the process is faster.

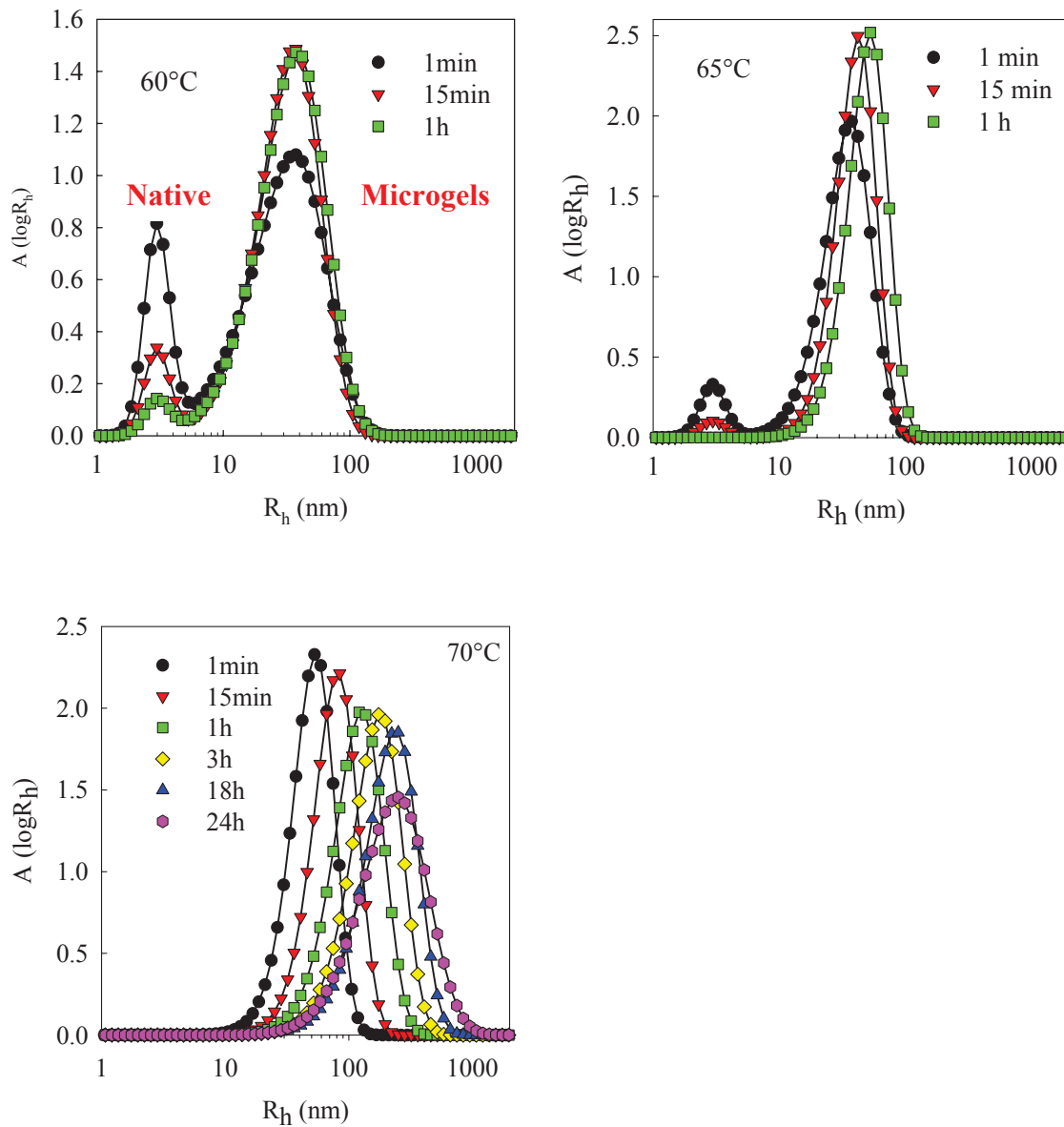


Figure 3.13: Amplitude of the light scattering signal as a function of the hydrodynamic radius of  $\beta$ -lg solutions heated for different times and at different temperatures indicated in the figures (pH 5.8,  $C = 40$  g/L)

Figure 3.14 shows the evolution of  $R_{hz}$  of the microgels at  $T=75^{\circ}\text{C}$  as a function of heating time (a) and as a function of the fraction of aggregated proteins ( $F_{ag}$ ) (b). Initially, for  $F_{ag}<10\%$ , microgels with  $R_{hz}=40\text{nm}$  were formed. Then, the size increased rapidly until about  $F_{ag}\approx 30\%$ , after which it increased weakly until all protein had aggregated.

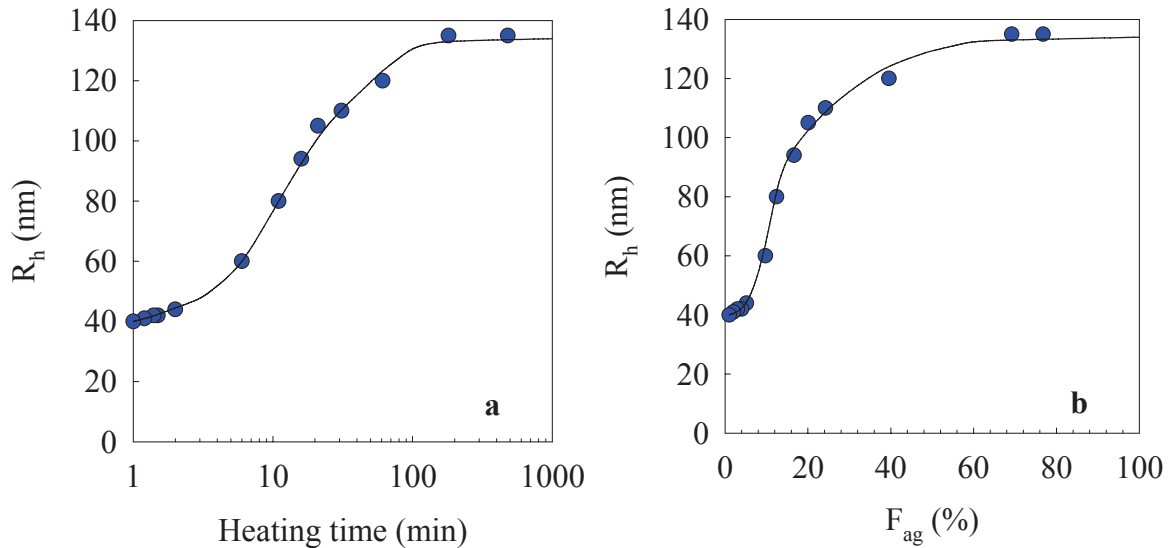


Figure 3.14: Evolution of the size of the microgels formed during heating at  $75^{\circ}\text{C}$  as a function of heating time (a) and the fraction of aggregated proteins (b) at  $\text{pH } 5.8$  and  $C=40 \text{ g/L}$

During the growth of the microgels, their number concentration decreased initially, which implies that the growth involves fusion (see paper I). At the later stage, the number concentration remained approximately constant showing that the growth occurred by addition of newly denatured proteins to existing microgels.

Figure 3.15a shows that the formation and growth of the microgels happen at the beginning of the heating process while strands are formed at a later stage. We also observed an increase of the pH during heating, see figure 3.15b, as was already reported by (Donato, Schmitt et al. 2009).

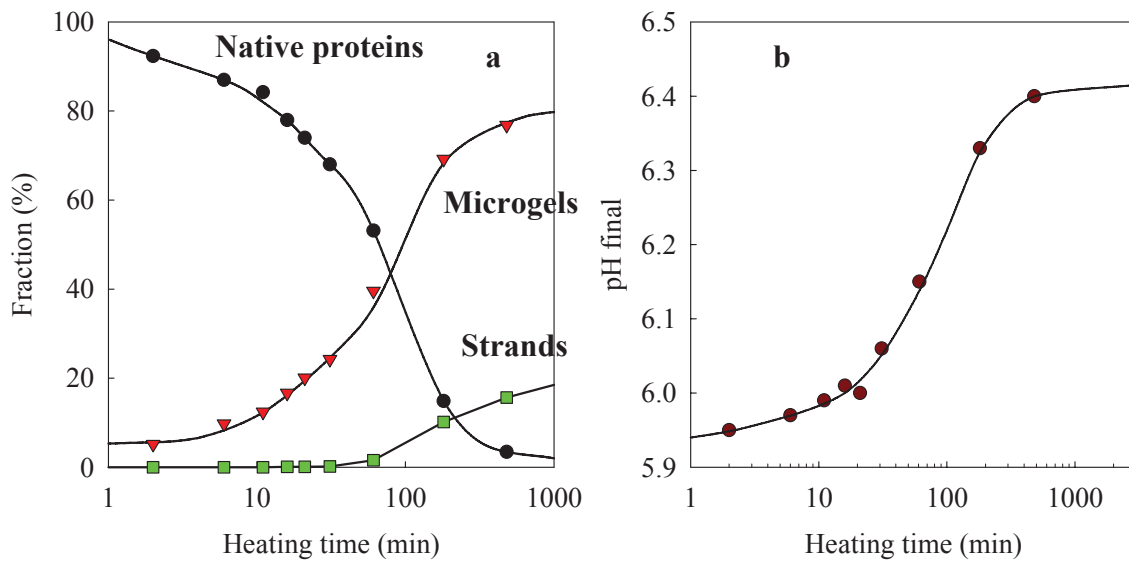


Figure 3.15: Fraction of native proteins, strands and microgels (a) and the pH (b) as a function of heating time at 75°C for a  $\beta$ -lg solution at  $C=40\text{g/L}$  and pH 5.8.

When we plot the fraction of microgels and strands as a function of the pH, see figure 3.16, it is clear that only microgels are formed when  $\text{pH} < 6.1$ . When  $\text{pH} > 6.1$ , denatured proteins form small strands, but can also still be incorporated into already formed microgels. If we keep the pH below 6.1 during heating, no strands are formed, but the microgels stick together to form bigger aggregates and precipitate. This behavior is similar to what we observe when we heat the system below pH 5.75. This means that the increase of the pH above 6.1 is crucial for the stabilisation of the protein suspension. When we start at  $\text{pH} < 5.75$  the increase of the pH during heating is not sufficient to stabilize the microgels.

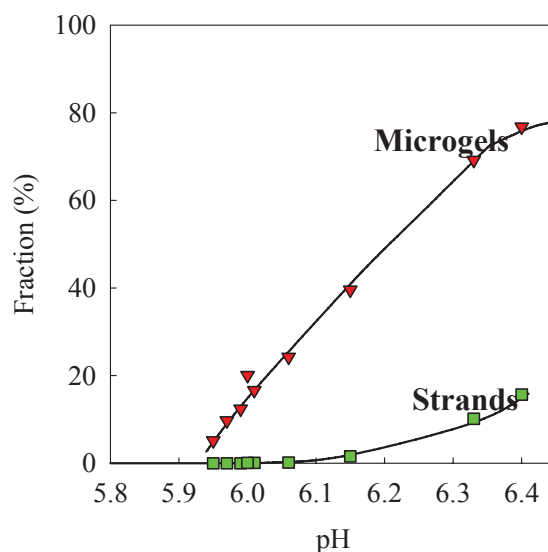


Figure 3.16: Fraction of microgels and strands as a function of the pH during heating at 75°C for a  $\beta$ -lg solution at  $C=40\text{g/L}$  and pH 5.8.

The increase of the pH implies that the microgels remove  $\text{H}^+$  from the solution to neutralize their charge inside. By consequence the residual native proteins become more strongly charged. It is likely that also the surface charge density of the microgels increases, and thus the electrostatic repulsion, favouring the formation of a stable suspension.

The internal structure of the microgels is not yet fully resolved. (Krebs, Devlin et al. 2007) suggested that initially short fibers are formed that subsequently condense into spherical particles. (Schmitt, Moitzi et al. 2010) also suggested that the microgels were formed by cross-linked protein strands based on small angle X-ray scattering. These experiments suggest that the initial stage of the aggregation process is the formation of protein strands independent of the pH. However we didn't see their presence with DLS, but it is possible that the strands are not stable and immediately associate into the microgels

### ***Evolution at neutral pH in the presence of calcium ions***

For this study, we choose a heating temperature of 62°C at which the evolution of the system is slow enough to observe the first step of aggregation process. DLS showed the same evolution in the presence of calcium ions at pH 7 as in pure water at pH 5.8, that we discussed in the previous section. Figure 3.17 shows the evolution of aggregate size as a function of heating time (a) and  $F_{\text{ag}}$  (b).  $R_{\text{hz}}$  was almost constant up to  $F_{\text{ag}} \approx 10\%$  and then increased progressively for  $R = 1, 1.5$  and  $2$ , where no microgels were formed. However, at  $R = 2.5$  and  $3$  where aggregates of small microgels were formed,  $R_{\text{hz}}$  increased initially

strongly above  $F_{ag} \approx 10\%$  and weakly at higher conversions similarly to the evolution in pure water at pH 5.8, see figure 3.13.

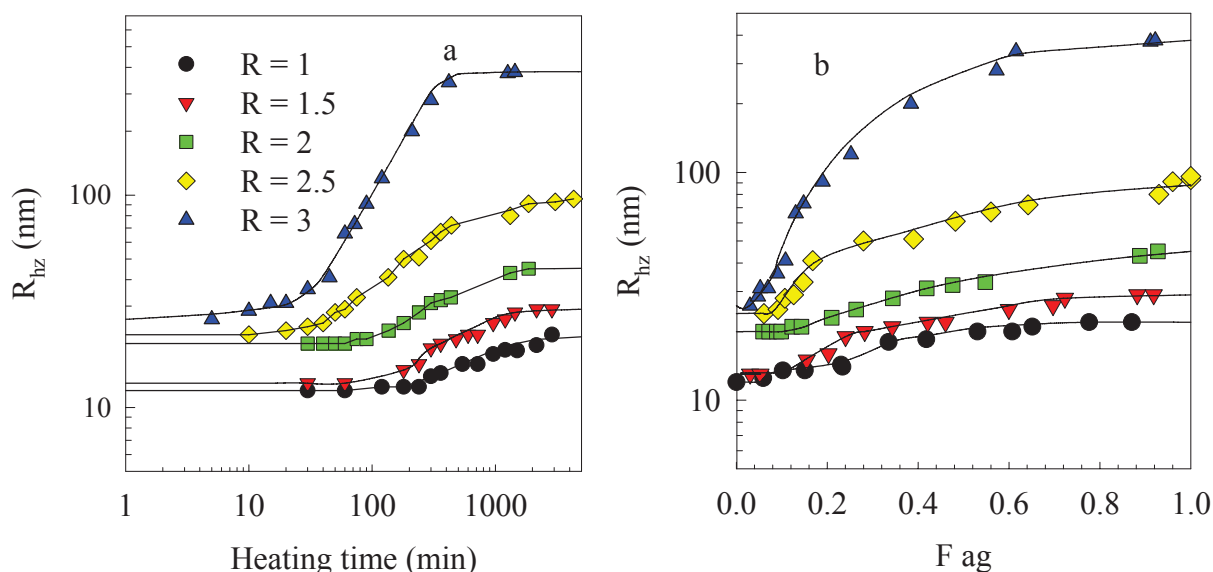


Figure 3.17: Evolution of the hydrodynamic radius of the aggregates as a function of heating time (a) and  $F_{ag}$  (b) formed by heating at  $62^\circ\text{C}$   $\beta$ -I $\text{g}$  solutions at  $C=40\text{g/L}$  and pH 7.0 in the presence of various amounts of calcium ions.

At low  $R$ , the number concentration of aggregates increased initially and then stabilized. The increase stagnated at smaller conversions with increasing  $R$ , see figure 9 in paper III. For  $R = 2.5$  and 3, we found that it decreased, implying that the growth of microgels by fusion dominated as was the case in pure water at pH 5.8.

### **Calcium bound to the proteins before and after heating**

The fraction of calcium ions bound to the protein can be determined using a calcium electrode. For native proteins, it decreased approximately linearly with increasing  $R$  down to 60% at  $R=3$ , see figure 3.18. After heating, almost all calcium was bound to the aggregates up to  $R = 2.2$  and still more than 90% at  $R=2.7$ .

These results can be used to determine the net protein charge (see table 3 in paper II). It appears that in order to form a significant amount of microgels, the net charge of the native proteins should be reduced to less than about -5. This value is remarkably similar to

that in pure water at pH 6.2, which shows that probably the net charge of the protein is the crucial parameter for the formation of the microgels.

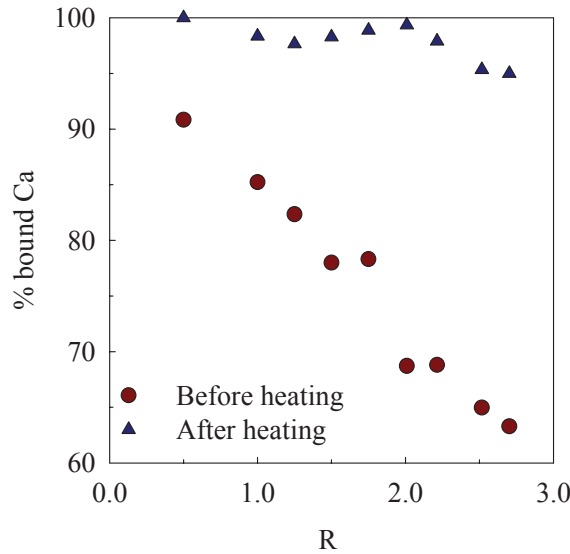


Figure 3.18: Fraction of bound calcium ions before and after heating  $\beta$ -lg solutions at  $C=40$  g/L and pH 7.0 as a function of  $R$ .

### ***III.3. Mechanism of the formation and stabilization of strands and microgels.***

DLS showed that in all cases relatively large aggregates were formed even at the earliest stage of the process, implying that nucleation is the first step of the aggregation process. At larger conversions the nuclei grow which, at least in the case of microgel formation, involves fusion of aggregates.

The transition between the nucleation of strands or microgel is controlled by the net charge of the native proteins. At neutral pH in the presence of calcium ions, the net charge on native protein decreases, because Ca ions are bound. Stable microgels were formed if the charge density was in between about -5 and -4, see figure 3.19. In pure water, the charge density has to be reduced by lowering the pH to within approximately the same range in order to form stable microgels, see figure 3.19. At higher charge densities, microgels were no longer formed, but instead small strands were formed. At smaller charge densities, microgels associate to form bigger aggregates that can lead to precipitation or gelation.

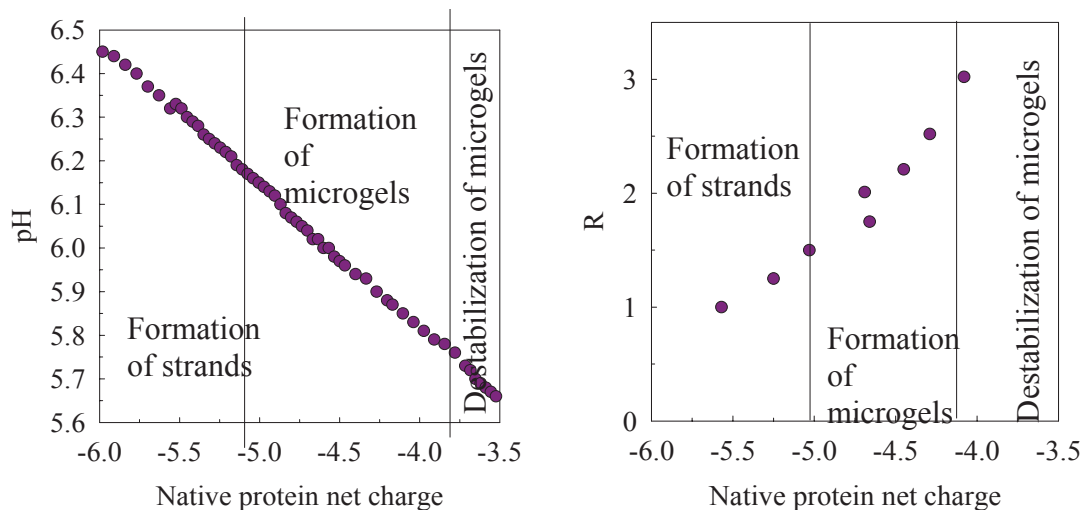


Figure 3.19: Net charge of native proteins for different pH in pure water and different R at pH 7 for a  $\beta$ -lg solution at  $C=40$  g/L. The different structures that formed after heating at different charge densities are indicated in the figures.

The proposed mechanism of the formation and stabilisation of microgels by lowering the pH or by adding calcium ions is schematically shown in figure 3.20. The formation of microgels reduces the concentration of free  $\text{Ca}^{2+}$  ( $[\text{Ca}^{2+}]_f$ ) or increases the pH of the solutions during heating. In both situations, the net charge of residual native protein increases. When it is larger than -5, microgels are no longer formed, but instead only small strands are formed. The microgel suspensions remain stable because their surface charge density increases. The microgels aggregate if the pH is kept below 6.2 or if R is larger than a critical value that depends on the pH. As discussed above, the transition between the formation of strands and microgels in the presence of  $\text{Ca}^{2+}$  is gradual when  $T < 70^\circ\text{C}$  and the two types of structure were never observed in the same solution in this case.

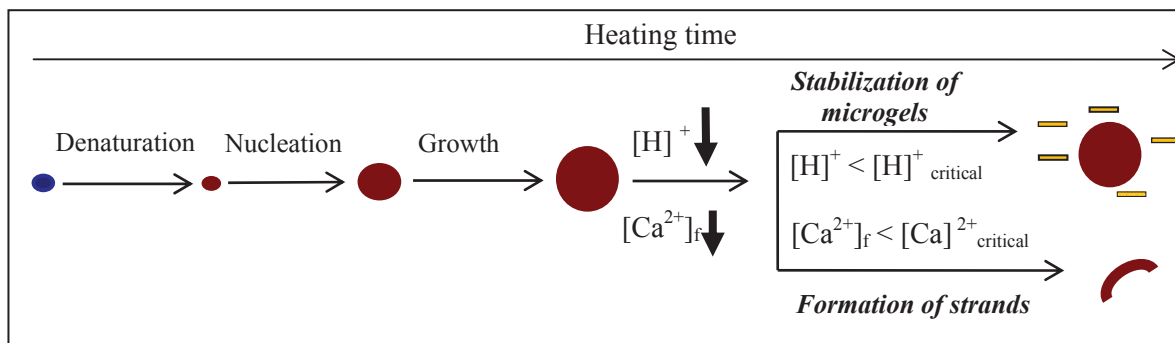


Figure 3.20: Schematic representation of the microgel formation and stabilization in heated  $\beta$ -lg solutions.

### III.4. Secondary aggregation and gelation

In this section, we discuss the aggregation and gelation at high protein concentration. We will show first the structures of the aggregates close to the gel point, then we'll discuss the sol-gel state diagram and finally structure of the gels as a function of the pH and the calcium concentration.

#### III.4.1. Secondary aggregation and gelation in pure water

At higher protein concentrations the strands or microgels are still formed in a first step, but they subsequently randomly associate into larger polydisperse clusters with a self-similar structure. By using static light scattering, we found for aggregates formed at pH 5.8 a fractal dimension of  $d_f = 2$ , see figure 3.21. This value is the same as was reported by (Mehalebi, Nicolai et al. 2008) for aggregates formed by secondary aggregation of strands at higher pH. With increasing concentration the size of the self-similar clusters increases and diverges at the gel point, see figure 3 in paper I.

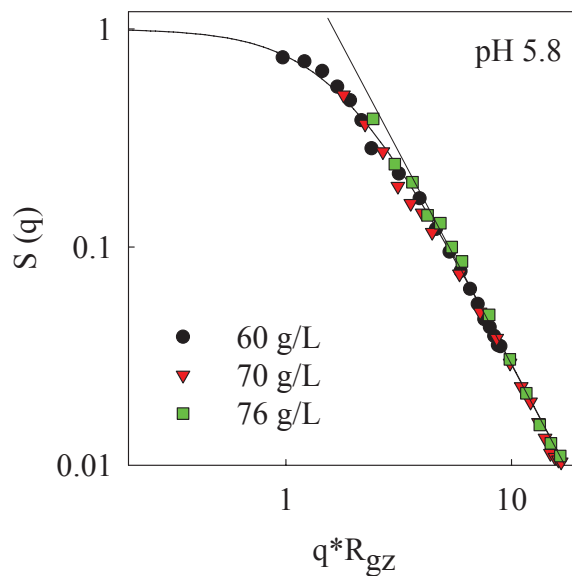


Figure 3.21: Static structure factor as a function of  $q \cdot R_{gz}$  of large  $\beta$ -lg aggregates formed at different protein concentrations in pure water at pH 5.8 by heating at 85°C until steady state. The straight line has slope -2.

As expected, the gelation concentration decreased with decreasing pH, because the protein charge density decreased, see figure 3.22. However, we found a remarkable maximum at pH 5.8, which we suggest is due to the formation of microgels for  $\text{pH} < 6.0$

and the concomitant increase of the pH. The microgels are denser than aggregates with the same size formed by associated strands. Therefore between 6.0 and pH 5.8 the increase of the fraction of microgels and their size leads to an increase of  $C_g$ , but at lower pH the overall reduction of the charge density dominates.

The gel structure can be studied using CLSM (Ako, Nicolai et al. 2009). The transition between homogeneous gels (finely-stranded gels) and heterogeneous gels (particulate gels) is indicated by the dashed line in the figure 3.22. This transition depends on the protein concentration and the pH. Heterogeneous gels were formed at pH 5.8 at  $C=80$  g/L, but they were homogeneous at higher concentrations. With decreasing pH, the concentration range where particulate gels were formed widened and below pH 5.6 they formed over the whole concentration range up to 100 g/L. In the sol region, the dashed line indicates the transition between strands and microgels. The same concentration dependence behavior is observed as in the gel region, i.e. the critical pH increases with decreasing protein concentration.

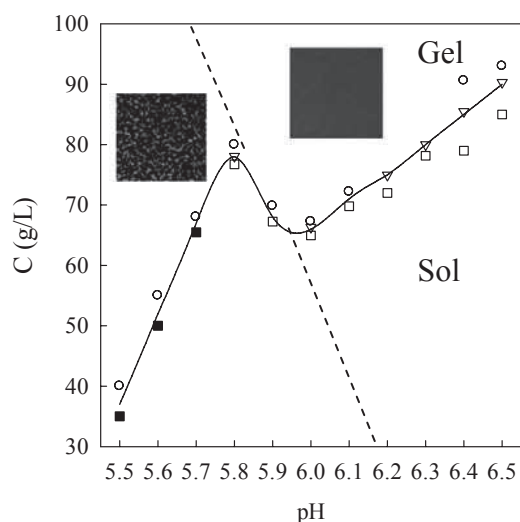


Figure 3.22: State diagram of  $\beta$ -Ig solutions at  $C=40$ g/L in pure water at pH 5.8 after heating at  $85^{\circ}\text{C}$  until steady state. Circles indicate systems that did not flow when tilted. Squares indicate free flowing homogeneous solutions. Triangles indicate very fragile gels that broke-up when tilted. Filled squares indicate macroscopically heterogeneous systems. The dashed line indicates the transition between the formation of strands (high pH) or microgels (low pH).

### III.4.2. Secondary aggregation and gelation at pH 7 in the presence of CaCl<sub>2</sub>

Figure 3.23 shows a sol-gel state diagram at pH 7.0 as a function of C and the total Ca<sup>2+</sup> concentration ([Ca<sup>2+</sup>] (a) or R (b)). The critical Ca<sup>2+</sup> concentration above which a gel or a precipitate is formed increased with increasing protein concentration up to 60 g/L and then decreased. However the critical ratio decreased progressively with increasing protein concentration. In the gel region, the dashed line indicates the transition between homogeneous gels and heterogeneous gels. The dashed line continues into the sol area where it indicates the transition between strand and microgel formation. Both sol and gel region the transition occurred at R = 1.5 ± 0.5 almost independent of C.

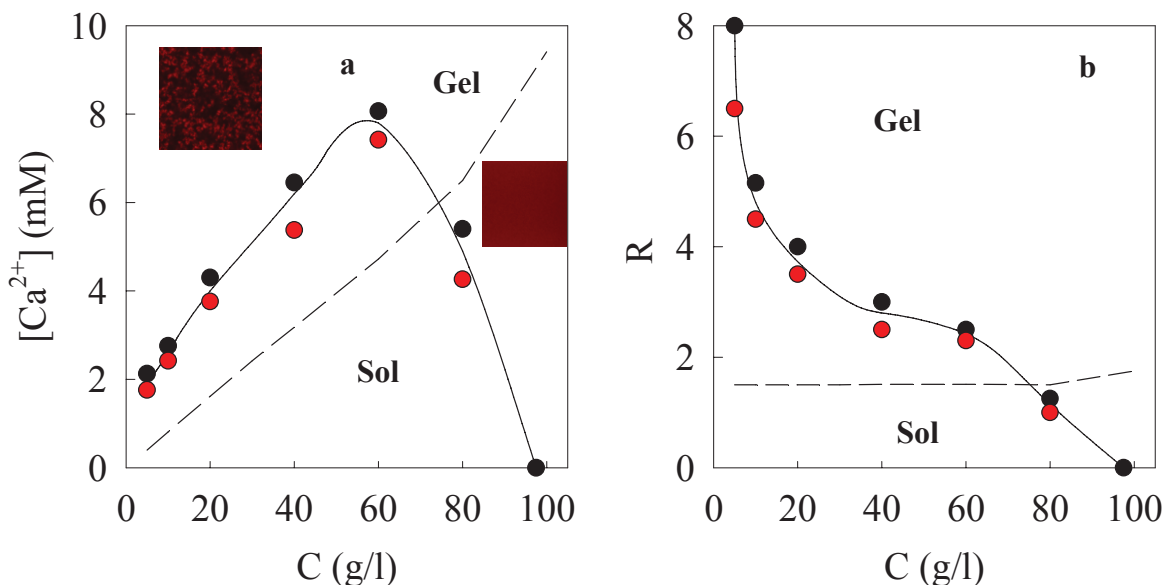


Figure 3.23: State diagram of  $\beta$ -Ig solutions at pH 7.0 heated at 85°C as a function of C and  $[Ca^{2+}]$  (a) or C and R (b). The black and red circles indicate solutions and gels, respectively. Solid lines are guide to the eye. Dashed lines indicate the boundary between the formation of strands (low  $[Ca^{2+}]$ ) and microgels (high  $[Ca^{2+}]$ ).

We also established sol-gel diagrams at other pH values between 6.0 and 7.5. Similar behaviors were observed as for pH 7.0, but the calcium concentration needed to induce gelation increased with increasing pH, see paper II. At pH 7.5 and 60 g/L we observed two sol-gel transitions with increasing calcium concentrations: one transition from a transparent liquid to a transparent gel at  $[Ca^{2+}] = 6$  mM and another one from a turbid liquid to a turbid gel at  $[Ca^{2+}] = 8$  mM, see figure 3.24. This remarkable behavior can be explained by the fact that the number concentration of the strands is much larger than that of the microgels. At the first transition, the electrostatic repulsion between strands is

sufficiently reduced to allow their association into a gel. However at the second transition, microgels are formed and the repulsion between the microgels is still sufficiently high to inhibit their association. Only above  $[Ca^{2+}] = 8$  mM the electrostatic repulsion is sufficiently reduced to allow gelation of the microgels. We expect that this behavior occurs in all systems close to the concentration where the sol-gel transition crosses the transition between the formation of strands and microgels.

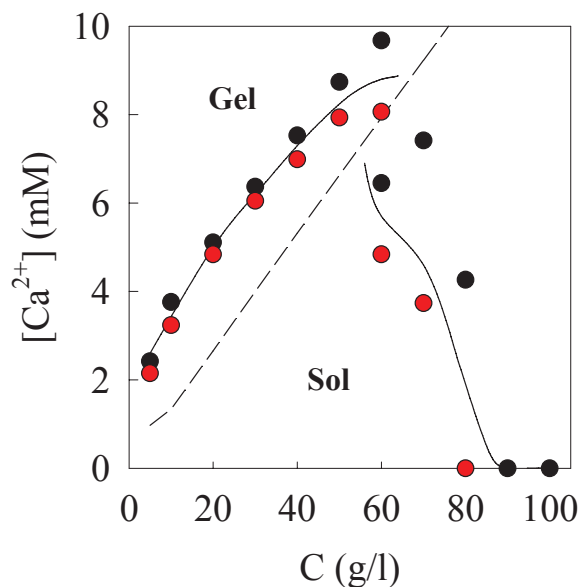


Figure 3.24: State diagram of heated  $\beta$ -Ig solutions as a function of  $C$  and  $[Ca^{2+}]$  at pH 7.5. The black and red circles indicated solutions and gels, respectively. Solid lines are guide to the eye. Dashed lines indicate the boundary between the formation of strands (low  $[Ca^{2+}]$ ) and microgels (high  $[Ca^{2+}]$ ).

### III.5. Comparison of aggregation and gelation at pH 7 in the presence of NaCl and $CaCl_2$

The effect of adding NaCl on the heat-induced aggregation and gelation of  $\beta$ -Ig at pH 7.0 has already been study in detail in the past. At low protein concentrations small strand- like aggregates are formed. The strands associate into larger fractal aggregates with a fractal dimension of 2 at higher concentrations and gel above a critical concentration that decreases with increasing NaCl concentration (Le Bon, Nicolai et al. 1999).

It appears that stable suspensions of microgels cannot be formed at pH 7.0 by screening the electrostatic repulsion with NaCl suggesting that it is necessary that the

protein charge is reduced by specific binding of (multivalent) ions. However, (Ako, Nicolai et al. 2010) found that NaCl can induce the transition between finely stranded and particulate gels. The particulate gels are formed for NaCl concentrations above about 0.2 M by association of spherical particles and have very similar structure as gels formed by microgels in the presence of CaCl<sub>2</sub>. These results were interpreted by assuming that above a critical NaCl concentration the aggregates of small strands were longer soluble and micro-phase separate occurred, leading to the formation of the microgels. Notice that the transition between the two types of gels occurs at much higher ionic strength in NaCl than in CaCl<sub>2</sub>, which shows once more the specific interaction of Ca ions with the proteins.

The process of particulate gel formation in NaCl has not yet been studied and it is not clear at what stage aggregates of small strands transform into microgels. Therefore we investigated the aggregation process of a  $\beta$ -lg solution at 40 g/L at 0.3 M NaCl where it leads to the formation of particulate gels. We choose a heating temperature of 65°C where the reaction is sufficiently slow to allow the whole process to be monitored. The evolution of  $R_{hz}$  in the presence of NaCl is compared with that in the presence of CaCl<sub>2</sub> ( $R = 4$ ) heated at 60°C in figure 3.25. At  $R = 4$ , microgels were formed already very early during the reaction. The size of the aggregates increased until it diverged and a gel was formed after about 500 minutes. At 0.3 M NaCl, small strands were formed initially with the same size as at low ionic strength. The aggregates grew rapidly with increasing heating time after about 20 min and formed self similar aggregates with a fractal dimension of 2 (see figure 13 in paper III). The aggregation process at 0.3 M NaCl was thus similar to that at lower salt concentrations, where finely-stranded gels are formed. In this system a gel was formed after about 330min.

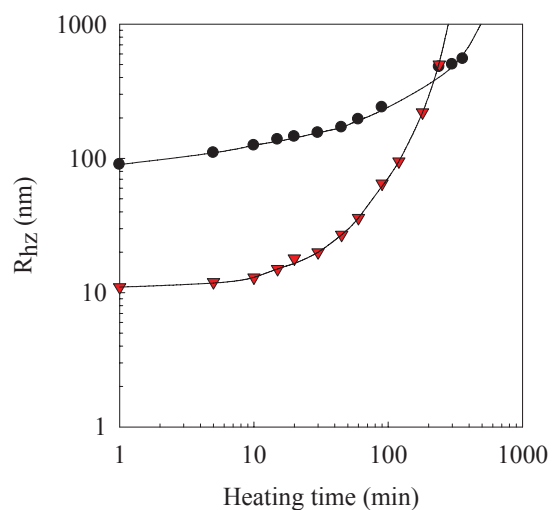
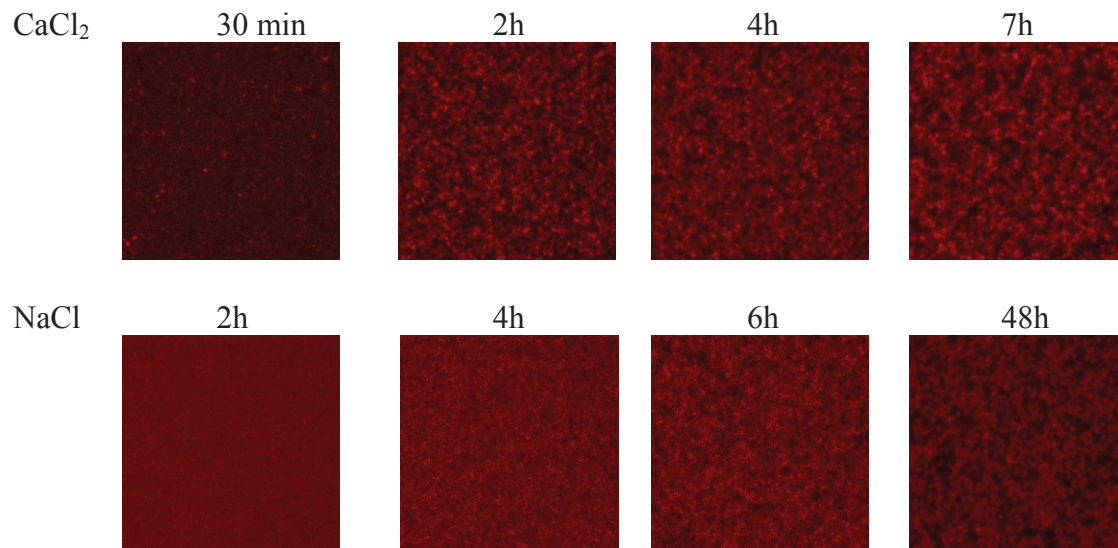


Figure 3.25: Evolution of  $R_{hz}$  as a function of the heating time for  $\beta$ -lg at  $C=40$  g/L and pH 7.0 in the presence of  $\text{CaCl}_2$  at  $R=4$  (circles) at  $T=60^\circ\text{C}$  or in the presence  $0.3$  M NaCl at  $T=65^\circ\text{C}$  (triangles). The gel times of the systems containing  $\text{CaCl}_2$  and NaCl were about 500 min and 330min, respectively.

CLSM images of the systems at different heating times are shown in figure 3.26. For  $R = 4$ , distinct protein particles were visible from the start of the aggregation process. However no features could be observed during the first few hours in the presence of NaCl even though the aggregate became large. The reason is that large aggregates formed in NaCl have a low density due to their fractal structure and can interpenetrate. At longer times close to and above the gel time the system in NaCl became increasingly heterogeneous similarly to gels formed in  $\text{CaCl}_2$ .



*Figure 3.26: CLSM images of solutions and gels of  $\beta$ -lg at  $C=40$  g/L and pH 7.0 in the presence of  $\text{CaCl}_2$  ( $R = 4$ ) during heating at  $60^\circ\text{C}$  or in the presence of  $0.3\text{M}$  NaCl during heating at  $65^\circ\text{C}$ . The images represent  $40 \times 40 \mu\text{m}$ .*

These results clearly show that although similar particulate gels are also formed at high NaCl concentrations as in the presence of  $\text{CaCl}_2$  (or low pH), the mechanism is different. Randomly aggregated small strands formed at the early stage of the process restructure into agglomerated dense spherical domains close to and beyond the gel point. It follows that, while the structure of the nuclei and the aggregates formed at low concentrations is mainly determined by the charge density of the proteins, the structure of the gel is also determined by the ionic strength.



## Chapter IV Conclusions and perspectives

### *IV.1. Conclusions*

The objective of the thesis was to study the formation and structural properties of spherical protein particles, called microgels, produced by heating  $\beta$ -lactoglobulin solutions at different conditions of pH, protein concentrations, heating temperatures, and added salt. The aim was to be able to control the size and density of the microgels in order to optimize their use in industrial applications.

We have shown that stable suspensions of microgels can be formed either by lowering the pH close to pI in pure water or at higher pH by adding calcium ions. Stable suspensions of spherical protein microgels are formed in pure water by heating  $\beta$ -lg at concentrations between 10 and 50 g/L when the pH is set within a small range between 5.75 - 6.0. The hydrodynamic radius of the microgels increases with decreasing pH between about 75 and 200nm, but the protein density of the microgels remains approximately constant at about 0.15 g/mL. At  $\text{pH} \leq 5.7$ , a fraction of the proteins precipitates, while at  $\text{pH} \geq 6.1$  mostly small protein strands with a hydrodynamic radius of 15-20 nm are formed. The upper limit shifts to somewhat larger pH at lower protein concentrations. For  $C > 50\text{g/L}$  the same aggregates are still formed as a first step, but they subsequently associate into larger self-similar aggregates or form a gel for  $C > C_g$ . In addition to the aggregates, denatured monomers and oligomers are formed, but they represent less than 5% for  $C > 10\text{g/L}$ .

In the presence of calcium ions, stable suspensions of microgels can also be formed by heating  $\beta$ -lg for  $\text{pH} > 6.1$ . The critical molar ratio of  $\text{Ca}^{2+}$  to  $\beta$ -lg needed to induce microgel formation was independent of the protein concentration for  $\text{pH} \geq 6.9$  and increased weakly with increasing pH from  $R \approx 1.5$  at pH 6.9 to  $R \approx 2.5$  at pH 7.5. In the pH-range 6.0 - 6.4 microgels are formed in pure water at low protein concentrations, but a small amount of  $\text{Ca}^{2+}$  is needed at higher concentrations. The size of the microgels increases with increasing R. Larger and denser microgels can be formed in the presence of  $\text{Ca}^{2+}$  at neutral pH than in pure water closer to pI. Stable suspensions of microgels with a size ranging from 100 to 400 nm and a density of about 0.2 – 0.45 g/ml can be formed in a

narrow range of  $\text{Ca}^{2+}$  concentrations. At  $R > 3$  or at  $C > 60\text{g/L}$ , the microgels randomly associate leading eventually to the formation of gel.

In all situations, the aggregation process starts by the formation of a distinct population of well-defined nuclei. As the aggregation proceeds, initially, more nuclei of the same size are formed, but as soon as a few percent of the proteins has converted, the nuclei grow by fusion and addition of denatured proteins.

The net charge density of the native protein is the crucial parameter for the formation of microgels and can be controlled either by the pH or by adding calcium ions, see figure 4.1. The formation of the microgels causes an increase of the pH or a decrease of the free calcium ions concentration, which leads to an increase of the net charge of residual native proteins. When the latter becomes larger than  $-5$ , small strands start to form instead of microgels at later stages of the reaction. Its increase also causes an increase of the electrostatic repulsion between the microgels and therefore leads to a stabilization of the microgel suspensions. When the charge density of the native proteins is less than about  $-4$ , secondary aggregation and gelation of the microgels occurs.

The heating temperature can influence the size and structure of the microgels. In pure water at pH 5.8, the size of the microgels was independent of the heating temperature in between  $75^\circ\text{C}$  and  $85^\circ\text{C}$  but microgels became bigger at  $70^\circ\text{C}$ . In the presence of calcium at neutral pH, the amount of  $\text{Ca}^{2+}$  per protein needed to induce the formation of microgels decreased with increasing heating temperature from between 1 and 1.5 at  $85^\circ\text{C}$  to between 2 and 2.5 at  $62^\circ\text{C}$ . The size of the microgels was independent of the heating temperature in the range  $85^\circ\text{C}$ - $75^\circ\text{C}$ , when the aggregation was fast, but at  $62^\circ\text{C}$  when it was very slow, much smaller microgels were formed. In addition, at this low temperature a gradual transition between the formation of strands and microgels was observed as a function of  $R$ .

Screening of the electrostatic interactions is not sufficient to form microgels as at pH 7 only small strands are formed even at high NaCl concentrations that randomly associate to form larger self-similar aggregates leading above a critical protein concentration to gelation. Homogeneous, so-called finely stranded, gels are formed at lower NaCl concentrations, but more heterogeneous particulate gels are formed at higher NaCl concentrations ( $>0.2\text{M}$ ). The structure of the latter type of gels is similar to the gels formed at pH close to pI or in presence of  $\text{CaCl}_2$ , but the mechanism of formation is different. Whereas the latter gels are formed by random association of microgels, the

former are formed by micro phase separation of the self similar aggregates at a later stage of the gelation process.

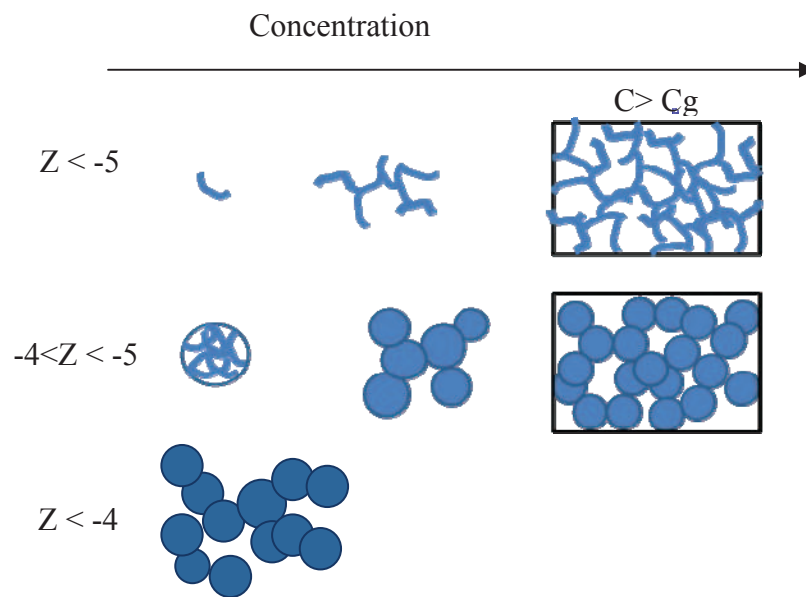


Figure 4.1: Schematic representation of the aggregation process of heat denatured  $\beta$ -Ig by lowering the pH in pure water or adding calcium ions. At large charge densities strands are formed. When the net charge of native proteins is less than -5, microgels are formed. At higher concentrations the strands or microgels associate into self-similar aggregates that grow with increasing concentration until they percolate into a system spanning gel at a critical gel concentration. When the charge density is less than about -4 the microgels associate even at very low concentrations leading to precipitation or gelation.

## *IV.2. Perspectives*

The results presented in this thesis allow us to better understand the formation of the spherical particles by heating globular protein solutions. Here we focused on pure  $\beta$ -lg, but the industrially more interesting whey protein isolate (WPI), which is the mixture of different globular proteins ( $\beta$ -lg  $\alpha$ -lac, BSA), can also form microgels. It would be interesting to study this system in more detail and compare the results with those obtained for pure  $\beta$ -lg presented here.

We have demonstrated that the net charge of the proteins is a crucial parameter for the formation and stabilization of the microgels and that it can be controlled either by lowering the pH or by adding calcium ions. Given the capability of calcium ions to induce the formation of microgels at neutral pH, we set out to investigate whether this feature is general for all bivalent ions or specific for calcium ions. We studied microgel formation in the presence of different bivalent cations ( $\text{Fe}^{2+}$  and  $\text{Mg}^{2+}$  in the form of  $\text{FeSO}_4$  and  $\text{MgCl}_2$ , respectively). After heating  $\beta$ -lg solutions at 40 g/L with these bivalent ions with different R at pH 7.0, microgels were found to be formed above a critical R that depends weakly on the kind of bivalent cations (Figure 4.2). This observation strongly suggests that the microgels induced formation is a generic property of all bivalent cations. From these results, we speculate that the key parameter that controls the formation of protein particles is the net charge of the protein that is reduced by absorption of bivalent cations.

The microgels in the presence of calcium ions can attain a higher density compared to those formed by lowering the pH. Further studies are needed to understand the localization of calcium ions in the structure of the microgels.

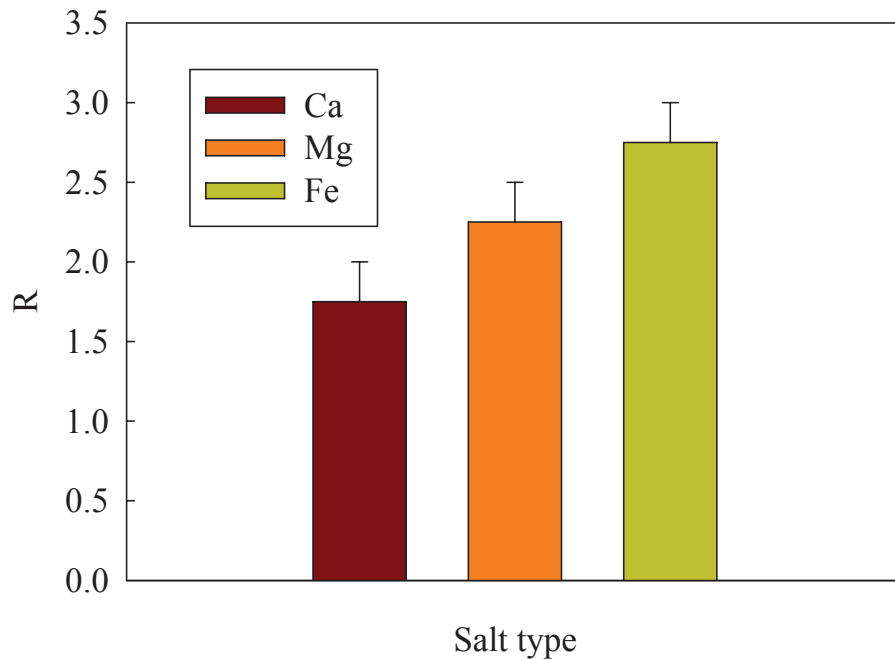


Figure 4.2: Critical molar ratio needed to induce the transition between the formation of strands and microgels for different bivalent ions indicated in the figure after heating at 85°C a  $\beta$ -lg solution at 40 g/L at pH 7.0.

Orthophosphates can act as a calcium chelating agent as it can bind at neutral pH 2 calcium ions per phosphate molecule. Orthophosphate is present in milk and to a small extent in WPI. In order to see the impact of orthophosphate on microgel formation, we established a state diagram for  $\beta$ -lg solution at pH 7.0 and  $C=40$  g/L heated at 85°C as a function of the molar ratios of  $\text{PO}_4^{3-}/\beta\text{-lg}$  and  $\text{Ca}^{2+}/\beta\text{-lg}$  (figure 4.3). The presence of phosphate increases the critical calcium concentration needed to induce the microgel formation. but the increase is much weaker than expected if orthophosphate simply acted as a chelating agent. It is clear that phosphate not only plays a role of calcium chelation, but probably also participates in the formation of the microgels. Further research is needed to elucidate the organization of calcium and phosphate in the structure of microgels.

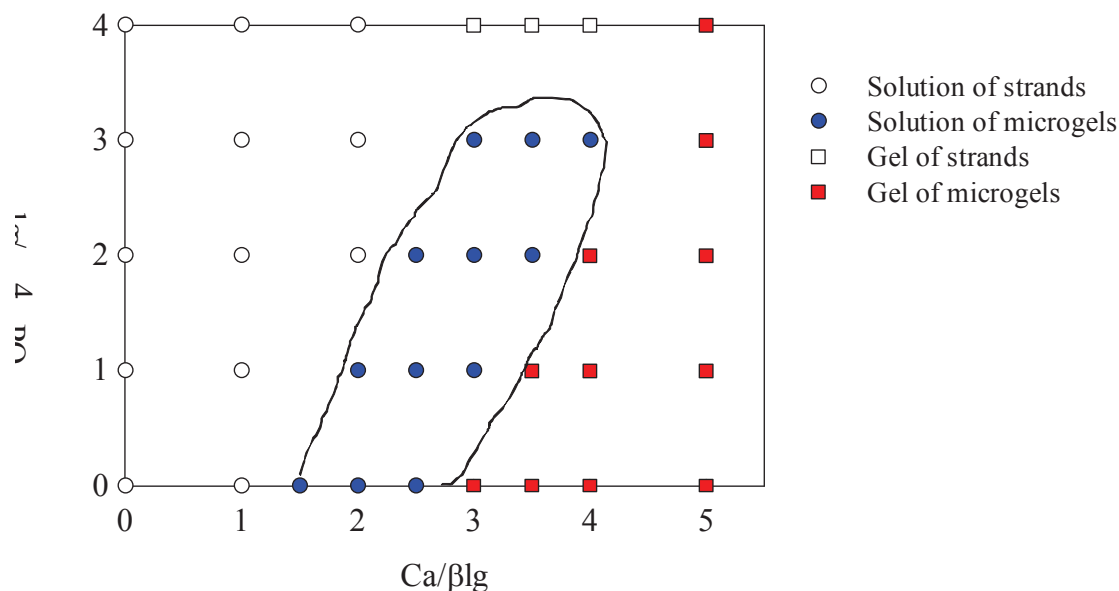


Figure 4.3: State diagram of  $\beta$ -lg solutions at pH 7.0-40g/L heated at 85°C as a function of the molar ratio  $PO_4^{3-}/\beta$ -lg and  $Ca^{2+}/\beta$ -lg. The blank and blue circles indicate solutions of strands and microgels, respectively. The blank and red squares refer to gel of strands and gels of microgels, respectively. Solid lines are guide to the eye indicate the area where solutions of microgels can be found.

In this study, we showed that the mechanism of the microgel formation follows by a nucleation and growth process. The nuclei with different sizes can be formed at the initial state of the heating process but they are not stable and become larger because the fusion of other nuclei or the addition of denatured proteins. Many questions remain in the formation and growth of the nuclei and their structure: what is the mechanism involved in the nuclei appearance? What is their structure? How it grows?

Spherical protein particulates can also be formed by heating other globular proteins when their net charge decreases (Krebs, Devlin et al. 2007). These proteins are all known to form fibrils at higher charge density. They proposed that this property of formation of particulates is general for a whole class of globular proteins. It would be interesting to study if they also form stable microgel suspensions via a similar mechanism as for  $\beta$ -lg.

The size and structure of microgels can easily controlled by altering the environmental conditions. This property makes these particles a potential tool for encapsulation of active ingredients. Further studies about interaction of microgels with such ingredients and stabilization of the complexes in the digestive system will be useful for food applications.

## References

- Adamcik, J., J. M. Jung, et al. (2010). "Understanding amyloid aggregation by statistical analysis of atomic force microscopy images." Nature Nanotechnology **5**(6): 423-428.
- Ako, K., T. Nicolai, et al. (2010). "Salt-Induced Gelation of Globular Protein Aggregates: Structure and Kinetics." Biomacromolecules **11**(4): 864-871.
- Ako, K., T. Nicolai, et al. (2009). "Micro-phase separation explains the abrupt structural change of denatured globular protein gels on varying the ionic strength or the pH." Soft Matter **5**(20): 4033-4041.
- Anema, S. G. and A. B. McKenna (1996). "Reaction kinetics of thermal denaturation of whey proteins in heated reconstituted whole milk." Journal of Agricultural and Food Chemistry **44**(2): 422-428.
- Apenten, R. K. O. and D. Galani (2000). "Thermodynamic parameters for beta-lactoglobulin dissociation over a broad temperature range at pH 2.6 and 7.0." Thermochemica Acta **359**(2): 181-188.
- Arakawa, T. and S. N. Timasheff (1984). "Mechanism of protein salting in and salting out by divalent cation salts: balance between hydration and salt binding. ." Biochemistry **23**(25): 5912–5923.
- Arnaudov, L. N., R. De Vries, et al. (2003). "Multiple steps during the formation of beta-lactoglobulin fibrils. ." Biomacromolecules **4**(6): 1614-1622.
- Aschaffenburg, R. (1959). "Crystal forms of  $\beta$ -lactoglobulin." Journal of Molecular Biology **13**(1): 194–201.
- Aymard, P., J. C. Gimel, et al. (1996). "Experimental evidence for a two-step process in the aggregation of beta-lactoglobulin at pH 7." Journal De Chimie Physique Et De Physico-Chimie Biologique **93**(5): 987-997.
- Aymard, P., T. Nicolai, et al. (1999). "Static and Dynamic Scattering of b-Lactoglobulin Aggregates formed after Heat-Induced Denaturation at pH2. ." Macromolecules **35**: 2542-2552.
- Basch, J. J. and S. N. Timasheff (1967). "Hydrogen ion equilibria of the genetic variants of bovine beta-lactoglobulin." Arch. Biochem. Biophys. **118**: 37-47.
- Bauer, R., S. Hansen, et al. (1998). "Detection of intermediate oligomers, important for the formation of heat aggregates of b-lactoglobulin. ." International Dairy Journal **8**: 105-112.

- Baussay, K., C. Le Bon, et al. (2004). "Influence of the ionic strength on the heat-induced aggregation of the globular protein beta-lactoglobulin at pH 7." International Journal of Biological Macromolecules **34**(12): 21-28.
- Berne, B. J. and R. Pecora (1993). Dynamic Light Scattering, Oxford University Press.
- Bromley, E. H. C., M. R. H. Krebs, et al. (2006). "Mechanisms of structure formation in particulate gels of beta-lactoglobulin formed near the isoelectric point." European Physical Journal E **21**(2): 145-152.
- Brown, W. (1996). Light Scattering: Principles and development, Clarendon Press: Oxford.
- Brownlow, S., J. H. Morais Cabral, et al. (1997 ). "Bovine beta-lactoglobulin at 1.8 Å resolution-still an enigmatic lipocalin." Structure **5**(4): 481-495.
- Bryant, M. C. and D. J. McClements (1998). "Molecular basis of protein functionality with special consideration of cold-set gels derived from heat-denatured whey." Trends in Food Science and Technology **9**: 143-151.
- Cairoli, S., S. Iametti, et al. (1994). "Reversible and irreversible modifications of beta-lactoglobulin upon exposure to heat. ." Journal of protein chemistry **13**(3): 347-354.
- Carrotta, R., L. Arleth, et al. (2003). "Small-Angle X-Ray Scattering studies of Metastable Intermediates of beta-lactoglobulin Isolated after heat-induced aggregation. ." Biopolymers **70**: 377-390.
- Creamer, L. K., M. Blair, et al. (2000). "Binding of small amphiphathic molecules to b-lactoglobulin. Abstract 424." Journal of Dairy Science **83**: 99.
- Creamer, L. K., D. D. Parry, et al. (1983). "Secondary Structure of bovine  $\beta$ -lactoglobulin B." Archives of Biochemistry and Biophysics **227** (1): 98-105.
- Croguennec, T., S. Bouhallab, et al. (2003). "Stable monomeric intermediate with exposed Cys-119 is formed during heat denaturation of b-lactoglobulin. ." Biochem. Biophys. Res. Comm.: 301-465.
- Croguennec, T., B. T. O'Kennedy, et al. (2004). "Heat-induced denaturation/aggregation of b-lactoglobulin A and B : kinetics of the first intermediates formed. ." International Dairy Journal **14**: 399–409.
- Dannenberg, F. and H.-G. Kessler (1988). "Reaction Kinetics of the Denaturation of Whey Proteins in Milk." Journal of Food Science **53**(1).
- De Wit, J. N. (2009). "Thermal behaviour of bovine beta-lactoglobulin at temperatures up to 150°C: A review. ." Trends Food Sci. Technol **20**: 27–34.

- Donato, L., C. Schmitt, et al. (2009). "Mechanism of formation of stable heat-induced beta-lactoglobulin microgels." International Dairy Journal **19**(5): 295-306.
- Durand, D., J. C. Gimel, et al. (2002). "Aggregation, gelation and phase separation of heat denatured globular proteins." Physica a-Statistical Mechanics and Its Applications **304**(1-2): 253-265.
- Elliot, M. S., S. B. Haddon, et al. (2001). "Direct observation of pre-critical nuclei in a metastable hard-sphere fluid." J. Phys. Condens. Matter **13**: L553-L558.
- Farrell, H. M., R. Jimenez-Flores, et al. (2004). "Nomenclature of the proteins of cows' milk - Sixth revision." Journal of Dairy Science **87**(6): 1641-1674.
- Galani, D. and R. K. O. Apenten (1999). "Heat-induced denaturation and aggregation of beta-Lactoglobulin: kinetics of formation of hydrophobic and disulphide-linked aggregates." International Journal of Food Science and Technology **34**(5-6): 467-476.
- Gosal, W. S., A. H. Clark, et al. (2004). "Fibrillar beta-lactoglobulin gels: Part 1. Fibril formation and structure." Biomacromolecules **5**(6): 2408-2419.
- Hambling, S. G., A. S. Mc Alpine, et al. (1992).  $\beta$ -lactoglobulin. Advanced Dairy Chemistry - 1: Proteins. P. F. Fox. London, Elsevier Applied Science: 141 - 190.
- Hoffmann, M. A. M. and P. J. J. M. van Mil (1997). "Heat-induced aggregation of  $\beta$ -lactoglobulin: role of free thiol group and disulfide bonds. ." J. Agric. Food Chem. **45**(29-42).
- Hoffmann, M. A. M. and P. J. J. M. van Mil (1999). "Heat-induced aggregation of beta-lactoglobulin as a function of pH." Journal of Agricultural and Food Chemistry **47**(5): 1898-1905.
- Iametti, S., L. Scaglioni, et al. (1998). "Structural features and reversible association of different quaternary structures of beta-lactoglobulin." Journal of Agricultural and Food Chemistry **46**(6): 2159-2166.
- Jeyarajah, S. and J. C. Allen (1994). "Calcium binding and salt-induced structural changes of native and preheated beta-lactoglobulin." J. Agric. Food Chem. **42**: 80-85.
- Jung, J. M., G. Savin, et al. (2008). "Structure of heat-induced beta-lactoglobulin aggregates and their complexes with sodium-dodecyl sulfate." Biomacromolecules **9**(9): 2477-2486.
- Kinsella, J. E. and D. M. Whitehead (1989 ). "Proteins in whey : chemical, physical and functional properties." Academic Press: 343-437.

- Kontopidis, G., C. Holt, et al. (2004). "Invited Review: beta-lactoglobulin: Binding properties, structure, and function." Journal of Dairy Science **87**(4): 785-796.
- Krebs, M. R. H., G. L. Devlin, et al. (2007). "Protein particulates: Another generic form of protein aggregation?" Biophysical Journal **92**(4): 1336-1342.
- Krebs, M. R. H., G. L. Devlin, et al. (2009). "Amyloid Fibril-Like Structure Underlies the Aggregate Structure across the pH Range for beta-Lactoglobulin." Biophysical Journal **96**(12): 5013-5019.
- Law, A. J. R. and J. Leaver (2000). "Effect of pH on the thermal denaturation of whey proteins in milk." Journal of Agricultural and Food Chemistry **48**(3): 672-679.
- Le Bon, C., T. Nicolai, et al. (1999). "Growth and structure of aggregates of heat-denatured beta-Lactoglobulin." International Journal of Food Science and Technology **34**(5-6): 451-465.
- Majhi, P. R., R. R. Ganta, et al. (2006). "Electrostatically driven protein aggregation: beta-lactoglobulin at low ionic strength." Langmuir **22**(22): 9150-9159.
- Mehalebi, S., T. Nicolai, et al. (2008). "The influence of electrostatic interaction on the structure and the shear modulus of heat-set globular protein gels." Soft Matter **4**(4): 893-900.
- Mehalebi, S., T. Nicolai, et al. (2008). "Light scattering study of heat-denatured globular protein aggregates." International Journal of Biological Macromolecules **43**(2): 129-135.
- Mounsey, J. S. and B. T. O'Kennedy (2007). "Conditions limiting the influence of thiol-disulphide interchange reactions on the heat-induced aggregation kinetics of beta-lactoglobulin." International Dairy Journal **17**(9): 1034-1042.
- Nicolai, T., M. Britten, et al. (2011). "beta-Lactoglobulin and WPI aggregates: Formation, structure and applications." Food Hydrocolloids **25**(8): 1945-1962.
- Nicolai, T., D. Durand, et al. (1996). Scattering properties and modelling of aggregating and gelling systems. . Light Scattering : Principles and development. . W. Brown. Oxford, Clarendon Press: 201-231.
- O'Kennedy, B. T. and J. S. Mounsey (2009). "The dominating effect of ionic strength on the heat-induced denaturation and aggregation of beta-lactoglobulin in simulated milk ultrafiltrate." International Dairy Journal **19**(3): 123-128.
- Oliveira, K. M., V. L. Valente-Mesquita, et al. (2001). "Crystal structures of bovine beta-lactoglobulin in the orthorhombic space group C222(1). Structural differences

- between genetic variants A and B and features of the Tanford transition." Eur J Biochem **268**(2): 477-483.
- Otte, J., M. Zakora, et al. (2000). "Involvement of disulfide bonds in bovine beta-lactoglobulin B gels thermally at various pH. ." Journal of Food Science **65**(3): 384-389.
- Pace, C., B. Shirley, et al. (1996). "Forces contributing to the conformational stability of proteins." FASEB J. **10**: 75-83.
- Papiz, M. Z., L. Sawyer, et al. (1986). "The structure of  $\beta$ -lactoglobulin and its similarity to plasma retinol-binding protein." Nature **324**: 383 - 385.
- Pouzot, M., D. Durand, et al. (2004). "Influence of the ionic strength on the structure of heat-set globular protein gels at pH 7. beta-lactoglobulin." Macromolecules **37**(23): 8703-8708.
- Pouzot, M., T. Nicolai, et al. (2005). "X-ray and light scattering study of the structure of large protein aggregates at neutral pH." Food Hydrocolloids **19**(2): 231-238.
- Prasad, V., D. Semwogerere, et al. (2007). "Confocal microscopy of colloids." Journal of Physics-Condensed Matter **19**(11).
- Renard, D. and J. Lefebvre (1992). "Gelation of Globular-Proteins - Effect of Ph and Ionic-Strength on the Critical Concentration for Gel Formation - a Simple-Model and Its Application to Beta-Lactoglobulin Heat-Induced Gelation." International Journal of Biological Macromolecules **14**(5): 287-291.
- Renard, D., J. Lefebvre, et al. (1998). "Effects of pH and salt environment on the association of beta-lactoglobulin revealed by intrinsic fluorescence studies." International Journal of Biological Macromolecules **22**(1): 41-49.
- Roefs, S. P. F. M. and C. G. De Kruif (1994). "A Model for the Denaturation and Aggregation of  $\beta$ -Lactoglobulin." Eur. J. Biochem. **226**: 883-889.
- Roefs, S. P. F. M. and H. A. Peppelman (2001). Aggregation and gelation of whey proteins: Specific effect of divalent cations? Food Colloids, fundamentals of formulation. E. Dickinson and R. Miller. Cambridge, The Royal Society of Chemistry: 358-368.
- Sawyer, L., S. Brownlow, et al. (1998). "beta-lactoglobulin: Structural studies, biological clues." International Dairy Journal **8**(2): 65-72.
- Schmitt, C., C. Bovay, et al. (2007). "Whey protein soluble aggregates from heating with NaCl: Physicochemical, interfacial, and foaming properties." Langmuir **23**(8): 4155-4166.

- Schmitt, C., C. Bovay, et al. (2009). "Multiscale Characterization of Individualized beta-Lactoglobulin Microgels Formed upon Heat Treatment under Narrow pH Range Conditions." Langmuir **25**(14): 7899-7909.
- Schmitt, C., C. Moitzi, et al. (2010). "Internal structure and colloidal behaviour of covalent whey protein microgels obtained by heat treatment." Soft Matter **6**(19): 4876-4884.
- Schokker, E. P., H. Singh, et al. (2000). "Heat-induced aggregation of beta-lactoglobulin A and B with alpha-lactalbumin." International Dairy Journal **10**(12): 843-853.
- Schokker, E. P., H. Singh, et al. (1999). "Characterization of intermediates formed during heat-induced aggregation of [beta]-lactoglobulin AB at neutral pH. ." International Dairy Journal **9**(11): 791-800.
- Simons, J. W. F. A., H. A. Kusters, et al. (2002). "Role of calcium as trigger in thermal beta-lactoglobulin aggregation." Archives of Biochemistry and Biophysics **406**(2): 143-152.
- Stading, M. and A. M. Hermansson (1990). "Viscoelastic behaviour of  $\beta$ -lactoglobulin gel structures." Food Hydrocolloids **4**(2): 121-135.
- Surroca, Y., J. Haverkamp, et al. (2002). "Towards the understanding of molecular mechanisms in the early stages of heat-induced aggregation of beta-lactoglobulin A B. ." Journal of Chromatography A **970**(12): 275-285.
- Timasheff, S. N., R. Townend, et al. (1966). "The optical rotary dispersion of the  $\beta$ -lactoglobulins." J. Biol. Chem. **241**: 2496-2501.
- Tolkach, A., S. Steinle, et al. (2005). "Optimization of thermal pretreatment conditions for the separation of native alpha-lactalbumin from whey protein concentrates by means of selective denaturation of beta-lactoglobulin." Journal of Food Science **70**(9): E557-E566.
- Unterhaslberger, G., C. Schmitt, et al. (2007). Beta-lactoglobulin aggregates from heating with charged cosolutes: formation, characterization and foaming, . Food Colloids: Self assembly and material science, E. Dickinson and M. Leser, The Royal Society of Chemistry, Cambridge: 175–192.
- Veerman, C., H. Ruis, et al. (2002). "Effect of electrostatic interactions on the percolation concentration of fibrillar beta-lactoglobulin gels." Biomacromolecules **3**(4): 869-873.
- Verheul, M., J. S. Pedersen, et al. (1999). "Association behavior of native beta-lactoglobulin." Biopolymers **49**(1): 11-20.

- Verheul, M., S. P. F. M. Roefs, et al. (1998). "Kinetics of heat-induced aggregation of b-lactoglobulin." J. Agric. Food Chem. **46**: 896-903.
- Xiong, Y. L., K. A. Dawson, et al. (1993). "Thermal Aggregation of Beta-Lactoglobulin - Effect of Ph, Ionic Environment, and Thiol Reagent." Journal of Dairy Science **76**(1): 70-77.
- Zittle, D. Monica, et al. (1957). "The Binding of Calcium Ions by b-Lactoglobulin Both before and after Aggregation by Heating in the Presence of Calcium Ions." Contribution From The Eastern Regional Research Laboratory **79**: 4661-4666.
- Zuniga, R. N., A. Tolkach, et al. (2010). "Kinetics of Formation and Physicochemical Characterization of Thermally-Induced beta-Lactoglobulin Aggregates." Journal of Food Science **75**(5): E261-E268.



## PAPER I

### **On the crucial importance of the pH for the formation and self-stabilization of protein microgels and strands**

#### **Abstract**

Stable suspensions of protein microgels are formed by heating salt free  $\beta$ -lactoglobulin solutions at concentrations up to about  $C = 50 \text{ g.L}^{-1}$  if the pH is set within a narrow range between 5.75 and 6.1. The internal protein concentration of these spherical particles is about  $150 \text{ g.L}^{-1}$  and the average hydrodynamic radius decreases with increasing pH from 200 nm to 75 nm. The formation of the microgels leads to an increase of the pH, which is a necessary condition to obtain stable suspensions. The spontaneous increase of the pH during microgel formation leads to an increase of their surface charge density and inhibits secondary aggregation. This self-stabilization mechanism is not sufficient if the initial pH is below 5.75 in which case secondary aggregation leads to precipitation. Microgels are no longer formed above a critical initial pH, but instead short curved protein strands are obtained with a hydrodynamic radius of about 15-20 nm.

---

Tuan Phan-Xuan, Dominique Durand, Taco Nicolai

*Polymères, Colloïdes, Interfaces, UMR CNRS Université du Maine, 72085 Le Mans cedex 9, France*

Laurence Donato, Christophe Schmitt, Lionel Bovetto

*Department of Food Science and Technology, Nestlé Research Center, Vers-chez-les-Blanc, CH-1000 Lausanne 26, Switzerland*

Published in *Langmuir* 2011, 27, 15092 – 15101

## Introduction

Globular proteins have a well-defined dense structure with a radius of a few nanometers. They are most often charged and form stable solutions in water through electrostatic repulsion. Upon heating intra-molecular interactions weaken so that the protein chains become more mobile and expose different amino acids to the surface. As a consequence, physical and even covalent (disulfide) bonds may be formed between the heat-denatured proteins. Heating may therefore lead to aggregation of globular proteins or even gelation if the concentration is sufficiently high. Here we report on an investigation of  $\beta$ -lactoglobulin ( $\beta$ -lg), which is the major whey protein in cow's milk.  $\beta$ -lg is a globular protein with a molar mass of  $18.2 \text{ kg}\cdot\text{mol}^{-1}$ , a radius of about 2 nm an iso-electric point  $pI = 5.2$ .(Hambling, Mc Alpine et al. 1992)

Heat-induced aggregation of  $\beta$ -lg has been studied extensively and has recently been reviewed in detail.(Nicolai, Britten et al. 2011) The morphology of the aggregates depends strongly on the pH and the ionic strength. At pH 2-3 and low ionic strength large rigid rod-like aggregates are formed, while closer to the iso-electric point the aggregates are spherical. Far above the iso-electric point ( $pI$ ) the aggregates are small and elongated at low concentrations, but with increasing protein concentration larger randomly branched aggregates with a self-similar structure are formed. A more detailed investigation at pH 7.0 showed that the elementary units of these self-similar aggregates were very similar to the small strands formed at lower concentrations.(Aymard, Gimel et al. 1996; Pouzot, Nicolai et al. 2005) It was therefore suggested that the larger aggregates were formed by random association of the small strands formed in a first step.

At and very close to  $pI$ ,  $\beta$ -lg aggregates do not form stable suspensions, but flocculate and eventually precipitate. However, it was found that in a narrow ranges of the pH above  $pI$  (around pH 5.9) and below  $pI$  (around pH 4.6) stable suspensions of rather monodisperse spherical particles with a radius of about a hundred nanometers were formed at concentrations up to  $40 \text{ g}\cdot\text{L}^{-1}$ .(Jung, Savin et al. 2008; Donato, Schmitt et al. 2009; Schmitt, Bovay et al. 2009; Moitzi, Donato et al. 2011) These spherical particles were called microgels and can also be formed by whey protein isolate (WPI) that contains a majority of  $\beta$ -lg, but also other globular proteins such as  $\alpha$ -lactalbumin.(Schmitt, Moitzi et al. 2010) Stable suspensions of the microgels can be obtained at concentrations up to about  $200 \text{ g}\cdot\text{L}^{-1}$  even after moderate amounts of salt was added (up to 0.2 M NaCl at pH 7.0).

Small angle X-ray scattering experiments showed that the microgels did not have a crystalline structure, but that they possibly consisted of randomly connected dense aggregates with a size of about 9nm(Schmitt, Moitzi et al. 2010).

The objective of the work presented here was to investigate the mechanism of formation of the microgels. Following a brief discussion the aggregation kinetics, we will describe the structure and the size distribution of aggregates formed in  $\beta$ -lg solutions after extensive heat treatment when steady state has been reached, i.e. when these properties no longer depend on the heating time. We have studied the effect of the pH between pH 5.6 and pH 7.0 in order to establish the transition between formation of microgels at lower pH and small strands at higher pH. In the second part we will discuss in more detail the evolution of the formation of microgels at pH 5.8. The most interesting result is, no doubt, the finding that microgel suspensions are self-stabilized by the spontaneous increase of the pH during their formation. We will also show that the pH is a crucial parameter for the formation of either microgels or small strands and suggest that the formation of both types of aggregates is most likely by nucleation and growth.

## **Materials and methods**

**Materials** The  $\beta$ -lactoglobulin (Biopure, lot JE 001-8-415) used in this study was purchased from Davisco Foods International, Inc. (Le Sueur, MN, USA). The powder contained about 89.6 wt% protein (Kjeldahl, N x6.38) and the protein composition was 55.4% and 41.6% of the variants A and B, respectively, and less than 2% of other whey proteins (based on HIC-HPLC analysis(Donato, Schmitt et al. 2009)). The powder was dissolved in salt free Milli-Q water with 200 ppm  $\text{NaN}_3$  added to avoid bacterial growth. Stock solutions with a protein concentration of about 100 g/L were dialysed at room temperature against the solvent for a period of 8 hours with four exchanges of the solvent. The pH was set to the desired value by drop wise addition of 0.1M HCl under vigorous stirring. The solutions were filtered through 0.2  $\mu\text{m}$  pore size Anotop filters before heating.

The native protein concentration was measured after filtration by UV absorption at 278 nm using extinction coefficient  $0.96 \text{ Lg}^{-1}\text{cm}^{-1}$ . Solutions were heated in air tight cylindrical glass vials with a diameter of 10 mm using a thermostated water bath. The heating rate was fast as the set temperature was reached within 4 min. The samples were cooled rapidly by holding the vial under running tap water. As will be discussed below, the pH changed during heating. In a few cases the pH was maintained at an approximately

constant value. This was done by quickly cooling the sample at regular intervals, which arrests the aggregation process. The pH was subsequently measured and adjusted at room temperature by drop wise addition of 0.1M HCl under vigorous stirring after which the sample was heated again in a water bath and the aggregation process was continued.

**Dynamic and static light scattering** measurements were done using a commercial apparatus (ALV-Langen). The light source was a He-Ne laser with wavelength  $\lambda = 632$  nm. The temperature was controlled by a thermostat bath to within  $\pm 0.2$  °C. Measurements were made at angles of observation ( $\theta$ ) between 12 and 150 degrees. The relative scattering intensity ( $I_r$ ) was calculated as the intensity minus the solvent scattering divided by the scattering intensity of toluene at 20°C.

In dilute solutions  $I_r$  is related to the weight average molar mass ( $M_w$ ) and the structure factor ( $S(q)$ ) of the solute:(Brown 1996; Nicolai 2007)

$$I_r / KC = M_w S(q) \quad (1)$$

with K an optical constant:

$$K = \frac{4\pi^2 n_s^2}{\lambda^4 N_a} \left( \frac{\partial n}{\partial C} \right)^2 \left( \frac{n_{tol}}{n_s} \right)^2 \frac{1}{R_{tol}} \quad (2)$$

Here  $N_a$  is Avogadro's number,  $(\partial n / \partial C)$  the refractive index increment and the Rayleigh constant of toluene at 20°C. We have used for the refractive index increment  $0.189 \text{ mL.g}^{-1}$  and for the Rayleigh constant  $1.35 \times 10^{-5} \text{ cm}^{-1}$ . The structure factor describes the dependence of the intensity on the scattering wave vector ( $q$ ) and depends on the structure and the size of the solute. The z-average radius of gyration ( $R_{gz}$ ) can be determined from the initial  $q$ -dependence of  $S(q)$ :

$$S(q) = \left[ 1 + \frac{q^2 R_{gz}^2}{3} \right]^{-1} \quad qR_{gz} \leq 1 \quad (3)$$

The intensity autocorrelation function measured with DLS ( $g_2(t) = \langle I(0).I(t) \rangle / \langle I \rangle^2$ ) is related to the normalized electric field correlation function,  $g_1(t)$ , by the Siegert

relation.(Berne and Pecora 1993)  $g_1(t)$  was analysed in terms of a distribution of relaxation times:

$$g_1(t) = \int A(\log \tau) \exp(-t / \tau) d \log \tau \quad (4)$$

In most cases the scattering intensity was dominated by that of the protein aggregates and  $g_1(t)$  could be analyzed in terms of a monomodal distribution of relaxation times and we used the so-called generalized exponential (GEX) distribution:  $A(\tau)=k.\tau^p \exp[-(\tau/\tau^*)^s]$ . The GEX distribution contains two parameters ( $p,s$ ) to describe the shape of a wide range of single peaked distributions such as the Schultz-Zimm and the Pearson distribution.(Nicolai, Gimel et al. 1996)  $\tau^*$  is the characteristic relaxation time and  $k$  is a normalisation constant. In some cases we could observe in addition a distinct contribution of the residual native proteins. In that case  $g_1(t)$  was fitted to the sum of a GEX distribution to describe the aggregates and a log-normal distribution to describe the native proteins. For the latter the average relaxation time and the width of the distribution, but not the relative amplitude, were fixed at the values obtained on unheated solutions.

In dilute solutions the relaxation is caused by self diffusion of the particles and  $\tau$  is related to the diffusion coefficient ( $D$ ):  $\tau = (q^2.D)^{-1}$ . The hydrodynamic radius ( $R_h$ ) may be calculated using the Stokes-Einstein equation:

$$D = \frac{k.T}{6.\pi.\eta.R_h} \quad (5)$$

with  $\eta$  the viscosity,  $k$  Boltzman's constant and  $T$  the absolute temperature. The z-average hydrodynamic radius ( $R_{hz}$ ) was calculated from the average diffusion coefficient.

**Centrifugation experiments** were done at room temperature with an Allegra 64R centrifuge (Beckman Coulter, USA) at different rotor speeds (50-50,000 g) during 1 h. The heated  $\beta$ -lg solutions were diluted before centrifugation to  $10 \text{ g.L}^{-1}$ . After each centrifugation, the supernatant was taken 1.5 cm from the top of the solution and analyzed.

**Turbidity** measurements were done as a function of the wavelength in rectangular air tight cells using a UV-Visible spectrometer Varian Cary-50 Bio (Les Ulis, France). Different pathlengths (1 or 10mm) were used depending on the turbidity of the samples in

order to avoid saturation. Measurements were done at different temperatures that were controlled within 0.2°C using a thermostat bath.

**Size exclusion chromatography (SEC)** experiments were carried out at room temperature with a TSK PW 5000 + PW 6000 column set (30 cm + 60 cm) in series in addition to a Zorbax GF-450 pre-column (25 cm). The refractive index was measured at the exit of the columns using a differential refractive index detector (SHODEX RI 71). A volume of 300 µl of the protein solution was injected using an automatic injection system (Autoinjector 234, Gilson) at a concentration of approximately 1 g.L<sup>-1</sup>. The system was eluted at 20°C with 0.1 M NaNO<sub>3</sub> at pH 7 with a flow rate of 1 ml.min<sup>-1</sup>.

**Transmission electron microscopy.** The microstructure of heated protein dispersions was investigated by transmission electron microscopy (TEM) using the negative staining method. A drop of the protein dispersion diluted to 0.1wt% in Millipore water was deposited onto a formvar-carbon coated copper grid. The excess product was removed after 30 s using a filter paper. A droplet of 1% phosphotungstic acid at pH7.0 was added for 15 s, removing any excess. After drying the grid at room temperature for 5 min, micrographs were taken using a Philips CM12 transmission electron microscope operating at 80 kV. Images were recorded using a Gatan Multiscan Camera Model 794.

## Results and Discussion

### 1. Aggregation kinetics.

The most straightforward method to study the kinetics of the aggregation process is to measure the turbidity ( $\tau$ ) as a function of heating time. We measured the evolution of the turbidity for solutions at  $C = 10\text{g.L}^{-1}$  adjusted at different pH between 5.6 and 6.0 while heating at different heating temperatures between 72°C and 85°C. As we will discuss below, the pH increased during heating and the pH values stated in this article are those before the samples were heated, unless otherwise specified. At pH 5.6 and 5.7 heating led to precipitation of a fraction of the proteins which perturbed the measurements. Turbidity results obtained at pH 5.8, 5.9 and 6.0 are shown in figure 1 for two temperatures. In all cases the turbidity increased until it reached a plateau at a characteristic time  $t_p$ , which may be considered as the time needed to reach steady state.  $t_p$  increased strongly with decreasing temperature, but did not depend significantly on the pH in this range. Verheul et al. (Verheul, Roefs et al. 1998) also found no dependence of the aggregation rate in this pH

range at 75°C, but an increase with increasing pH below 70°C. On the other hand, a small decrease of the rate with decreasing pH was reported at 80°C.(Donato, Schmitt et al. 2009; Zuniga, Tolkach et al. 2010)

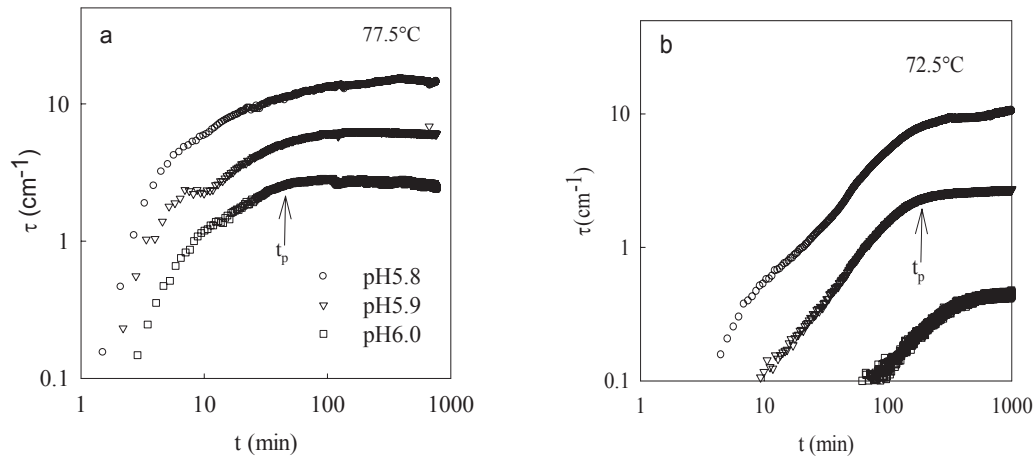


Figure 1. Time dependence of the turbidity at 750 nm during heating  $\beta$ -lg solutions ( $C = 10 \text{ g.L}^{-1}$ ) at different pH and temperatures indicated in the figure. The arrow illustrates the time where the turbidity reaches a plateau.

When  $t_p$  is plotted in an Arrhenius representation the data obtained at pH 5.8, 5.9 and 6.0 can be described by a single straight line and from the slope we can deduce an apparent activation energy of about  $300 \text{ kJ.mol}^{-1}$ , see figure 2, close to the values found at pH 7 (Le Bon, Nicolai et al. 1999) and at pH 6.5.(Tolkach and Kulozik 2005) Most often a reaction order close to 1.5 was found independent of the pH above pI.(Nicolai, Britten et al. 2011) We may therefore conclude that the kinetics of the aggregation process does not vary strongly over the whole range of  $\text{pH} > \text{pI}$  where stable aggregate suspensions can be formed even though different types of aggregates are formed. Most likely, this is the case because denaturation of native proteins is the rate limiting step of the aggregation process.

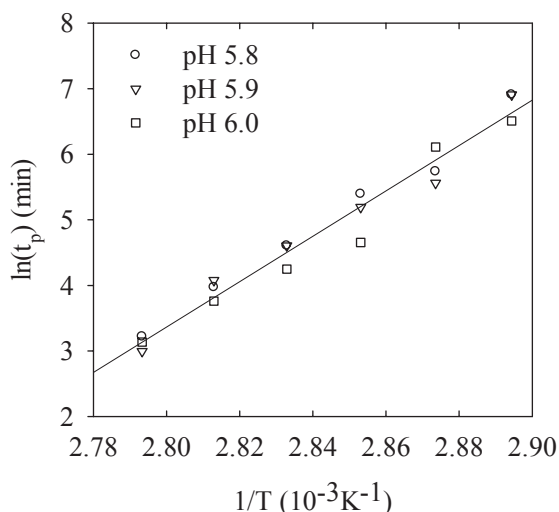


Figure 2. Arrhenius plot of temperature dependence of the time needed to reach a plateau turbidity for  $\beta$ -lg solutions ( $C=10 \text{ g.L}^{-1}$ ) at different pH indicated in the figure.

## 2. Characterisation at steady state.

We made a systematic investigation of the effect of the protein concentration for solutions at different pH between 5.6 and 7.0. In this section we focus on the structure and the composition of the aggregates after prolonged heating (overnight) when the system no longer evolved and had reached steady state. The results shown in this section did not depend on the actual heating time as long as steady state was reached.

Heated protein solutions were highly diluted so that interactions between the aggregates could be neglected and subsequently investigated using light scattering.  $M_w$ ,  $R_{gz}$  and  $R_{hz}$  were determined as described in the experimental section. The results for  $R_{hz}$  are shown in figure 3, to which those at pH 7.0 reported by Mehalebi et al. (Mehalebi, Nicolai et al. 2008) were added for comparison. The average size of the aggregates was approximately independent of the protein concentration except close to the gel concentration, where a sharp increase was observed. For pH 6.1, 6.2 and 6.3 we found that the aggregate size also increased with decreasing concentration for  $C < 30 \text{ g.L}^{-1}$ . We will discuss the origin of this behavior below. Repeat measurements at lower temperatures showed that the heating temperature had no influence on the size of the aggregates at steady state at least in the range 75-85°C, see figure S1 of the supplementary information. However, as we will show below, larger aggregates were obtained at 70°C.

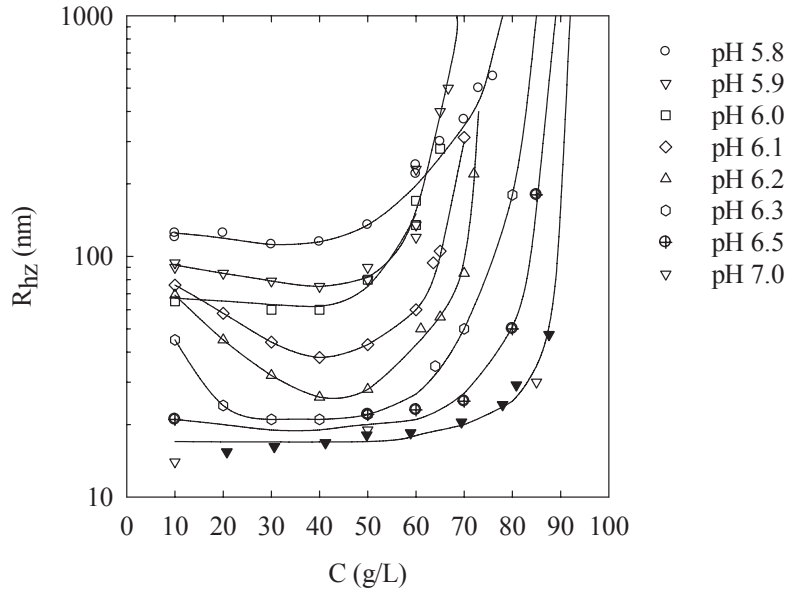


Figure 3. Concentration dependence of the z-averaged hydrodynamic radius of aggregates formed by heating at 85°C  $\beta$ -lg solutions at different pH until steady state was reached. Results obtained at pH 7.0 obtained from ref (Mehalebi, Nicolai et al. 2008) are represented as filled symbols. A few measurements at pH 7 were repeated in this study and are shown as open symbols.

Figure 4 shows that  $M_w$  and  $R_{hz}$  increased strongly with decreasing pH for pH < 6.2 in the intermediate concentration range (30-50 g.L<sup>-1</sup>) where they depended little on the protein concentration. As mentioned above, the lowest pH where stable suspensions were obtained was pH 5.75. The observed increase of  $R_{hz}$  with decreasing pH is in agreement with results reported for heat-denatured  $\beta$ -lg aggregates in the literature.(Jung, Savin et al. 2008; Mehalebi, Nicolai et al. 2008; Donato, Schmitt et al. 2009; Schmitt, Bovay et al. 2009; Zuniga, Tolkach et al. 2010) However, there is significant variation of the reported absolute values of  $R_{hz}$ . This may be in part explained by the fact that not in all cases steady state was reached, but it is also caused by the strong sensitivity to the pH and the mineral content.

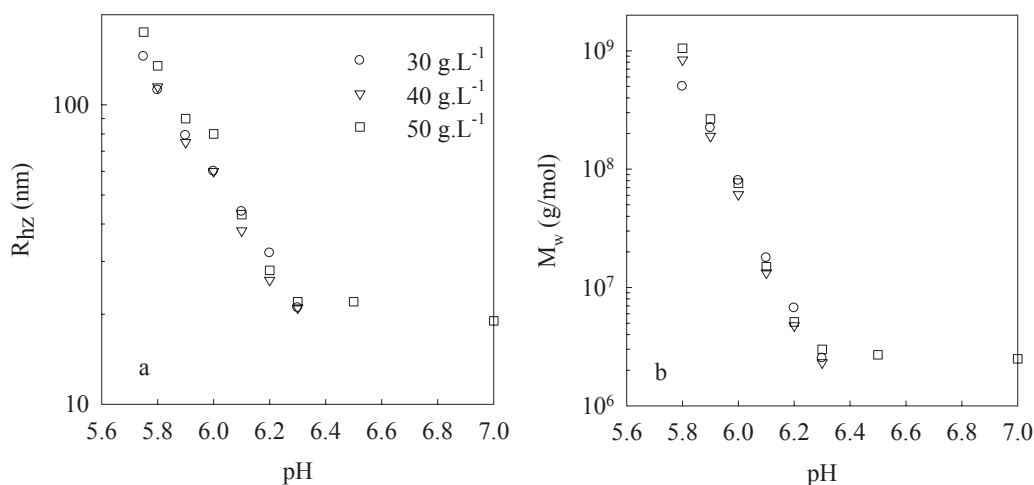
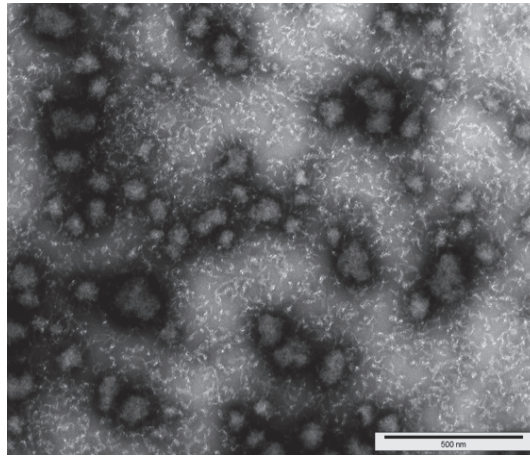


Figure 4. pH dependence of the z-averaged hydrodynamic radius (a) and the weight averaged molar mass (b) of aggregates formed by heating  $\beta$ -lg solutions at 85°C until steady state was reached for different protein concentrations indicated in the figure.

The aggregates were not large enough to deduce their shape from the structure factors obtained by light scattering. However, electron microscopy images of the aggregates formed at different pH have been reported in the literature. At pH 7.0 the aggregates are curved strands with a diameter of about 10 nm and a length of about 50 nm (Durand, Gimel et al. 2002; Jung, Savin et al. 2008; Donato, Schmitt et al. 2009; Schmitt, Bovay et al. 2009) TEM images at pH 6.8 and 6.4 also showed small strands, (Zuniga, Tolkach et al. 2010) but at pH 6.0 and lower the aggregates were more spherical. (Bromley, Krebs et al. 2006; Jung, Savin et al. 2008; Donato, Schmitt et al. 2009; Krebs, Devlin et al. 2009; Schmitt, Bovay et al. 2009; Zuniga, Tolkach et al. 2010) TEM images of the systems studied here showed similar structures and, strikingly, at pH 6.1 we observed both strands and spheres in the same sample, see figure 5. Notice that no intermediate structures were formed. The reason why these two fundamentally different morphologies can be formed in the same sample will become clear below.



*Figure 5. Negative staining TEM micrograph of the aggregates formed by heating a  $\beta$ -lg solution at 85°C until steady state was reached ( $C= 40\text{g.L}^{-1}$  and  $\text{pH} = 6.1$ ). The scale bar represents 500 nm.*

At higher concentrations approaching the gel concentration, the size of the aggregates increased sharply caused by secondary aggregation of the small strands or the microgels. Analysis of the structure factor of these large aggregates showed that they had a self-similar structure as was shown in detail by Mehalebi et al.(Mehalebi, Nicolai et al. 2008).

**Size distribution of the aggregates.** The size distribution of the microgels was investigated at various protein concentrations (30 or 40  $\text{g.L}^{-1}$ ) and pH (5.75-6.0), by using a combination of size exclusion chromatography (SEC) and sedimentation experiments. The latter were necessary because the majority of the aggregates were large and completely excluded from the columns used in SEC. Supernatants obtained after centrifugation for 1h at different rotor speeds (50-50,000 g) were analysed by light scattering and the values of  $M_w$  and  $R_{hz}$  were determined. The residual protein fraction in the supernatant (F) was determined by UV absorption. It turned out that the extinction coefficient of the microgels was slightly larger. This has been taken into account using a method explained in the supplementary information. F is plotted as a function of  $M_w$  and  $R_{hz}$  in figure 6 for different pH.

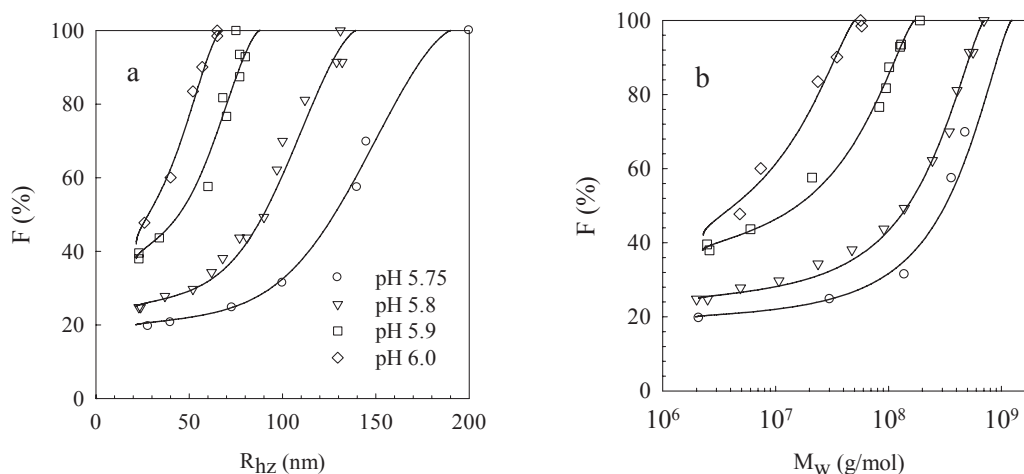


Figure 6. Fraction of proteins as a function of  $R_{hz}$  (a) and  $M_w$  (b) for supernatants obtained after centrifugation at different rotor speeds. The pH was set before heating at different values indicated in the figure.  $C = 40 \text{ g.L}^{-1}$  except at pH 5.75 where  $C = 30 \text{ g.L}^{-1}$ . Before centrifugation the solutions were heated at  $85^\circ\text{C}$  until steady state was reached.

A significant fraction of the proteins with  $M_w < 2 \times 10^6 \text{ g.mol}^{-1}$  and  $R_{hz} < 22 \text{ nm}$  did not sediment even at 50,000 g. Light scattering experiments showed that the supernatant contained the small protein strands that are formed in addition to the microgels. Thus centrifugation at 50,000 g can be used to roughly separate the protein microgels from the protein strands. Figure 7 shows the fraction of microgels determined in this way as a function of the pH for different protein concentrations. It decreased sharply with increasing pH at a critical pH and was in all cases very small for  $\text{pH} \geq 6.5$ . In fact, no microgels are observed at high pH implying that a small fraction of the small strands sediments at 50,000 g.

If the fraction of the larger microgels decreases and that of the smaller strands increases the average molar mass and the average hydrodynamic radius decrease. Thus the drop in the fraction of microgels explains in part the drop in  $M_w$  and  $R_{hz}$  shown in figure 4. However, as we will see below, the decrease of  $M_w$  and  $R_{hz}$  is also partly explained by a decrease in the size of the microgels themselves with increasing pH. The critical pH above which only strands are formed shifts to slightly higher values at lower protein concentrations. Therefore at lower protein concentrations, for given starting pH, the critical pH is reached after a larger fraction of protein has formed microgels. A larger fraction of microgels leads to larger average molar masses and radii. This explains the initial decrease of the  $R_{hz}$  with increasing protein concentration at intermediate pH values (figure 3).

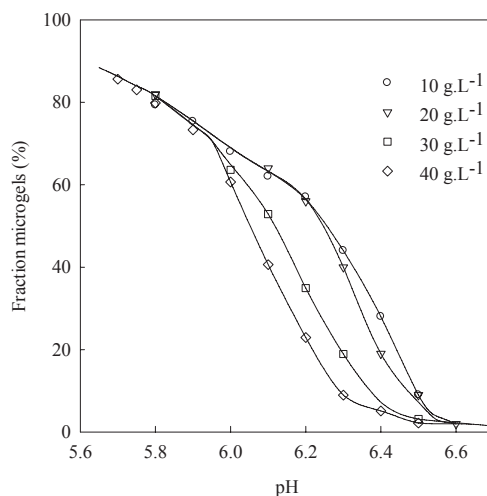


Figure 7. Dependence on the pH of the fraction of proteins that sedimented in the form of microgels after centrifugation at 50,000 g for solutions at different protein concentrations that were heated at 85°C until steady state was reached. This fraction corresponds roughly to the fraction of microgels.

The supernatant obtained at pH 5.8 after centrifugation at 50,000g was further analyzed by SEC. The chromatograph shows a peak (I) at elution volume ( $V_e$ ) around 18 ml and a second well separated peak (II) close to the total exclusion volume ( $V_e=10$ ml), see figure 8. Integration over the whole chromatograph showed that no proteins were retained in the columns. Peak I is situated close to that of native  $\beta$ -lg that is also shown for comparison. The fraction of native protein in the supernatant was determined by measuring the UV absorption after precipitation of non-native proteins at pH 4.6 and was found to be less than 2%. Peak II represents the small protein strands that were formed in addition to the microgels.

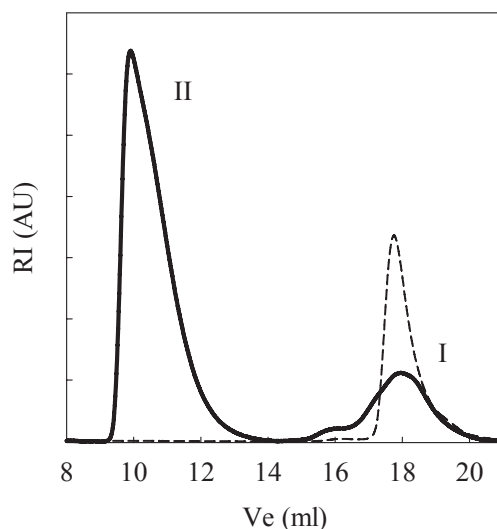


Figure 8. The solid line represents the refractive index signal ( $RI \propto C$ ) as a function of the elution volume ( $V_e$ ) for the supernatant obtained after centrifuging at 50,000g of a heated  $\beta$ -lg solution at  $C = 40 \text{ g.L}^{-1}$  and pH 5.8. Peak I represents monomers, dimers and a small amount of larger oligomers and peak II represents small protein strands. The dashed line indicates the result for an unheated  $\beta$ -lg solution.

Peak I represents about 5% of the total amount of proteins. It contains denatured monomers, dimers and a small amount of larger oligomers, which precipitated at pH 4.6, in addition to residual native proteins. A third population of proteins (III) in the heated samples consisted of mainly microgels that precipitated at 50,000g. Its mass distribution could be deduced from the data shown in figure 4, by considering that at a given rotor speed aggregates with  $M > M'$  were removed from the supernatant. The fraction of proteins with  $M < M'$  that remained in the supernatant was equal to:

$$F(M') = \int_0^{M'} A(M) dM \quad (6)$$

where  $A(M)$  is the normalized molar mass distribution of all proteins and also contains contributions of peaks I and II:  $A(M) = A_I(M) + A_{II}(M) + A_{III}(M)$ . Experimentally  $M_w$  is determined for each value of  $F(M')$  and can be compared with theoretical values that are calculated assuming  $A(M)$ :

$$M_w = \int_0^{M'} M \cdot A(M) dM \quad (7)$$

The true mass distribution was obtained by varying  $A(M)$  via a process of iteration until there was agreement between the experiments and the calculation.

For the calculation of  $M_w$  using eq.7, it is necessary to know the fraction of proteins in peaks I and II and their average molar masses.  $M_w$  of peak II was deduced from light scattering ( $2.6 \times 10^6 \text{ g.mol}^{-1}$ ), while for peak I we have taken  $M_w$  equal to that of the dimer, but the calculations are insensitive to the choice of the latter. We do not need to know the shape of  $A_I$  and  $A_{II}$ , because all proteins of peaks I and II are in the supernatant. However, we need a functional form for  $A_{III}(M)$  in order to do the calculation. We have tried first Gaussian or log-normal distributions, but they did not give satisfactory descriptions of the data. Therefore we have used the same versatile GEX distribution that we used to analyse the DLS results:

$$A_{III}(M)=k. M^p \exp[-(M/M^*)^s] \quad (8)$$

where  $M^*$  a characteristic molar mass. This function yielded a good fit of the data. The calculated values are compared with the experimental values in figure 6a. Satisfactory agreement with the data was obtained using the same values for  $p$  (1.7) and  $s$  (1) at each pH, but different values of  $M^*$ . We have assumed that peak I contained about 5% of the proteins at each pH, but the results are not sensitive to the exact value. The fraction in peak II increased with increasing pH: 15, 20, 33, 37% at pH 5.75, 5.8, 5.9 and 6.0, respectively. The corresponding mass distributions of the microgels ( $A_{III}(M)$ ) are shown in figure 9a.

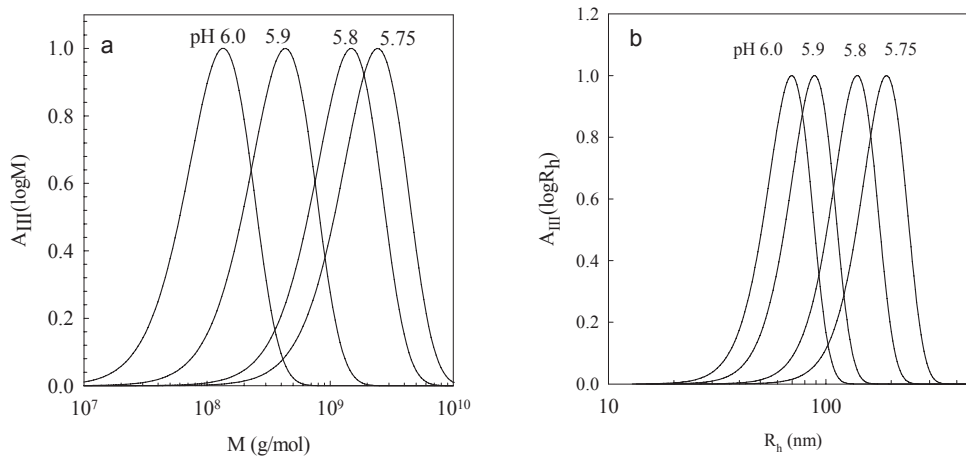


Figure 9. Distribution of the molar mass (a) and the hydrodynamic radius (b) of the microgels formed by heating solutions 85°C until steady state was reached. For clarity the distributions were normalized. The pH was set before heating at different values indicated in the figure.  $C = 40 \text{ g.L}^{-1}$  except at pH 5.75 where  $C = 30 \text{ g.L}^{-1}$ .

In order to calculate the distribution of  $R_h$  we have assumed that the aggregates of fraction III are spherical and homogeneous, which means that  $R_h = a.M^{1/3}$ . This assumption is justified by transmission electron microscopy (TEM) images which showed that the particles were approximately spherical. Experimentally,  $R_{hz}$  was derived from the average diffusion coefficient and can be calculated as:

$$R_{hz} = M_w \left[ \int_0^M R_h^{-1} \cdot M \cdot A(M) dM \right]^{-1} \quad (9)$$

Knowing  $A(M)$ , the only adjustable parameter in the calculation of  $R_{hz}$  is the prefactor  $a$ ,

$$\rho = \frac{M}{\frac{4}{3}\pi R_h^3 \cdot N_A}$$

which depends on the protein concentration in the microgels:  $\rho = \frac{M}{\frac{4}{3}\pi R_h^3 \cdot N_A}$ . The values of  $a$  and thus  $\rho$  that led to the best fits (see figure 6b) varied somewhat for the different pH values investigated: 0.12, 0.185, 0.164 and 0.106 g.mL<sup>-1</sup> for pH 6.0, 5.9, 5.8 and 5.75, respectively, but the variation is probably not significant in view of the sensitivity of the calculated  $\rho$  values to small errors in  $R_h$ . The corresponding size distributions ( $A_{III}(R_h)$ ) are shown in figure 9b.

It is important to realize that the values of  $R_{hz}$  and  $M_w$  plotted in figure 4 are averages over all the aggregates present in the samples that are mainly microgels in this pH range, but also contain small strands. The fraction of small strands increases with increasing pH, which partially explains the strong decrease of  $R_{hz}$  and  $M_w$  with increasing pH. The true size of the microgels decreases less strongly with increasing pH than suggested by figure 4, especially between pH 6.0 and 6.2.

### 3. Evolution of the system during heating.

The system can be quenched at different stages of the aggregation process by rapid cooling to room temperature. In this way the composition and the structure of the aggregates can be characterized as a function of heating time. We will present here a detailed characterization of the system at pH 5.8 at  $C = 40$  g.L<sup>-1</sup>, where a stable suspension of mainly microgels (80%) is formed. We determined the residual fraction of native proteins; the fraction of small strands and the fraction of microgels in the same way as described above. The fraction of denatured monomers and oligomers was in all cases at most a few percent and is ignored in the following. The results obtained as a function of heating time at 75°C and 70°C are shown in figure 10. At both temperatures we find that native proteins are initially converted into microgels and only at a later stage also into small strands. The same was found very recently by Moitzi et al. (Moitzi, Donato et al. 2011) during heating at 85°C, pH 5.9 and  $C = 10$  g.L<sup>-1</sup>. Notice that in the latter study (Moitzi, Donato et al. 2011), the small strands were called soluble aggregates. The conversion rate is much smaller at 70°C than at 75°C in agreement with the strong temperature dependence discussed above and about 30% of the proteins is still in the native state after 24h heating at 70°C.

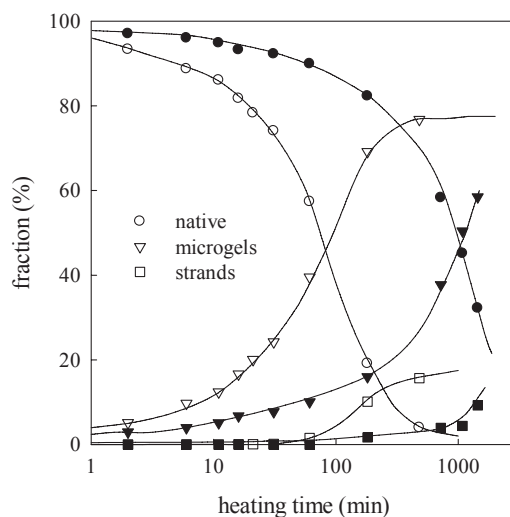


Figure 10. Fraction of native proteins, small strands and microgels in  $\beta$ -lg solutions as a function of heating time at 75°C (open symbols) or 70°C (filled symbols) (pH = 5.8, C = 40 g.L<sup>-1</sup>).

The hydrodynamic radius of the microgels was determined using dynamic light scattering.  $R_{hz}$  is plotted as a function of the fraction of aggregated proteins ( $F_a$ ) in figure 11. At both temperatures we observed a sharp increase of  $M_w$  and  $R_{hz}$  at conversions up to about 30% and almost no growth during further conversion. Notice that it took about 40 min to reach 30% conversion at 75°C and 6 h at 70°C, see figure 10. Growth at low conversions and stagnation of the radius at higher conversion was already reported by Aymard et al.(Aymard, Gimel et al. 1996) for  $\beta$ -lg solutions heated at pH 7.0. Zuniga et al.(Zuniga, Tolkach et al. 2010) observed an almost constant radius already after a short heating time at 80°C between pH 6.0 and pH 6.8. An almost constant radius was also rapidly found at pH 5.9 by Moitzi et al.(Moitzi, Donato et al. 2011). A possible reason for the stagnation of growth once the aggregates have reached a critical size may be that accumulation of charge at the surface inhibits merging with other aggregates. This would explain why the microgels are larger closer to pI where the net surface charge is lower.

Bigger particles were formed at 70°C ( $R_{hz} = 300$  nm) than at 75°C ( $R_{hz} = 110$  nm), which may be surprising as we had found no significant effect of the temperature on the particle size between 75°C and 85°C. Bromley et al.(Bromley, Krebs et al. 2006) also observed an increase of the particle size at lower temperatures at pH 5.3 and attributed it to the lower fraction of denatured proteins available for aggregation.

The number concentration of microgels ( $v$ ) can be calculated if it is assumed that their density is constant ( $\rho \approx 0.15 \text{ g.ml}^{-1}$ ):  $v = CF_a / (4/3 \pi R^3 \rho)$ . The insert of figure 11 shows that  $v$  decreases initially sharply, but stagnates above about 20% conversion. The number of microgels can only decrease by fusion of two microgels into one larger microgel. This means that during the early stage of the aggregation process microgels grow by fusion and at the later stage by addition of proteins to existing microgels.

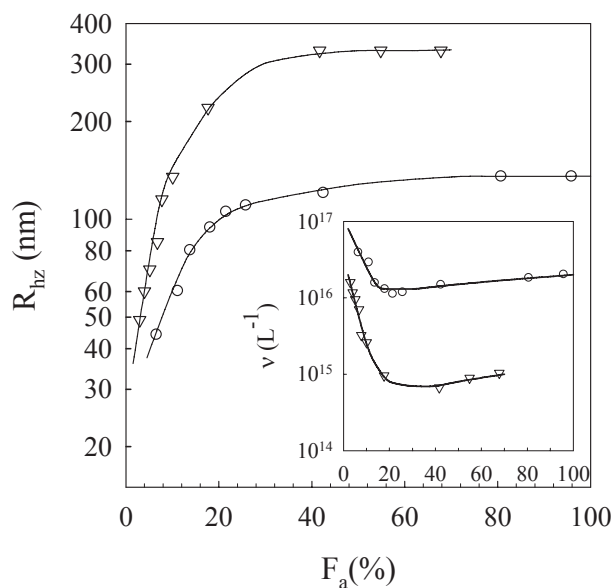
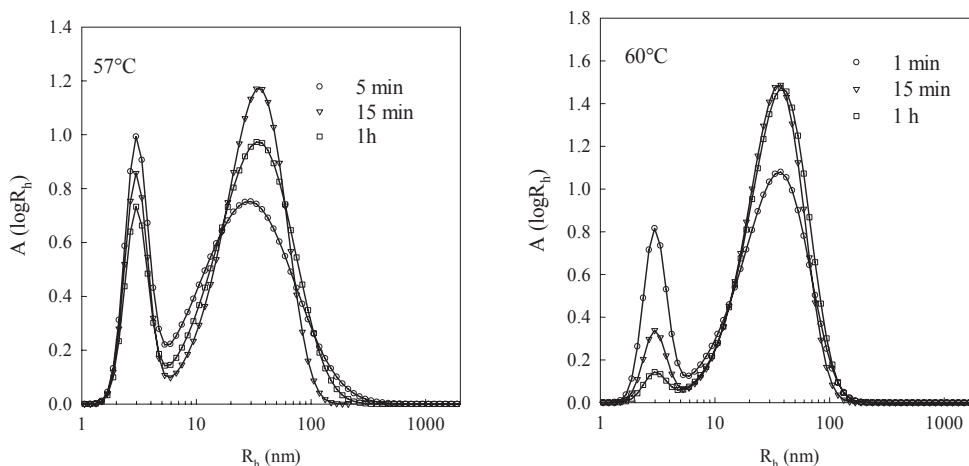


Figure 11. z-average hydrodynamic radius of the microgels as a function of the fraction of aggregated proteins in  $\beta$ -lg solutions that were heated for different times at 75°C (circles) or 70°C (triangles). (pH 5.8,  $C = 40 \text{ g.L}^{-1}$ ). The insert shows the number concentration of microgels.

Even though it takes more than 24 hours to reach steady state at 70°C, the system evolved rapidly already during the first few minutes of heating. In order to study in more detail the initial phase of the aggregation process, we heated at even lower temperatures (65°C, 60°C and 57°C) where steady state cannot be obtained within a period of days. During the first hour of heating at these temperatures the fraction of proteins that aggregated was too small to be measured accurately and SEC showed only a peak corresponding to native proteins. Nevertheless, the aggregates contributed significantly to the light scattering, because the signal is proportional to the molar mass that is orders of

magnitude larger for the aggregates than for the native proteins. Therefore one can observe the aggregates with light scattering even if their weight fraction is very small.

Solutions obtained after heating at 70, 65, 60 and 57°C for different times were diluted and characterized with DLS. Relaxation time distributions were obtained and transformed into distributions of the hydrodynamic radius ( $A(\log R_h)$ ) using the Stokes-Einstein relation, see Materials and methods section. The distributions are shown in figure 12 and in many cases contain two peaks: one at  $R_h \approx 3$  nm representing native proteins and one centered at larger  $R_h$  representing the aggregates. We note that unheated protein solutions contained a small fraction of aggregates and showed a peak situated at  $R_h \approx 100$ nm, but its relative amplitude was much smaller than after 5 min at 57°C, see figure S6 of the supplementary information. It is clear that the very first step of the aggregation process is the formation of aggregates with  $R_h$  centered at about 40nm. As aggregation proceeded more native proteins were converted into aggregates with the same size. When  $F_a$  became larger than a few percent the aggregates started to grow. This can be clearly seen at 70°C for which the DLS results are shown in fig. 12 for heating times up to 24h. Size distributions obtained by DLS as a function of heating time at pH 7.0 showed a similar bimodal distribution during the very early stage of the aggregation process, but the aggregates were much smaller in this case ( $R_{hz} \approx 10$ nm).(Aymard, Gimel et al. 1996)



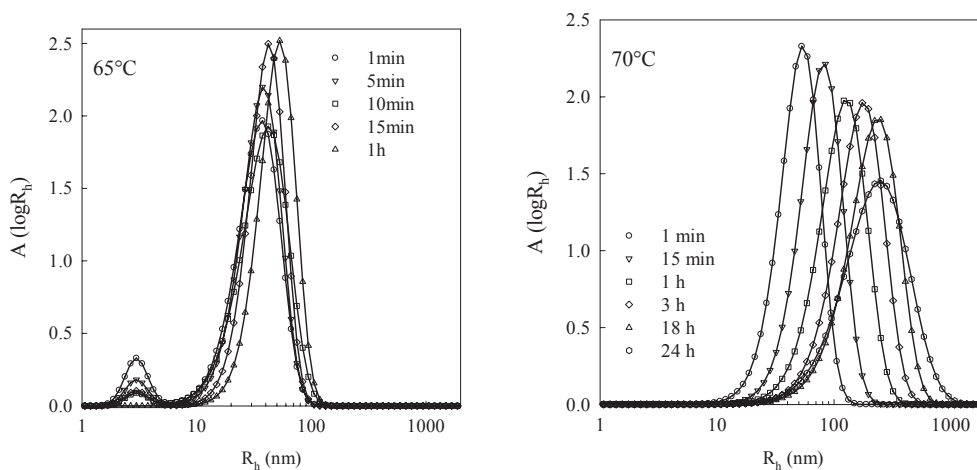


Figure 12. Amplitude of the light scattering signal as a function of the hydrodynamic radius for  $\beta$ -Ig solutions heated for different times and at different temperatures indicated in the figures (pH 5.8,  $C = 40 \text{ g.L}^{-1}$ ).

**pH during heating.** We found that the pH increased during heating, which is an important observation that was already reported in the literature. (Donato, Schmitt et al. 2009; Moitzi, Donato et al. 2011) The relative increase of the pH was less important when starting at higher pH and was no longer significant at pH 6.9. The effect appears to be stronger at lower protein concentrations. The increase of the pH is correlated to the conversion of native proteins into aggregates, which can be clearly seen in figure 13 where the fractions of aggregates and native proteins are plotted as a function of the pH for 70°C and 75°C. Figure 10 shows that when plotted as a function of heating time the results obtained at the two temperatures were very different, because of the different aggregation rates. Remarkably, when the same results are plotted as a function of the pH, they are quite similar. In this representation it can be seen that at both temperatures small strands started to form only when  $\text{pH} > 6.1$ . It is clear, however, that not all residual native proteins converted into strands as soon as the pH rises above 6.1, because the fraction of proteins that converted into microgels also continued to rise. In other words, only microgels were formed as long as the pH remained less than 6.1, but when it rose above 6.1 the residual native proteins could either form small strands or could be incorporated into the already formed microgels.

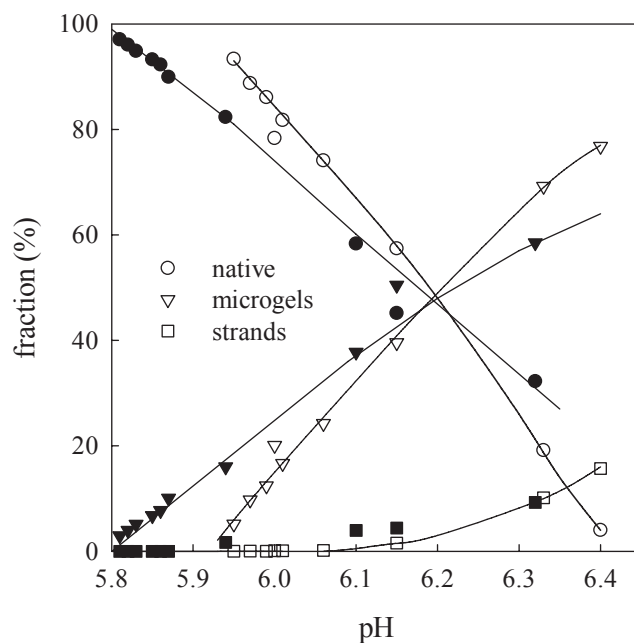


Figure 13. Fraction of native proteins, small strands and microgels in  $\beta$ -lg solutions as a function of the pH obtained after heating for different times at 75°C (open symbols) or 70°C (filled symbols) (pH = 5.8,  $C = 40 \text{ g.L}^{-1}$ ).

When the pH was maintained at  $\text{pH} \leq 6.0$  during heating a precipitate was formed similar to that observed for solutions with starting  $\text{pH} \leq 5.7$ . Stable suspensions were obtained only if the pH was maintained at pH 6.1 or higher during heating. This is an important observation, because it shows that the increase of the pH driven by the formation of microgels is a necessary condition to obtain stable suspensions. We expect that the same phenomena occur at other protein concentrations below 50g/L except that the critical pH for the transition between the formation of microgels and strands shifts to slightly higher values at lower protein concentrations, see figure 7.

It should be realized that even though the pH increases the number of  $\text{H}^+$  ions that are depleted from the solution (order  $10^{-6} \text{ M}$ ) is negligible compared to the number of proteins (order  $10^{-4} \text{ M}$ ). Therefore the average net charge of the proteins is practically the same, but the pH at this net charge density is different for microgels. The proteins have a large buffering capacity so that the pH is determined by the structure of protein aggregates and not by their concentration. The fact that the pH after formation of the microgels varies with the concentration implies that the structure of the microgels is different. Why this leads to a higher critical pH cannot be answered by the measurements done in this study.

#### **4. Mechanism of the formation and self-stabilisation of protein microgels.**

Stable suspensions of protein strands or spherical microgels can be formed by heating  $\beta$ -lg at  $\text{pH} \geq 5.75$  at low ionic strength and at concentrations below about  $50 \text{ g.L}^{-1}$ . Light scattering experiments suggest that the microgels are formed by a process of nucleation and growth, where the growth involves fusion of smaller particles. Here we have shown that the pH is a crucial parameter for the formation of stable microgel suspensions. A very small increase of the pH at a critical value results in the formation of strands rather than microgels. The critical pH increases weakly with decreasing protein concentration from about 6.1 at  $40 \text{ g/L}$  to 6.4 at  $10 \text{ g/L}$ . In general, protein aggregate suspensions are stabilized by electrostatic repulsion, which explains why they associate and gel at increasingly lower concentrations if more salt is present during heating. If the initial pH is set lower than 5.75 or if the pH is maintained below the critical pH during heating, the electrostatic repulsion between the aggregates is not sufficient and a fraction of the proteins precipitates even at very low protein concentrations.

The reason that stable microgel suspensions are formed is that the pH increases during the aggregation process. We hypothesize that the pH increase is caused by partial charge neutralization of proteins in the interior of the microgels, which leads to depletion of  $\text{H}^+$  ions, that is for a large part compensated by an increased charge density of the residual native proteins and probably the proteins at the surface of the microgels. The increased surface charge density may account for the stability of the suspensions as it leads to an increase of electrostatic repulsion between the microgels as already reported from  $\zeta$ -potential measurements.<sup>5</sup> We may therefore conclude that without pH-regulation the particles self-stabilize via the increase of the surface charge density. The increase of the pH and concomitant increase of the charge density of the residual native proteins also explains the formation of small strands at the later stage of the aggregation process. This idea is corroborated by the observation that when the pH was maintained below the critical pH during heating almost no small strands were formed.

#### **Conclusion**

When the pH is set within a small range between 5.75-6.0 in the absence of added salt, stable suspensions of spherical protein microgels can be formed by heating  $\beta$ -lg at concentrations between 10 and  $50 \text{ g.L}^{-1}$ . The hydrodynamic radius of the microgels

increases with decreasing pH between about 75 and 200nm, but the protein concentration within the microgels remains approximately constant at about 0.15 g.mL<sup>-1</sup>. At pH ≤ 5.7, secondary aggregation leads to precipitation of protein. At pH ≥ 6.1 mostly small protein strands with a hydrodynamic radius of 15-20 nm are formed. At higher concentrations the same aggregates are still formed as a first step, but they subsequently associate into larger self-similar aggregates or form a gel above a critical gel concentration. In addition to the aggregates, denatured monomers and oligomers are formed, but they represent less than 5% at the higher protein concentration investigated here.

The aggregation process starts by the formation of a distinct population of well-defined nuclei. As the aggregation proceeds, initially, more nuclei of the same size are formed, but as soon as a few percent of the proteins has converted, the nuclei grow by fusion and addition of denatured proteins.

The formation of the microgels causes an increase of the pH, which in turn increases the electrostatic repulsion between the microgels. The latter is necessary to obtain stable suspensions, because if the pH is fixed at a value below 6.1 a fraction of the proteins precipitates. Thus the process of microgel formation self-stabilizes the suspensions if the initial pH is set between pH 5.75 and 6.1. The increase of the pH leads to the formation of small aggregates in addition to the microgels at the later stage of the aggregation process.

### **Acknowledgements**

Martine Rouvet (Nestlé Research Center, Lausanne) is thanked for carrying out the transmission electron microscopy experiments and Magali Martin (PCI, Le Mans) for doing the SEC experiments.

### **References**

1. Hambling, S. G.; Mc Alpine, A. S.; Sawyer, L.,  $\beta$ -lactoglobulin. In *Advanced Dairy Chemistry -1 : Proteins*, Fox, P. F., Ed. Elsevier Applied Science: London, 1992; pp 141-190.
2. Nicolai, T.; Britten, M.; Schmitt, C.,  $\beta$ -lactoglobulin and WPI aggregates: Formation, structure and applications. *Food Hydrocolloids* **2011**, 25 1945.

3. Pouzot, M.; Nicolai, T.; Visschers, R. W.; Weijers, M., X-ray and light scattering study of the structure of large protein aggregates at neutral pH. *Food Hydrocolloids* **2005**, 19, 231-238.
4. Aymard, P.; Gimel, J. C.; Nicolai, T.; Durand, D., Experimental evidence for a two-step process in the aggregation of  $\beta$ -lactoglobulin at pH7. *Journal de chimie physique* **1996**, 93, 987-997.
5. Schmitt, C.; Bovay, C.; Vuilliomenet, A. M.; Rouvet, M.; Bovetto, L.; Barbar, R.; Sanchez, C., Multiscale Characterization of Individualized beta-Lactoglobulin Microgels Formed upon Heat Treatment under Narrow pH Range Conditions. *Langmuir* **2009**, 25, (14), 7899-7909.
6. Jung, J. M.; Savin, G.; Pouzot, M.; Schmitt, C.; Mezzenga, R., Structure of heat-induced beta-lactoglobulin aggregates and their complexes with sodium-dodecyl sulfate. *Biomacromolecules* **2008**, 9, (9), 2477-2486.
7. Donato, L.; Schmitt, C.; Bovetto, L.; Rouvet, M., Mechanism of formation of stable heat-induced beta-lactoglobulin microgels. *International Dairy Journal* **2009**, 19, (5), 295-306.
8. Moitzi, C.; Donato, L.; Schmitt, C.; Bovetto, L.; Gillies, G.; Stradner, A., *Food Hydrocolloids*, accepted **2011**.
9. Schmitt, C.; Moitzi, C.; Bovay, C.; Rouvet, M.; Bovetto, L.; Donato, L.; Leser, M. E.; Schurtenberger, P.; Stradner, A., Internal structure and colloidal behaviour of covalent whey protein microgels obtained by heat treatment. *Soft Matter* **2010**, 6, 4876-4884.
10. Nicolai, T., Food structure characterisation using scattering methods. In *Understanding and controlling the microstructure of complex foods*, McClements, D. J., Ed. Woodhead: Cambridge, 2007; pp 288-310.
11. Brown, W., *Light Scattering : Principles and development*. Clarendon Press: Oxford, 1996.
12. Berne, B. J.; Pecora, R., *Dynamic Light Scattering*. Oxford University Press: Oxford, 1993.
13. Nicolai, T.; Gimel, J. C.; Johnsen, R., Analysis of relaxation functions characterized by a broad monomodal relaxation time distribution. *Journal de physique II* **1996**, 6, 697-711.
14. Verheul, M.; Roefs, S. P. F. M.; De Kruif, K. G., Kinetics of heat-induced aggregation of  $\beta$ -lactoglobulin. *J. Agric. Food Chem.* **1998**, 46, 896-903.

15. Zuniga, R. N.; Tolkach, A.; Kulozik, U.; Aguilera, J. M., Kinetics of Formation and Physicochemical Characterization of Thermally-Induced beta-Lactoglobulin Aggregates. *Journal of Food Science* **2010**, 75, (5), E261-E268.
16. Le Bon, C.; Nicolai, T.; Durand, D., Kinetics of Aggregation and Gelation of Globular Proteins after Heat-Induced Denaturation. *Macromolecules* **1999**, 32, 6120-6127.
17. Tolkach, A.; Kulozik, U., Effect of pH and temperature on the reaction kinetic parameters of the thermal denaturation of beta-lactoglobulin. *Milchwissenschaft-Milk Science International* **2005**, 60, (3), 249-252.
18. Mehalebi, S.; Nicolai, T.; Durand, D., Light scattering study of heat-denatured globular protein aggregates. *Int. J. Biol. Macromol.* **2008**, 43, 129-135.
19. Durand, D.; Gimel, J. C.; Nicolai, T., Aggregation, gelation and phase separation of heat denatured globular proteins. *Physica A: Statistical Mechanics and its Applications* **2002**, 304, (1-2), 253-265.
20. Bromley, E. H. C.; Krebs, M. R. H.; Donald, A. M., Mechanisms of structure formation in particulate gels of beta-lactoglobulin formed near the isoelectric point. *European Physical Journal E* **2006**, 21, (2), 145-152.
21. Krebs, M. R. H.; Devlin, G. L.; Donald, A. M., Amyloid Fibril-Like Structure Underlies the Aggregate Structure across the pH Range for beta-Lactoglobulin. *Biophysical Journal* **2009**, 96, (12), 5013-5019.

## Supplementary information

### Effect of the heating temperature

Figure S1 shows that the heating temperature does not influence the size of the microgels at least if  $T \geq 75^\circ\text{C}$ .

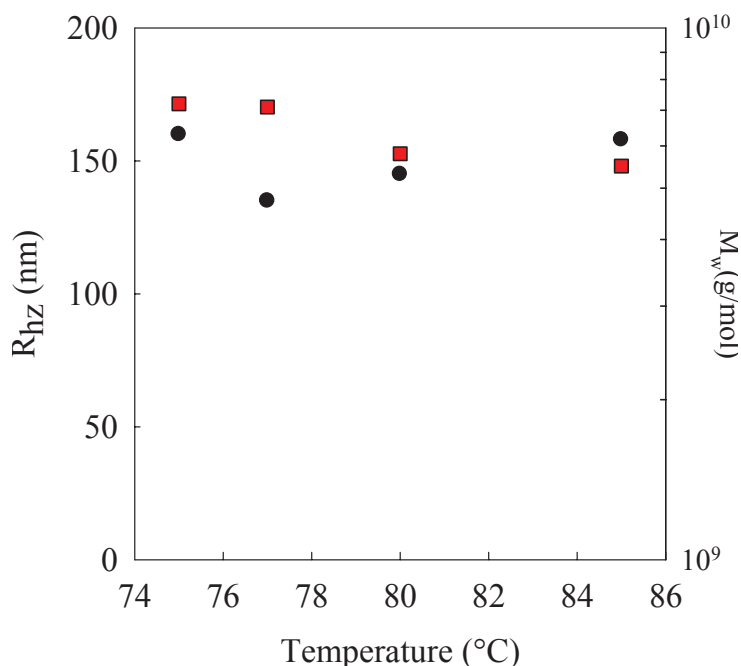


Figure S1. Dependence of the weight averaged molar mass and the z-averaged hydrodynamic radius of aggregates formed by heating  $\beta$ -lg solutions ( $\text{pH}=5.8$ ,  $C=10\text{g/L}$ ) until steady state was reached as a function the heating temperature.

### Determination of the protein concentration in the supernatant.

The protein concentration of the supernatant was determined by measuring the optical absorbance (OA) of the solutions. After heating the solutions were turbid which contributed to the measured OA. The turbidity decreased with increasing wavelength following a power law, see fig. S2 and was subtracted from the data. The OA of the heated samples at pH 5.8 was larger than that of the native proteins and had different wavelength dependence, see figure S3. Such a difference was not observed for samples heated at  $\text{pH}>6.1$ .

Figure S4 shows results for supernatants obtained at different rotor speeds after dilution by the same factor. As expected the OA decreased with increasing rotor speed, but

also the wavelength dependence changed. This is better seen if the data are normalized by the peak value at  $\lambda=280\text{nm}$ , see fig. S5. Comparison with native proteins shows that for centrifugal forces larger than about 4000g, the absorption spectrum is the same as that of native proteins. Notice that at these rotor speeds the supernatant contains relatively little protein in the form of microgels.

In order to derive the protein concentration at larger rotor speeds we have assumed that the supernatant consists of two populations of proteins with fractions  $F_1$  and  $F_2$ , respectively. Smaller aggregates that absorb like native proteins ( $OA_1$ ) and larger aggregates (microgels) that absorb more strongly ( $OA_2$ ):  $OA=F_1.OA_1+F_2.OA_2$ .  $F_2$  was assumed to be negligible at 4000g and  $F_1$  was calculated using the extinction coefficient of native proteins.  $F_1$  is constant up to about 4000g and decreases weakly at higher rotor speeds. For lower rotor speeds the contribution of the larger aggregates was calculated as  $F_2.OA_2=OA-F_1.OA_1$ . The wavelength dependence of  $OA_2$  was found to be almost the same for all supernatants, which justifies our assumption of two distinct populations. Before centrifugation  $F_2=(1-F_1)$ , which enabled us to deduce  $OA_2$ . The values of  $F_2$  at higher rotor speeds were obtained by fitting  $OA$  to  $F_1.OA_1+F_2.OA_2$ , see solid lines in fig. S4.

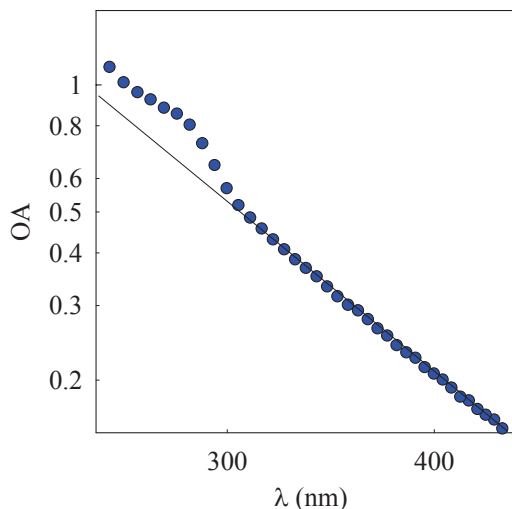


*Figure S2. Double logarithmic representation of the optical absorption before correction for the turbidity. The solid line represents the power law dependence of the turbidity.*

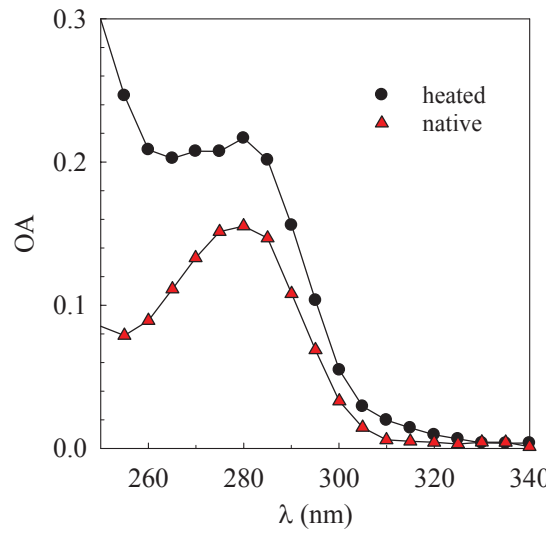


Figure S3. Optical absorption after correction for the turbidity before and after heating.

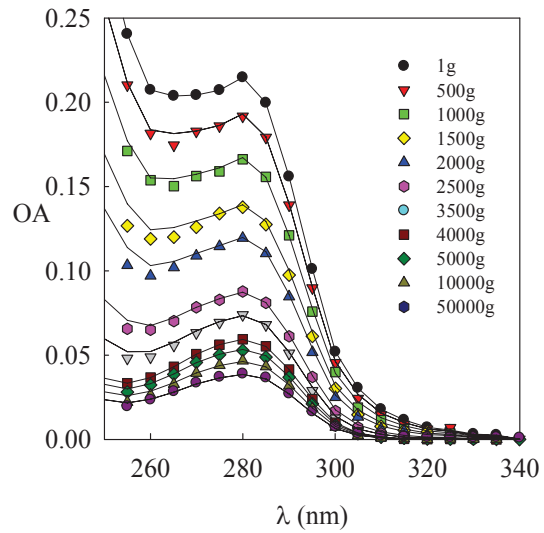


Figure S4. Optical absorption after correction for the turbidity of the supernatants of heated samples after centrifugation at different rotor speeds. The solid lines represent  $F_1.OA_1+F_2.OA_2$ , see text.

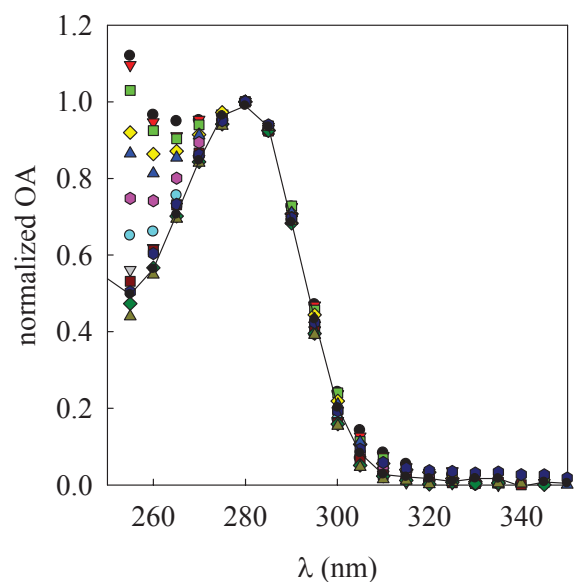


Figure S5. Normalized optical absorption after correction for the turbidity of the supernatants of heated samples after centrifugation at different rotor speeds. The filled symbols represent the results for native proteins. The open symbols are as in figure S4.

#### Dynamic light scattering results for unheated $\beta$ -lg.

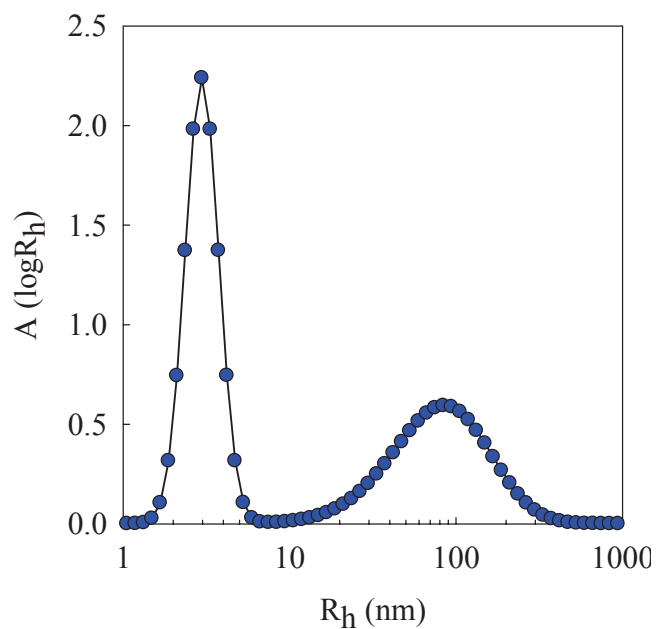


Figure S6. Amplitude of the light scattering signal as a function of the hydrodynamic radius for a dilute solution of unheated  $\beta$ -lg.



## PAPER II

### **Heat induced formation of beta-lactoglobulin microgels driven by addition of calcium ions**

#### **Abstract**

Stable suspensions of spherical protein particles (microgels) can be formed by heating beta-lactoglobulin solutions in the presence of calcium ions. The conditions for the calcium induced microgel formation were studied at different pH between 5.8 and 7.5 and different protein concentrations between 5 – 100 g/l. The results showed that a critical molar ratio of calcium to proteins ( $R$ ) is needed to form microgels independent of the protein concentration.  $R$  decreases with decreasing pH. The microgels have a hydrodynamic radius ranging from 100 to 300 nm and their internal protein concentration ranges from 0.2 to 0.45 g/ml. The amount of calcium bound to the proteins was determined and the results suggest that the crucial parameter for microgel formation is the net charge density of the native proteins. The microgel suspensions are stable in a narrow range of  $R$  but the microgels aggregate at higher calcium concentrations.

---

Tuan Phan-Xuan, Dominique Durand, Taco Nicolai

*LUNAM Université du Maine, IMMM UMR-CNRS, Polymers, Colloids, Interfaces, 72085  
Le Mans Cedex 9, France.*

Laurence Donato, Christophe Schmitt, Lionel Bovetto

*Food Science and Technology Department, Nestec Ltd, Nestlé Research Center, P.O. Box  
44, CH-1000 Lausanne 26, Switzerland.*

Published in *Food Hydrocolloids* <http://dx.doi.org/10.1016/j.foodhyd.2012.09.008>

## Introduction

Beta-lactoglobulin ( $\beta$ -lg), which is the major whey protein in cow's milk, is a globular protein with a molar mass of  $18.2 \text{ kg}\cdot\text{mol}^{-1}$ , a radius of about 2 nm and an iso-electric point  $\text{pI} = 5.2$  (Hambling, Mc Alpine et al. 1992). In aqueous solution,  $\beta$ -lg denatures when heated and aggregates or even forms a gel if the concentration is sufficiently high. Heat-induced aggregation of  $\beta$ -lg has been studied extensively in past, see for a recent detailed review (Nicolai, Britten et al. 2011). The morphology of the aggregates depends strongly on the pH. In salt free solutions large rigid rod-like aggregates are formed at pH 2-3, whereas closer to the iso-electric point the aggregates are spherical. At  $\text{pH} > 6.3$  small strands are formed at low concentrations that associate at higher protein concentrations into larger randomly branched aggregates with a self-similar structure (Aymard, Gimel et al. 1996; Pouzot, Nicolai et al. 2005).

At and very close to  $\text{pI}$ ,  $\beta$ -lg aggregates do not form stable suspensions, but associate and eventually precipitate. However, it was found that in a narrow range of the pH just above  $\text{pI}$  (around pH 5.9) and just below  $\text{pI}$  (around pH 4.6) stable suspensions of rather monodisperse spherical particles were formed with a radius of about a hundred nanometers (Schmitt, Bovay et al. 2009); (Jung, Savin et al. 2008); (Donato, Schmitt et al. 2009); (Moitzi, Donato et al. 2011). These spherical particles were called microgels and can also be formed by whey protein isolate (WPI) that contains a majority of  $\beta$ -lg together with other globular proteins such as  $\alpha$ -lactalbumin (Schmitt, Moitzi et al. 2010). In a recent study (Phan-Xuan, Nicolai et al. 2011), we have shown that the pH is a crucial parameter for the formation of stable microgel suspensions in pure water. Stable suspensions are only obtained if the pH is set between 5.75 and 6.2 before heating and involves a process of self-stabilization.

The presence of calcium ions enhances heat induced aggregation of  $\beta$ -lg (Sherwin and Foegeding 1997); (Xiong, Dawson et al. 1993), but the specific interaction between  $\text{Ca}^{2+}$  and  $\beta$ -lg is still poorly understood at the molecular level (Simons, Kusters et al. 2002). It has been suggested that three effects or a combination of them might be responsible for calcium-induced protein aggregation:

- Intermolecular cross linking of adjacent negatively charged or carboxylic groups by the formation of protein- $\text{Ca}^{2+}$ -protein complexes ((Bryant and McClements 1998); (Hongsprabhas, Barbut et al. 1999); (Xiong, Dawson et al. 1993);

- Reduction of the net negative charge of the proteins by binding of calcium ions (Hongprabhas and Barbut 1997);
- Ion induced conformation changes, which lead to altered hydrophobic interactions and aggregation at elevated temperatures ((Kinsella 1989); (Wang and Damodaran 1991)).

However, (Xiong, Dawson et al. 1993) demonstrated that the role of  $\text{Ca}^{2+}$  in the formation of intermolecular bridges was unlikely and that the main effect of  $\text{Ca}^{2+}$  is to reduce the net protein charge. Excess  $\text{Ca}^{2+}$  may even have an inhibitory effect on the protein aggregation rate (Roefs S.P.F.M. 2001).

(Sherwin and Foegeding 1997) demonstrated that aggregation rates were affected by  $\text{CaCl}_2$ /protein stoichiometry rather than the  $\text{Ca}^{2+}$  and protein concentrations separately. (Simons, Kusters et al. 2002) suggested that calcium was bound to carboxylates with a threshold affinity. Subsequent site specific screening of surface charges resulted in protein aggregation, driven by partial unfolding of  $\beta$ -lg at elevated temperatures, which was facilitated by the absence of electrostatic repulsion.

The aim of the study presented here was to investigate the effect of adding calcium ions on the formation of stable  $\beta$ -lg microgel suspensions. We will first discuss in detail the effect of adding  $\text{CaCl}_2$  on heat induced aggregation at pH 6.9 and then show the influence of the pH between 6.0 and 7.5. The size and density of the microgels formed at different conditions was determined using light scattering techniques. Finally, we will discuss the mechanism of the formation and stable  $\beta$ -lg microgels suspensions in the presence of calcium ions and propose a process of self stabilization analogous to that in pure water at lower pH.

## **Materials and methods**

**Materials.** The  $\beta$ -lactoglobulin (Biopure, lot JE 001-8-415) used in this study was purchased from Davisco Foods International, Inc. (Le Sueur, MN, USA). The powder contained about 89.6 wt% protein (Kjeldahl, N x6.38) and the protein composition was 55.4% and 41.6% of the variants A and B, respectively, and less than 2% of other whey proteins (based on HIC-HPLC analysis) (Donato, Schmitt et al. 2009). The powder was dissolved in salt free Milli-Q water with 200 ppm  $\text{NaN}_3$  added to avoid bacterial growth. The solutions were dialysed against the solvent for a period of 8 hours with 4 exchanges of the solvent. The pH was set to the desired value by drop wise addition of 0.1M HCl or NaOH under vigorous stirring and aliquots of 0.1M or 0.5M  $\text{CaCl}_2$  were added to reach the

desired concentration. Because addition of  $\text{CaCl}_2$  reduces the pH of the solution, we used small amounts of 0.1 M NaOH to bring the pH back to the initial value. The amount of NaOH used to readjust the pH was noted for the calculation of the net charge of protein. The solutions were filtered through 0.2  $\mu\text{m}$  pore size Anotop filters before heating.

The native protein concentration was measured after filtration by UV absorption at 278 nm using an extinction coefficient of  $0.96 \text{ Lg}^{-1}\text{cm}^{-1}$  (Townend, Winterbottom et al. 1960). Solutions were heated at  $85^\circ\text{C}$  for a period between 5 and 15 hours in air tight cylindrical glass vials (7ml) with a diameter of 10 mm using a thermostat water bath. The heating rate was fast as the set temperature was reached within 4 min. The samples were cooled rapidly to  $20^\circ\text{C}$  by holding the vials under running tap water. The fraction of residual native protein after heating was determined by precipitation at pH 4.6 and measuring the UV absorption of the supernatant. We checked by light scattering that no aggregates were present in the supernatant.

Heating led to a small decrease of the pH when it was set above 6.9 (from 7.5 to 7.1 – 7.3 and from 7.2 to 7-7.15) and a small increase of the pH when it was set below 6.9 (from 6 to 6.4 – 6.6, from 6.2 to 6.6 – 6.7 and from 6.4 to 6.7 – 6.9) as was reported for salt free solutions by (Donato, Schmitt et al. 2009)

**Dynamic and static light scattering** measurements were done using a commercial apparatus (ALV-Langen, Germany). The light source was a He-Ne laser with wavelength  $\lambda = 632 \text{ nm}$ . The temperature was controlled by a thermostat bath to within  $\pm 0.2^\circ\text{C}$ . Measurements were made at angles of observation ( $\theta$ ) between 12 and 150 degrees. The relative scattering intensity ( $I_r$ ) was calculated as the intensity minus the solvent scattering divided by the scattering intensity of toluene at  $20^\circ\text{C}$ .

In dilute solutions  $I_r$  is related to the weight average molar mass ( $M_w$ ) and the scattering wave vector ( $q$ ) dependent structure factor ( $S(q)$ ) of the solute (Nicolai 2007) (Brown 1996):

$$I_r / KC = M_w S(q) \tag{1}$$

with  $K$  an optical constant depending on the refractive index increment. We have used for the refractive index increment  $0.189 \text{ mL.g}^{-1}$ . The structure factor describes the dependence of the intensity on the scattering wave vector ( $q$ ) and depends on the structure and the size

of the solute. The z-average radius of gyration ( $R_g$ ) can be determined from the initial q-dependence of S(q):

$$S(q) = \left[ 1 + \frac{q^2 R_g^2}{3} \right]^{-1} \quad qR_g \leq 1 \quad (3)$$

The intensity autocorrelation function was measured with dynamic light scattering (DLS) (Berne and Pecora 1993). In all cases the correlation functions could be described in terms of a narrow relaxation time distribution. The average relaxation rate ( $\Gamma$ ) was found to be proportional to  $q^2$ . In dilute solutions the relaxation is caused by self diffusion of the particles and  $\Gamma$  is related to the diffusion coefficient (D):  $\Gamma = (q^2 \cdot D)$ . The average hydrodynamic radius ( $R_h$ ) may be calculated using the Stokes-Einstein equation:

$$D = \frac{k \cdot T}{6 \cdot \pi \cdot \eta \cdot R_h} \quad (5)$$

with  $\eta$  the viscosity, k Boltzman's constant and T the absolute temperature. The density of the particles was calculated from  $M_w$  and  $R_h$  by assuming that they were spherical:

$$\rho = \frac{M_w}{4 \cdot \pi \cdot R_h^3 N_{av}} \quad (6)$$

with  $N_{av}$  Avogadro's number.

**Confocal Laser Scanning Microscopy (CLSM)** was used in the fluorescence mode. Observations were made with a Leica TCS-SP2 (Leica Microsystems Heidelberg, Germany). A water immersion objective lens was used HCxPL APO 63x NA=1.2 with theoretical resolution of 0.3 $\mu$ m in the x-y plane. A small fraction of  $\beta$ -Ilg was labelled with the fluorochrome rhodamine B isothiocyanate, by adding a small amount of a concentrated rhodamine solution (5ppm) to the  $\beta$ -Ilg solutions before heat treatment. No effect of labelling on the aggregation process was observed.

**Transmission electron microscopy.** The microstructure of heated protein dispersions was investigated by transmission electron microscopy (TEM) using the negative staining method. A drop of the protein dispersion diluted to 0.1wt% in Millipore

water was deposited onto a formvare-carbon coated copper grid. The excess product was removed after 30 s using a filter paper. A droplet of 1% phosphotungstic acid at pH7.0 was added for 15 s, removing any excess. After drying the grid at room temperature for 5 min, observations were made with a FEI Tecnai G2 Spirit BioTWIN transmission electron microscope operating at 120 kV (FEI company, The Netherlands)”. Images were recorded using a Quemesa camera (Olympus soft imaging solutions, Germany).

**Centrifugation experiments** were done at room temperature with an Allegra 64R centrifuge (Beckman Coulter, USA) at  $5 \cdot 10^4$  g during 1 h. The heated  $\beta$ -lg solutions were diluted before centrifugation to  $10 \text{ g}\cdot\text{L}^{-1}$ .

**Calcium binding measurements.** The calcium ion activity in solution was determined using a calcium-specific electrode (Fisher Scientific, USA). A calibration curve was obtained by measuring  $\text{CaCl}_2$  solutions in water at concentrations ranging from 0 to 25 mM. We have calculated the concentration of free calcium ions by assuming that the activity of bound  $\text{Ca}^{2+}$  was zero and the activity of free  $\text{Ca}^{2+}$  was the same as in pure water.

## Results and discussion

### Effect of the calcium concentration on microgel formation at pH 6.9

$\beta$ -lg solutions with different  $\text{CaCl}_2$  ( $C_s$ ) and protein ( $C$ ) concentrations were heated at  $85^\circ\text{C}$  until steady state was reached (5-15h) and the fraction of residual native proteins had become negligible ( $< 5\%$ ). After the samples were cooled to  $20^\circ\text{C}$  they were checked for gelation, defined here by the absence of flow when the vials were tilted. At protein concentrations below about  $10 \text{ g/L}$ , the gels were not self-supporting and precipitation was observed. In pure water, the solutions remained transparent liquids below  $C \approx 95 \text{ g/L}$ , whereas transparent gels were formed at higher concentrations. The critical protein concentration needed to form a gel was lower in the presence of  $\text{CaCl}_2$ , see below.

At higher calcium concentrations, the systems became turbid, see fig. 1. The transition between clear and opaque systems as a function of  $C_s$  was rather sharp and occurred in the liquid state for  $C < 80 \text{ g/L}$  and in the gel state at higher protein concentrations.



Figure 1:  $\beta$ -lg solutions after heating at  $85^{\circ}\text{C}$  during 12h at  $C=40$  g/L,  $\text{pH} = 6.9$  and different  $\text{CaCl}_2$  concentrations:  $C_s= 0$  mM (0), 2.15 mM (1), 3.23 mM (1.5), 4.3 mM (2). The numbers between parentheses indicate the molar ratio of  $\text{CaCl}_2$  to  $\beta$ -lg.

CLSM images, showed no distinguishing features for the transparent solutions and gels. As was mentioned in the introduction, in the absence of added salt aggregates are formed resembling curved short strands with a length of about 50nm and a diameter of about 10nm that are smaller than the resolution of CLSM. At high protein concentration these strands aggregate and form homogeneous gels. The CLSM images of turbid solutions showed particles at the limit of the resolution of the light microscope, see fig.2a. More detailed characterization of the systems using light scattering, see below, showed that these aggregates are similar to the microgels that are formed in pure water at lower pH. Turbid gels appear to be system spanning networks formed by randomly aggregated microgels, see fig.2b.

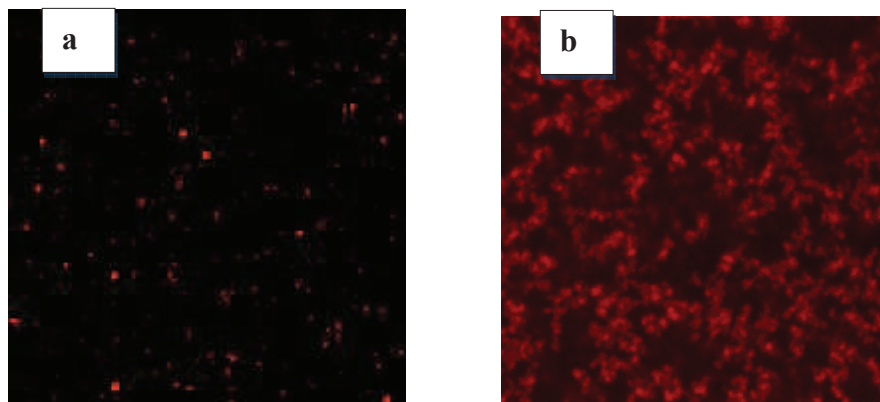


Figure 2: CLSM images of a stable microgel suspension formed at  $C = 40$  g/L and  $C_s = 5.38$  mM (2.5) (a) and a gel formed at  $C = 40\text{g/L}$  and  $C_s= 8.6$  mM (4). The images represent  $40\times 40\mu\text{m}$

We have shown earlier (Phan-Xuan, Nicolai et al. 2011) that the microgels sediment when centrifuged at  $5.10^4$  g for 1h, whereas most of the small strands remained

in the supernatant. In this way the fraction of proteins that formed microgels (F) could be determined, see fig. 3a. Within the experimental uncertainty, F did not depend on the protein concentration and increased from about 20% at R=1 to more than 90% at R=2.5. To illustrate that two distinct populations of aggregates are formed we show a transmission electron microscopy image of the system at R=1.75, see fig.3b. One can clearly observe both the approximately spherical microgels and the small strand-like aggregates.

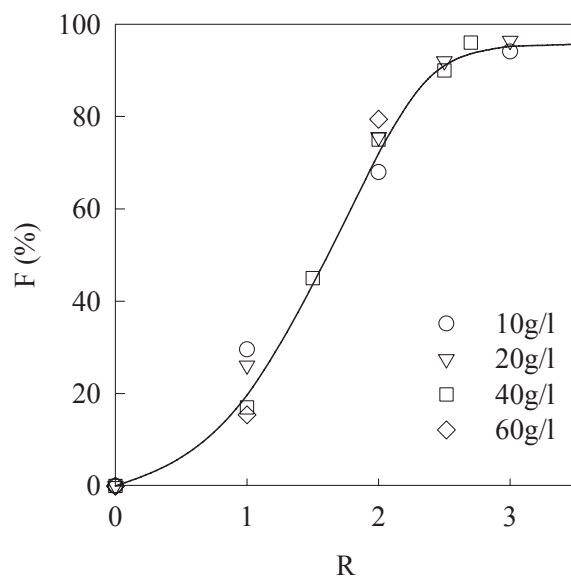


Figure 3a: Fraction of proteins that form microgels at pH 6.9 as a function of the molar ratio of  $\text{CaCl}_2$  to  $\beta\text{-lg}$  at different protein concentrations indicated in the figure. The solid line is a guide to the eye

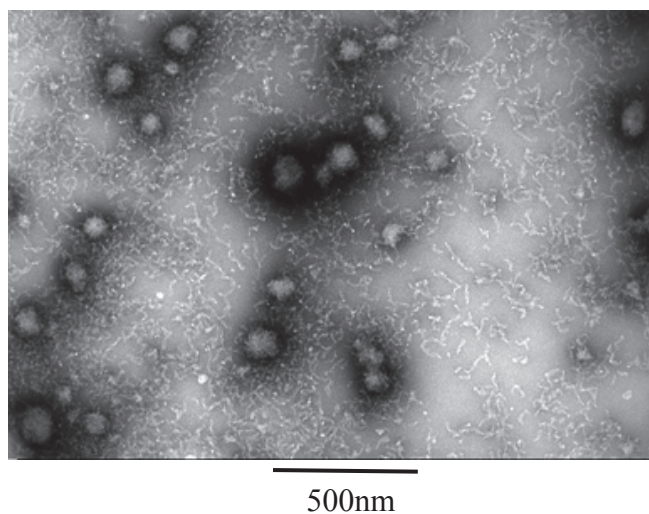


Figure 3b: TEM image of stable microgel suspension formed at pH 6.9,  $C = 40 \text{ g/L}$  and  $R=1.75$

Four different states could be distinguished after heating: I) transparent liquid; II) turbid liquid containing microgels; III) transparent gel; IV) turbid gel or precipitate. A state diagram was composed as a function of  $\text{CaCl}_2$  and protein concentrations, see fig.4a. An alternative representation in terms of the molar ratio between  $\text{Ca}^{2+}$  and  $\beta\text{-Ig}$  ( $R$ ) is shown in fig.4b. The critical  $\text{CaCl}_2$  concentration above which a gel or a precipitate is formed increased with increasing protein concentration up to  $C \approx 60\text{g/L}$  and then decreased. However, the critical ratio decreased progressively with increasing protein concentration.

The boundary between the formation of strands and microgels was defined in the liquid state by the values of  $C_s$  or  $R$  where  $F \approx 0.5$ , whereas in the gelled state it was determined by the transition from a homogeneous to a heterogeneous structure in CLSM images as illustrated in Figure 2. Remarkably, the transition between the formation of strands and microgels occurred at almost the same ratio ( $R=1.5$ ) at all concentration investigated.

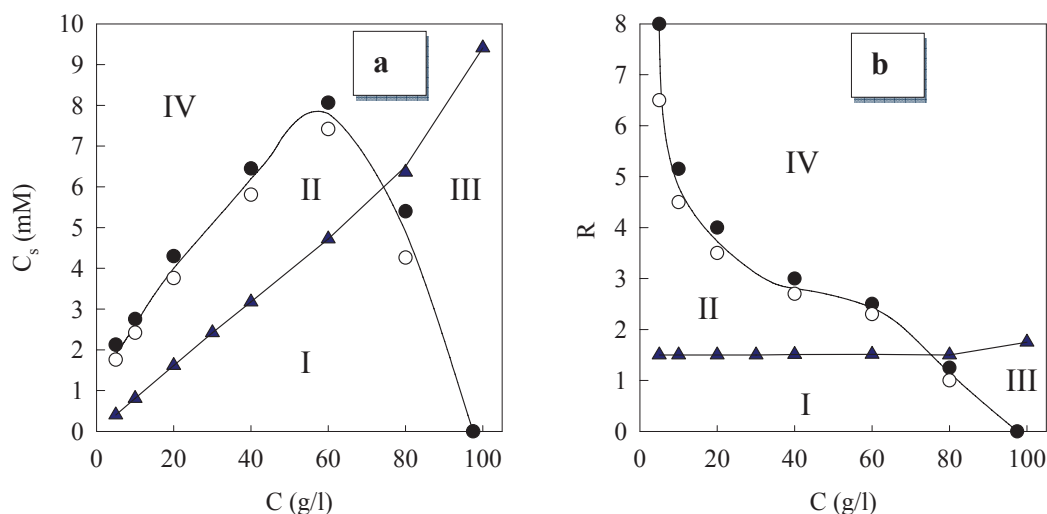


Figure 4: State diagram of heated  $\beta\text{-Ig}$  solutions as a function of  $C$  and  $C_s$  (a) or  $C$  and  $R$  (b) at pH 6.9. The open and close circles indicate solutions and gels, respectively. The blue triangles indicate the boundary between formation of small strands and microgels. Lines are guides to the eye. Four different states are distinguished: transparent liquid (I); turbid liquid containing microgels (II); transparent gel (III); turbid gel or precipitate (IV).

The region where stable microgel suspensions can be formed is rather small. In fact, the region in which individual microgels are formed is even smaller than domain (II), because close to the gel line the microgels associate into larger aggregates. The range of calcium concentrations in which stable suspensions of individual microgels can be formed narrows with increasing protein concentration.

We have determined the hydrodynamic radius ( $R_h$ ), and the density ( $\rho$ ) of the microgels using static and dynamic light scattering, see materials and methods. In order to avoid the effects of interaction and multiple scattering, measurements were made on highly diluted solutions. Earlier we reported that the  $R_h$  of microgels formed in pure water in the pH range between 5.75 and 6.1, varied between 60 nm to 200 nm with the larger microgels formed at lower pH. The density of these microgels was about 0.2g/ml.

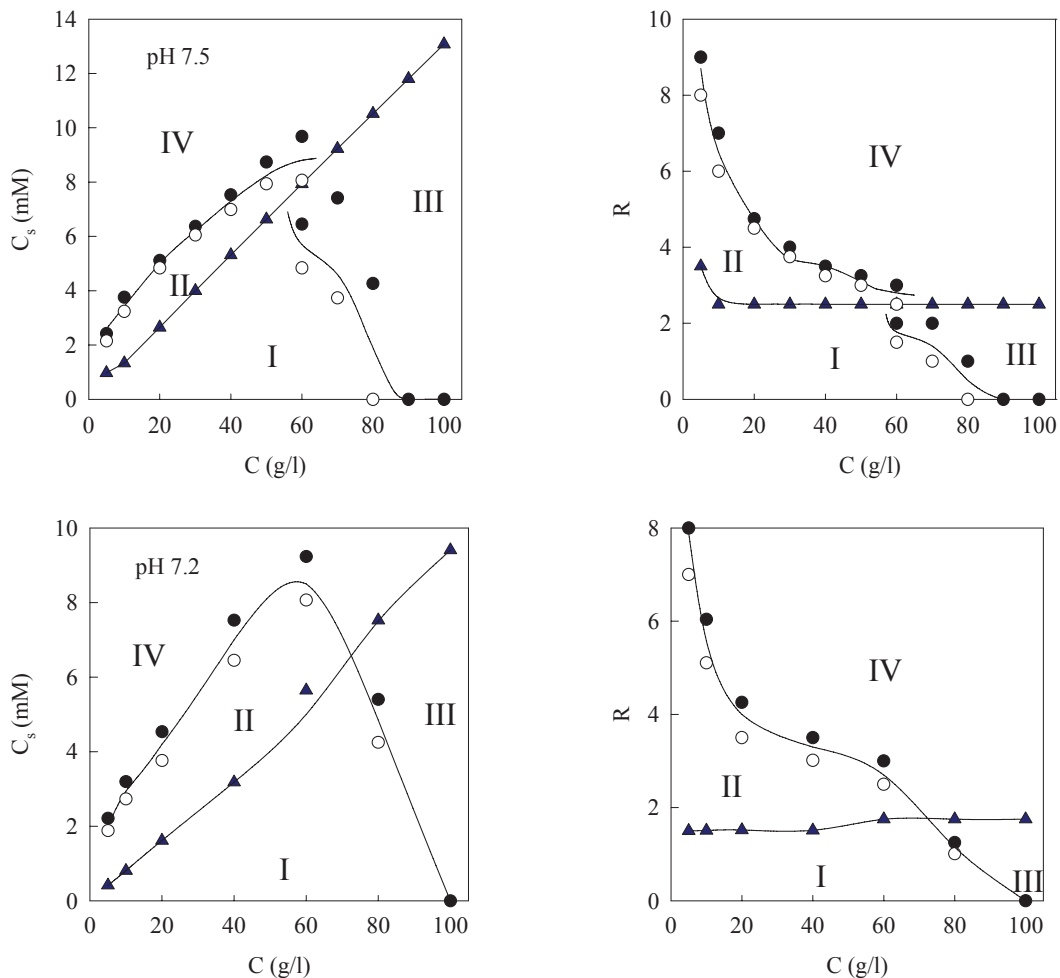
Values of  $R_h$  and  $\rho$  obtained by heating  $\beta$ -lg solutions at  $C=40\text{g/L}$  in the presence of  $\text{CaCl}_2$  at pH 6.9 are summarized in table 1. Notice that the densities are more uncertain, because small errors in  $R_h$  lead to much larger errors in the calculated density. Nevertheless, the general tendency is clear. The size and the density of the microgels increased with increasing  $\text{CaCl}_2$  concentration. For a given molar ratio no systematic dependence on the protein concentration was found. We also observed a weak increase of the hydrodynamic radius of the strands with increasing  $\text{CaCl}_2$  concentration from 15nm in pure water to 25nm at  $R=2$ .

**Table 1: Combined effects of added  $\text{CaCl}_2$ , protein concentrations and  $R$  on the weight fraction, the size and the density of the microgels formed by heating  $\beta$ -lg solutions at pH6.9.**

<b>C</b>	<b>R</b>	<b>F (%)</b>	<b><math>R_h</math> (nm)</b>	<b><math>\rho</math> (g/ml)</b>
10	2	68	140	0.27
20	2.	76	140	0.24
40	2	75	140	0.25
10	2.5	92	132	0.32
20	2.5	92	135	0.38
40	2.5	90	220	0.42
10	3	94	145	0.43
20	3	96	195	0.49
40	2.7	96	200	0.45

## Influence of the pH

We investigated the effect of the  $\text{CaCl}_2$  and the protein concentrations on the formation of microgels for solutions prepared at different pH between 6.0 and 7.5. Figure 5 shows state diagrams for each pH. It was reported elsewhere that in the absence of added salt, the critical gel concentration increases weakly from about 65g/L at pH 6.0 to about 95g/L at neutral pH and then decreases slightly at higher pH (Mehalebi, Nicolai et al. 2008). The results obtained here in pure water are consistent with this earlier investigation. Less calcium ions are needed to induce gelation at lower pH, but at each pH the critical concentration has a maximum at  $C \approx 50\text{-}60\text{g/L}$ . Remarkably, at pH 7.5 and  $C=60\text{ g/l}$ , we observed two sol-gel transitions with increasing calcium concentration: a transition from a transparent liquid at  $C_s=4\text{mM}$  to a transparent gel at  $C_s=6\text{mM}$  and a transition between a turbid liquid at  $C_s \approx 8\text{mM}$  and a turbid gel at  $C_s=10\text{mM}$ . This behavior will be discussed below.



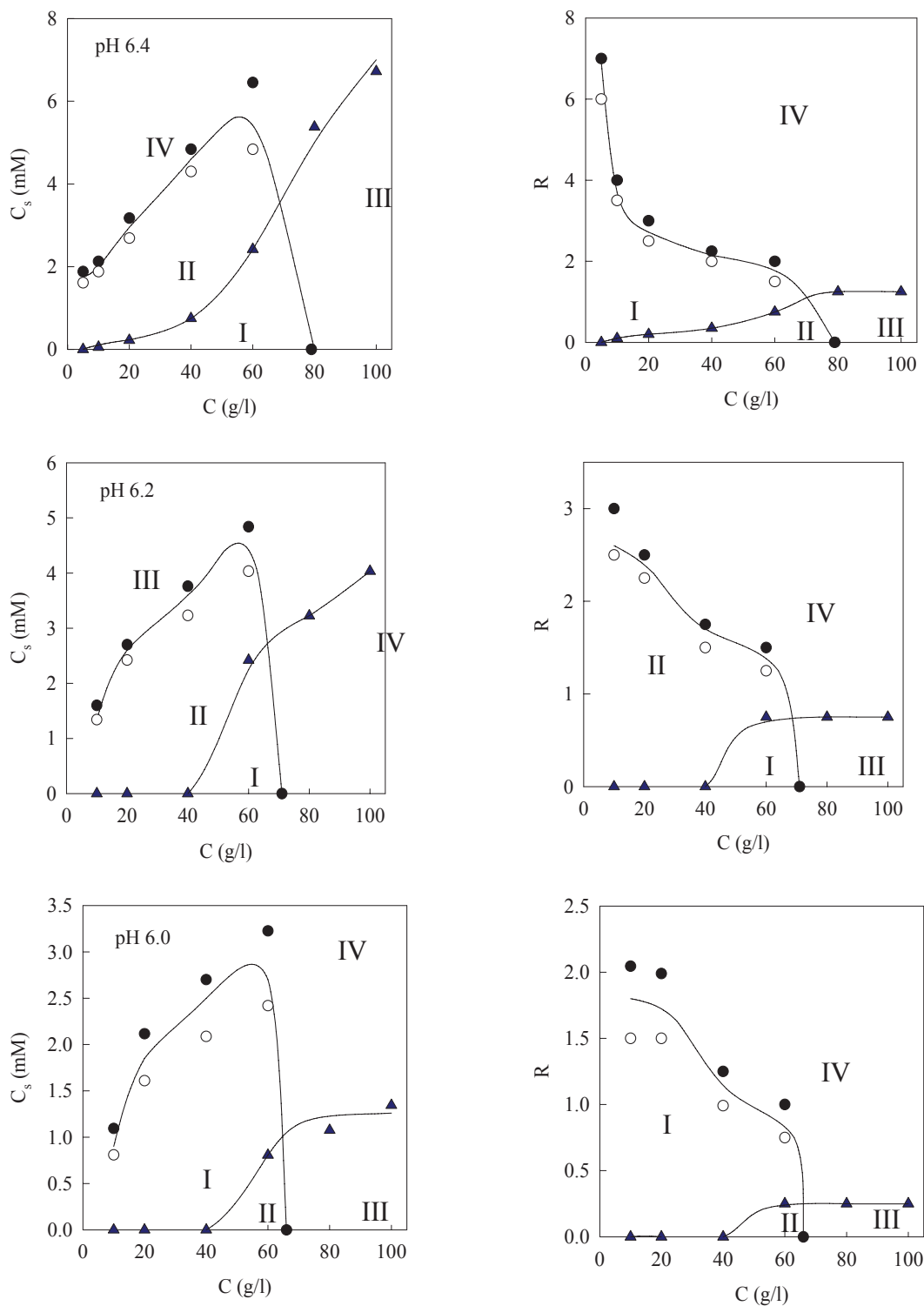


Figure 5: State diagram of heated  $\beta$ -lg solutions as a function of  $C$  and  $C_s$  (left) or  $C$  and  $R$  (right) at different pH. The open and close circles indicate solutions and gels, respectively. The blue triangles indicate the boundary between formation of small strands and microgels. Lines are guides to the eye. Four different states are distinguished: transparent liquid (I); turbid liquid containing microgels (II); transparent gel (III); turbid gel or precipitate (IV).

The critical molar ratio ( $R$ ) remains independent of  $C$  when the pH is increased from 6.9 to 7.5, but more  $\text{CaCl}_2$  needs to be added to form microgels at higher pH. At pH=6.4 microgels are formed even in the absence of  $\text{Ca}^{2+}$  at  $C \leq 20\text{g/L}$ , but the critical molar ratio increases with increasing protein concentration. At pH 6.2 and 6.0, microgels are formed in pure water up to  $C=40\text{g/L}$ , but small amounts of  $\text{Ca}^{2+}$  are still needed at higher concentrations. In pure water, the heterogeneous gels are formed at  $C=100\text{g/L}$  below pH 5.6.

The fraction of microgels as a function of  $R$  at  $C=40\text{g/L}$  is shown in figure 6 for different pH.  $F$  increased sharply to about 95% above a critical value of  $R$ , that shifted to larger values with increasing pH. We found that  $F$  did not depend significantly on the protein concentration for  $\text{pH} > 6.4$ , but at lower pH it decreased with increasing protein concentrations. At lower pH, very small amounts of  $\text{Ca}^{2+}$  have a strong impact on the microgel formation.

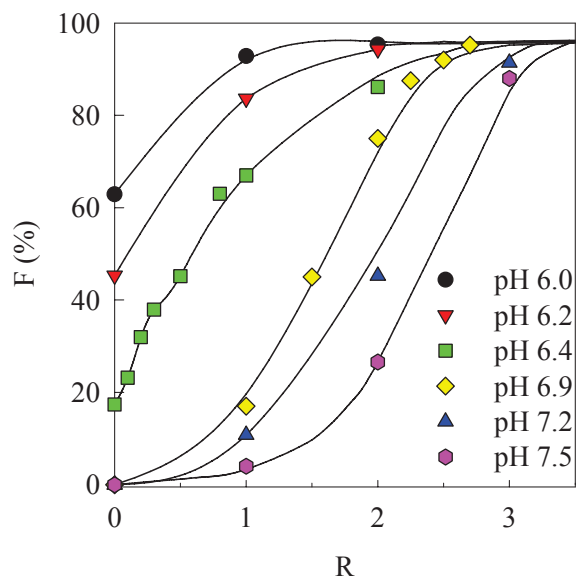


Figure 6: Dependence of the fraction of microgels (sedimented proteins after centrifugation at 50.000 g during 1h) on  $R$  at different pH and  $C=40 \text{ g.L}^{-1}$

Values of  $R_h$  and  $\rho$  for microgels obtained for  $C=40\text{g/L}$  at different pH and  $R$  are summarized in table 2. For a given  $\text{Ca}^{2+}$  concentration the size of the microgels decreases with increasing pH. For a given pH the size and the density increase with increasing  $R$ . It is thus possible to modulate the size and structure of microgels by changing the amount of calcium and pH.

**Table 2: Combined effects of added  $\text{CaCl}_2$  and pH on the weight fraction, the size and the density of microgels formed by heating  $\beta$ -lg solutions at  $C=40\text{g/L}$ .**

pH	R	F (%)	$R_h$ (nm)	$\rho$ (g/ml)
5.8	0	80	115	0.22
5.9	0	75	80	0.20
6.0	0	63	70	0.13
	1	93	300	0.27
6.2	0	57	50	0.08
	1	85	150	0.3
	2	95	300	0.4
6.4	1	60	110	0.3
	2	86	140	0.45
6.9	2	75	140	0.25
	2.5	90	220	0.42
	2.7	96	200	0.45
7.2	2	76	100	0.2
	3	95	150	0.35

### **Mechanism of the formation and self-stabilisation of the microgels.**

In an attempt to relate our observations to the net protein charge, we have determined the fraction of calcium ions bound to the proteins before and after heating the solutions, see materials and methods. Figure 7 shows the fraction of bound calcium ions as a function of R at pH 7.0 and  $C=40 \text{ g.L}^{-1}$ . Before heating it decreased almost linearly to about 60% at  $R=3$ . After heating almost all calcium was bound to the protein aggregates up to  $R=2.2$ . These results are similar to those reported by (Zittle, Monica et al. 1957) and (Baumy and Brulé 1988).

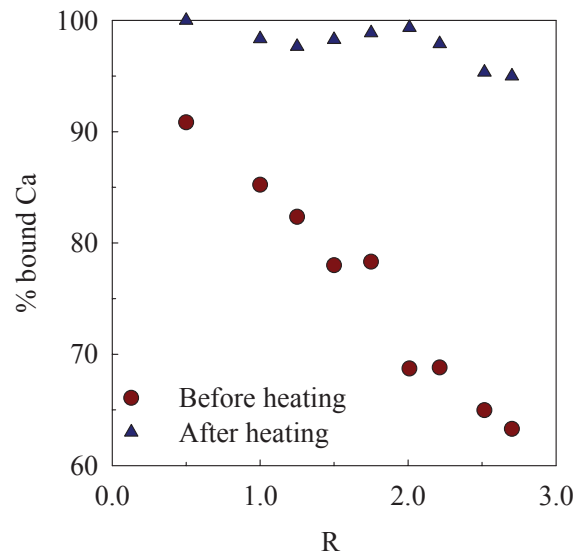


Figure 7: Fraction of bound calcium ions before and after heating  $\beta$ -lg solutions at  $C=40$   $\text{g.L}^{-1}$  and  $\text{pH } 7.0$  as a function of  $R$ .

The net charge of the proteins can be calculated from the fraction of bound calcium ions as follows. In pure water, the net charge of  $\beta$ -lg at  $\text{pH } 7.0$  is about  $-7$  (McKenzie 1971). The change of the net charge after addition of  $\text{CaCl}_2$  was calculated by adding the amount of  $\text{NaOH}$  per protein needed to restore the  $\text{pH}$  to  $7.0$  and subtracting twice the number of bound  $\text{Ca}^{2+}$  ions per protein. Table 3 summarizes the results. It appears that in order to form a significant amount of microgels ( $R > 1.5$ ) the net charge should be reduced to less than about  $-5$ . We note, however, that at lower  $\text{pH}$  the microgel formation also depends somewhat on the protein concentration.

The microgel suspensions remained stable during heating as long as their surface charge density was sufficiently high and the concentration of free ions was sufficiently low so that electrostatic repulsion was not screened effectively. Above a critical value of  $R$  the microgels associate and can form a gel. At  $\text{pH } 7.0$  and  $C=40\text{g/L}$ , the microgels started to associate when  $R$  exceeded about  $3$ , i.e. when the net charge became less than  $-2$  and the fraction of free  $\text{Ca}^{2+}$  became significant. At lower  $\text{pH}$ , less  $\text{CaCl}_2$  was needed to reduce the charge density and therefore association started at lower values of  $R$ . Association of the microgels is easier at higher protein concentrations, which explains why the critical value of  $R$  for gelation decreased with increasing  $C$ . At very high protein concentrations even the small strands associated and could form a gel. We note that random aggregation of the small strands is favored by addition of  $\text{NaCl}$  (Mehalebi, Nicolai et al. 2008), but addition

of NaCl by itself does not drive the formation of stable microgel suspensions, probably because NaCl does not bind to the proteins, but only screens the electrostatic repulsion. The effect of adding NaCl in addition to CaCl<sub>2</sub> has not yet been investigated.

In most situations, a single sol-gel transition was observed when the CaCl<sub>2</sub> was increased either caused by gelation of strands or by gelation of microgels. However, at pH 7.5 and C = 60 g/L we observed the formation of a transparent gel at C<sub>s</sub>=6mM due to gelation of strands, but a stable turbid suspension of microgels at C<sub>s</sub>=8mM. Thus at this particular protein concentration, the formation of microgels instead of strands, driven by the reduced charge density of the proteins, inhibits gelation. This remarkable behaviour can be explained by the fact that the number concentration of the strands is much larger than that of the microgels. At C<sub>s</sub>=6mM the electrostatic repulsion between the strands is sufficiently reduced to allow their association into a gel. However, at C<sub>s</sub>=8mM, microgels are formed and the repulsion between the microgels is still sufficiently high to inhibit their association. Only at C<sub>s</sub>=10mM is the electrostatic repulsion sufficiently reduced to allow gelation of the microgels. We expect that this behaviour occurs in all systems close to the concentration where the sol-gel transition crosses the transition between the formation of small strands and microgels.

The present finding that the formation of microgels is correlated to the net charge density is consistent with the formation of microgels in salt free water as a function of the pH. At C=40g/L a significant amount of microgels is formed in pure water below pH 6.2. Remarkably, the net negative charge of β-lg in pure water at pH 6.2 is close to -5. It appears that a crucial parameter for the formation of microgels is the net charge density of the native proteins that can be controlled either by the pH or by adding calcium ions.

When the proteins form microgels, they bind more calcium ions, which reduces the concentration of free ions and thereby increases the net charge of residual native proteins. A similar process occurs when microgels are formed in pure water (Phan-Xuan, Nicolai et al. 2011). In this case, microgel formation causes a significant increase of the pH and thus an increase of the charge density of the residual native proteins. In both situations, when the net charge of the residual native proteins becomes larger than about -5, they will no longer form microgels, but small strands.

Formation of the microgels led to removal of free Ca<sup>2+</sup> from the solution. This leads to an increase of the net charge of the residual native proteins. We believe that it also leads to an increase of the surface charge density of the microgels as the calcium ions will preferentially neutralize the core of the micelles. As a consequence, electrostatic repulsion

between microgels in contact will increase. This mechanism of self-stabilisation is similar to the one we proposed for the formation of microgels in pure water, where it led to an increase of the pH. We suppose that in this case the core of the microgels was preferentially neutralized by hydrogen ions leading to an increase of the surface charge density of the microgels.

All results reported here were obtained with systems heated at 85°C, where aggregation is very rapid. Measurements at pH 7 at lower heating temperatures showed that the critical CaCl<sub>2</sub> concentration for formation of microgels shifts to slightly higher CaCl<sub>2</sub> concentrations with decreasing temperature. This observation indicates that the heating temperature influences not only the kinetics of the aggregation, but also the transition between the formation of strands and microgels. We will discuss the dependence of the heating temperature in more detail elsewhere.

**Table 3: Amount of bound calcium ions per protein and the net protein charge before and after heat treatment for  $\beta$ -lg at  $C=40 \text{ g.L}^{-1}$  and pH 7.0**

R	Bound Ca <sup>2+</sup> per protein before heating	Bound Ca <sup>2+</sup> per protein after heating	NaOH added per protein	Net protein charge before heating	Net protein charge after heating	F (%)
2.7	1.71	2.56	0.6	-4.18	-2.48	96
2.52	1.63	2.40	0.55	-4.29	-2.75	92
2.21	1.52	2.17	0.49	-4.45	-3.15	87
2.01	1.38	2.00	0.45	-4.69	-3.45	65
1.75	1.37	1.73	0.40	-4.66	-3.94	70
1.5	1.17	1.47	0.37	-5.03	-4.43	45
1.25	1.03	1.22	0.31	-5.25	-4.87	19.5
1	0.85	0.98	0.27	-5.57	-5.31	17
0.5	0.45	0.50	0.16	-6.26	-6.16	
0	0	0	0	-7	-7	0

## Conclusion

Stable suspensions of spherical protein microgels can be formed by heating  $\beta$ -lg in the presence of calcium ions for  $\text{pH} > \text{pI}$  at least up to 7.5. The critical molar ratio  $\text{Ca}^{2+}/\beta$ -lg needed to induce microgel formation is independent of the protein concentration for  $\text{pH} \geq 6.9$  and increases weakly with increasing pH from  $R \approx 1.5$  at pH 6.9 to  $R \approx 2.5$  at pH 7.5. In the pH-range 6.0-6.4 microgels are formed in pure water at low protein concentrations, but a small amount of  $\text{Ca}^{2+}$  is needed at higher concentrations. The net charge of the native proteins is the crucial parameter for the formation of microgels and can be controlled either by the pH or by adding calcium ions. When the net charge becomes larger than about -5, microgels are no longer formed and instead small strands are formed.

Larger and denser microgels are formed in the presence of  $\text{Ca}^{2+}$  at neutral pH than in pure water closer to pI. Stable suspensions of microgels with a size ranging from 100 to 400 nm and a density of about 0.2 – 0.45 g/ml can be formed in a narrow range of  $\text{Ca}^{2+}$  concentrations. The microgels are charge stabilized, but if the fraction of free  $\text{Ca}^{2+}$  becomes significant they aggregate leading to precipitation or gelation.

Microgels bind  $\text{Ca}^{2+}$  more strongly than native  $\beta$ -lg, which leads to an increase of the net charge of residual native proteins. This may in turn cause the formation of small strands instead of microgels at later stages of the reaction. It also leads to stronger electrostatic repulsion between microgels.

Acknowledgement: The authors would like to thank Bertrand Schmitt for doing the TEM measurements.

## References

- Aymard, P., Gimel, J. C., Nicolai, T. & Durand, D. (1996), Experimental evidence for a two-step process in the aggregation of beta-lactoglobulin at pH 7, *Journal De Chimie Physique Et De Physico-Chimie Biologique*, **93**, 987-997.
- Baomy, J. J. & Brulé, G. (1988), Binding of bivalent cations to  $\alpha$ -lactalbumin and  $\beta$ -lactoglobulin: effect of pH and ionic strength, *Le Lait* **68**, 33 - 48.
- Berne, B. J. & Pecora, R. (1993), *Dynamic Light Scattering*. Oxford University Press.
- Brown, W. (1996), *Light Scattering: Principles and development*. Clarendon Press: Oxford.
- Bryant, C. M. & McClements, D. J. (1998), Molecular basis of protein functionality with special consideration of cold-set gels derived from heat-denatured whey, *Trends in Food Science & Technology*, **9**, 143-151.
- Donato, L., Schmitt, C., Bovetto, L. & Rouvet, M. (2009), Mechanism of formation of stable heat-induced beta-lactoglobulin microgels, *International Dairy Journal*, **19**, 295-306.
- Hambling, S. G., Mc Alpine, A. S. & Sawyer, L. (1992).  $\beta$ -lactoglobulin, In P. F. Fox *Advanced Dairy Chemistry - 1: Proteins* (pp. 141 - 190), London: Elsevier Applied Science
- Hongsprabhas, P. & Barbut, S. (1997), Structure-forming processes in Ca<sup>2+</sup>-induced whey protein isolate cold gelation, *International Dairy Journal*, **7**, 827-834.
- Hongsprabhas, P., Barbut, S. & Marangoni, A. G. (1999), The structure of cold-set whey protein isolate gels prepared with Ca<sup>++</sup>, *Food Science and Technology-Lebensmittel-Wissenschaft & Technologie*, **32**, 196-202.
- Jung, J. M., Savin, G., Pouzot, M., Schmitt, C. & Mezzenga, R. (2008), Structure of heat-induced beta-lactoglobulin aggregates and their complexes with sodium-dodecyl sulfate, *Biomacromolecules*, **9**, 2477-2486.
- Kinsella, J. E., Whitehead, D.M., Brady, J., Bringe, N.A. (1989). Milk proteins: possible relationships of structure and function, In P. E. Fox *Developments in dairy chemistry*. (4) (pp. 55–95), New York, NY, USA: Elsevier Applied Science
- McKenzie, H. A. (1971), *In Milk proteins : chemistry and molecular biology*. Academic Press : New York and London.

- Mehalebi, S., Nicolai, T. & Durand, D. (2008a), The influence of electrostatic interaction on the structure and the shear modulus of heat-set globular protein gels, *Soft Matter*, **4**, 893-900.
- Mehalebi, S., Nicolai, T. & Durand, D. (2008b), Light scattering study of heat-denatured globular protein aggregates, *International Journal of Biological Macromolecules*, **43**, 129-135.
- Moitzi, C., Donato, L., Schmitt, C., Bovetto, L., Gillies, G. & Stradner, A. (2011), Structure of beta-lactoglobulin microgels formed during heating as revealed by small-angle X-ray scattering and light scattering, *Food Hydrocolloids*, **25**, 1766-1774.
- Nicolai, T. (2007). Food structure characterisation using scattering methods, In D. J. McClements *Understanding and controlling the microstructure of complex foods* (pp. 288–310), Woodhead: Cambridge
- Nicolai, T., Britten, M. & Schmitt, C. (2011), beta-Lactoglobulin and WPI aggregates: Formation, structure and applications, *Food Hydrocolloids*, **25**, 1945-1962.
- Phan-Xuan, T., Nicolai, T., Durand, D., Schmitt, C., Donato, L. & Bovetto, L. (2011), On the crucial importance of the pH for the formation and self-stabilisation of protein microgels and strands, *Langmuir*, 15092–15101.
- Pouzot, M., Nicolai, T., Visschers, R. W. & Weijers, M. (2005), X-ray and light scattering study of the structure of large protein aggregates at neutral pH, *Food Hydrocolloids*, **19**, 231-238.
- Roefs S.P.F.M. , P. H. A. (2001). Aggregation and gelation of whey proteins: Specific effect of divalent cations?, In R. M. Dickinson Eric *Food Colloids: Fundamentals of Formulation* (pp. 358 - 368), Cambridge, UK: Royal Society of Chemistry
- Schmitt, C., Bovay, C., Vuillienet, A. M., Rouvet, M., Bovetto, L., Barbar, R. & Sanchez, C. (2009), Multiscale Characterization of Individualized beta-Lactoglobulin Microgels Formed upon Heat Treatment under Narrow pH Range Conditions, *Langmuir*, **25**, 7899-7909.
- Schmitt, C., Moitzi, C., Bovay, C., Rouvet, M., Bovetto, L., Donato, L., Leser, M. E., Schurtenberger, P. & Stradner, A. (2010), Internal structure and colloidal behaviour of covalent whey protein microgels obtained by heat treatment, *Soft Matter*, **6**, 4876-4884.
- Sherwin, C. P. & Foegeding, E. A. (1997), The effects of CaCl<sub>2</sub> on aggregation of whey proteins, *Milchwissenschaft-Milk Science International*, **52**, 93-96.

Simons, J. W. F. A., Kusters, H. A., Visschers, R. W. & de Jongh, H. H. J. (2002), Role of calcium as trigger in thermal beta-lactoglobulin aggregation, *Archives of Biochemistry and Biophysics*, **406**, 143-152.

Townend, R., Winterbottom, R. J. & Timasheff, S. N. (1960), Molecular interactions in  $\beta$ -lactoglobulin . II. Ultracentrifugal and electrophoretic studies of the association of  $\beta$ -lactoglobulin below its isoelectric point., *Journal of the American Chemical society*, **82**, 3161-3168.

Wang, C. H. & Damodaran, S. (1991), Thermal Gelation of Globular-Proteins - Influence of Protein Conformation on Gel Strength, *Journal of Agricultural and Food Chemistry*, **39**, 433-438.

Xiong, Y. L., Dawson, K. A. & Wan, L. P. (1993), Thermal Aggregation of Beta-Lactoglobulin - Effect of pH, Ionic Environment, and Thiol Reagent, *Journal of Dairy Science*, **76**, 70-77.

Zittle, Monica, D., Rudd & Custer (1957), The Binding of Calcium Ions by  $\beta$ -Lactoglobulin Both before and after Aggregation by Heating in the Presence of Calcium Ions, *J. Am. Chem. Soc.* , **79** 4661-4666.



## PAPER III

### Tuning the structure of protein particles and gels with calcium or sodium ions

#### Abstract

The effect of the addition of NaCl or CaCl<sub>2</sub> on the structure of the protein particles and gels was investigated in detail for aqueous solutions of the globular milk protein  $\beta$ -lactoglobulin ( $\beta$ -lg) at 40g/L and pH 7.0. When heated in the presence of NaCl or at very low CaCl<sub>2</sub> concentrations the proteins aggregate to form small strand-like particles, but if more than about two Ca<sup>2+</sup> ions per protein are present larger spherical particles (microgels) are formed, that increase in size with increasing CaCl<sub>2</sub> concentration. The effect of the heating temperature was investigated between 62 and 85°C. At lower heating temperatures more Ca<sup>2+</sup> ions per protein are needed to drive the formation of microgels. Particle size measurements done with dynamic light scattering suggest that the aggregation occurs via a nucleation and growth process. The nuclei grow either by dynamic interaction of themselves that could be considered as a fusion process or by addition of denatured proteins. If more than 3 Ca<sup>2+</sup> ions per protein are added, particulate gels are formed by random association of the microgels. Similar particulate gels are also formed at high NaCl concentrations (>200mM), but by a different mechanism. In this case the randomly aggregated small strands formed at the early stage of the heating process formed agglomerated dense spherical domains at a later stage of the heating process by a process of microphase separation mechanism.

---

Tuan Phan-Xuan, Dominique Durand, Taco Nicolai  
*LUNAM Université du Maine, IMMM UMR-CNRS, Polymers, Colloids, Interfaces, 72085  
Le Mans Cedex 9, France.*

Laurence Donato, Christophe Schmitt, Lionel Bovetto  
*Food Science and Technology Department, Nestec Ltd, Nestlé Research Center, P.O. Box  
44, CH-1000 Lausanne 26, Switzerland.*

Submitted in *Biomacromolecules*

## Introduction

Heat induced denaturation of globular proteins in aqueous solution induces aggregation leading to the formation of sub-micron size particles and above a critical protein concentration to gels<sup>1</sup>. The globular protein for which these phenomena have been studied in most detail is beta-lactoglobulin ( $\beta$ -lg) which is the major whey protein in bovine milk. It has a molar mass of  $18.2 \text{ kg}\cdot\text{mol}^{-1}$ , a radius of about 2 nm and an isoelectric point  $\text{pI} = 5.2$ <sup>2</sup>.

Depending on the pH, aggregates with different morphologies can be obtained. At acidic pH large rigid rod-like aggregates are formed<sup>3-8</sup>. At  $\text{pH} > 6.2$ , small curved strand-like aggregates are formed at low protein concentrations, that associate at higher concentrations into larger randomly branched aggregates with a self-similar structure<sup>9-10</sup>. Interestingly, in a narrow range of the pH just above pI (around pH 5.9) and just below pI (around pH 4.6) stable suspensions of rather monodisperse spherical particles were formed with a radius of about a hundred nanometers<sup>11-15</sup>. These spherical particles, which were called microgels, also formed by whey protein isolate (WPI) that contains a majority of  $\beta$ -lg together with in addition other globular proteins such as  $\alpha$ -lactalbumin<sup>16</sup>.

It has been shown that the pH is a crucial parameter for the formation of stable microgel suspensions<sup>15</sup>. Stable suspensions of microgels are only obtained if the pH is set before heat treatment between 5.75 and 6.2 and the protein concentration is less than about 50g/L. At lower pH the microgels agglomerate and precipitate, while at higher pH small strand-like aggregates are formed. At higher protein concentrations the microgels agglomerate and a gel is formed. It has been proposed that the microgels in suspension are stabilized by electrostatic repulsion. An increase of the pH of the suspension was measured during heating, which could result in an increase of the surface charge density of the microgel leading to their self-stabilisation. When pH increased above 6.1, the residual native protein form small strand-like aggregates. The fraction of proteins that form microgels and the structure of the latter are extremely sensitive to the pH.

It was suggested on the basis dynamic light scattering measurements that the microgels were formed by a process of nucleation and growth<sup>15</sup>. The aggregation rate increases sharply with increasing temperature as it is controlled by the protein denaturation step. No significant effect of the temperature on the particle size was found between 75°C and 85°C, where the aggregation is relatively fast. However, bigger microgels were formed at 70°C, Bromley et al.<sup>17</sup> also observed an increase of the particle size at lower

temperatures at pH 5.3 and explained this by the formation of fewer nuclei that subsequently grew to larger particles.

Very recently, we showed that stable suspension of microgels can also be obtained by heating  $\beta$ -lg at 85°C in the presence of  $\text{Ca}^{2+}$  for  $\text{pH} > 6.1$  at least up to  $\text{pH} 7.5$ <sup>18</sup>.  $\text{Ca}^{2+}$  binds specifically to  $\beta$ -lg and thereby reduces their net charge density<sup>18-19</sup>. Above a critical molar ratio between  $\text{Ca}^{2+}$  and  $\beta$ -lg ( $R = [\text{Ca}^{2+}]/[\beta\text{-lg}]$ ), mainly microgels are formed, while below this value mainly small strands are formed. The critical ratio is independent of the protein concentration (C) for  $\text{pH} \geq 6.9$ , but increased with increasing pH from  $R=1.5$  at  $\text{pH} 6.9$  to  $R=2.5$  at  $\text{pH}=2.5$ . At  $\text{pH} 6.4$  and lower, the critical ratio increased with increasing C from  $R=0$  at 10g/L to  $R=1.0$  at  $C=60\text{g/L}$ . At  $\text{pH} 6.2$  and lower a majority of microgels are formed even in the absence of  $\text{Ca}^{2+}$ . The addition of  $\text{Na}^+$  does not induce formation of microgels up to at least 400mM. Instead it drives aggregation of the small strands at lower protein concentrations by screening repulsive electrostatic interactions. This suggests that microgel formation can only occur if the net charge density of the proteins is reduced.

Above a critical gelation concentration, that decreases with decreasing pH and increasing amount of added NaCl<sup>10, 20-21</sup>, the proteins form a system spanning network. The gels are transparent when electrostatic interaction is strong, i.e. at low NaCl concentration away from the iso-electric point and highly turbid at pH close to pI or at high NaCl concentrations<sup>22</sup>. Microscopy showed that the turbid gels consisted of connected spherical particles with a radius of about a micrometer, so-called particulate gels, whereas the transparent gels were formed by cross-linked protein strands, so-called finely stranded gels<sup>17, 22-24</sup>. In the absence of added salt particulate gels are formed below  $\text{pH} 5.7$ . At higher pH the transition between finely stranded and particulate gels could be induced by adding NaCl. At  $\text{pH} 7$  the transition occurred at approximately 150mM NaCl. The transition between the two types of gel can also be induced by adding calcium ions<sup>25-29</sup>.<sup>18</sup> showed that the critical molar ratio R needed to induce this transition is independent of the protein concentration and increases with increasing pH. At  $\text{pH} 7$  the transition between the finely stranded and particulate gel occurs approximately at  $R=1.5$ , i.e. at the same R value as for the transition between the formation of strands and microgels at lower protein concentrations.

Here we present a detailed investigation study of the formation of strands, microgels and gels at  $\text{pH} 7$  at different heating temperatures in the presence of  $\text{Ca}^{2+}$  and compare it with aggregation and gelation in the presence of  $\text{Na}^+$ . We will show that the assembling of

native proteins into the different types of protein particles and gels can be modified by subtle changes of the  $\text{Ca}^{2+}$  concentration and that the process differs from that in the presence of  $\text{Na}^+$ .

### **Materials and methods:**

**Materials.** The  $\beta$ -lactoglobulin ( $\beta$ -lg) (Biopure, lot JE 001-8-415) used in this study was purchased from Davisco Foods International, Inc. (Le Sueur, MN, USA). The powder contained about 89.6 wt% protein (Kjeldahl, N x6.38) and the protein composition was 55.4% and 41.6% of the variants A and B, respectively, with less than 2% of other whey proteins (based on HIC-HPLC analysis)<sup>12</sup>. The powder was dissolved in Milli-Q water with 200 ppm  $\text{NaN}_3$  added to avoid bacterial growth. The  $\beta$ -lg solutions were dialysed against the solvent for a period of 8 hours with 4 exchanges of the solvent. 0.1M - 0.5M  $\text{CaCl}_2$  or 1M  $\text{NaCl}$  was added to reach the desired salt concentrations after which the pH was set to 7.0. The solutions were filtered through 0.2  $\mu\text{m}$  pore size Anotop filters before heating.

The  $\beta$ -lg concentration was measured by UV absorption at 278 nm using an extinction coefficient of  $0.96 \text{ Lg}^{-1}\text{cm}^{-1}$ . Solutions were heated at different heating temperatures from 60°C to 85°C in air tight cylindrical glass vials with a diameter of 10 mm using a thermostat water bath. The set temperature was reached within 4 min. The samples were cooled rapidly to 20°C to stop the aggregation process by holding the vials under running tap water. The fraction of residual native protein after heating was determined by precipitation at pH 4.6 and measuring the UV absorption of the supernatant.

**Dynamic and static light scattering** measurements were done using a commercial apparatus (ALV-Langen, Germany). The light source was a He-Ne laser with wavelength  $\lambda = 632 \text{ nm}$ . The temperature was controlled by a thermostat bath to within  $\pm 0.2 \text{ }^\circ\text{C}$ . Measurements were made at angles of observation ( $\theta$ ) between 12 and 150 degrees. The relative scattering intensity ( $I_r$ ) was calculated as the intensity minus the solvent scattering divided by the scattering intensity of toluene at 20°C.

In dilute solutions  $I_r$  is related to the weight average molar mass ( $M_w$ ) and the scattering wave vector ( $q$ ) dependent structure factor ( $S(q)$ ) of the solute<sup>30-31</sup>:

$$I_r / KC = M_w S(q) \quad (1)$$

with  $K$  an optical constant depending on the refractive index increment. We have used for the refractive index increment  $0.189 \text{ mL.g}^{-1}$ . The structure factor describes the dependence of the intensity on the scattering wave vector ( $q$ ) and depends on the structure and the size of the solute. The  $z$ -average radius of gyration ( $R_g$ ) can be determined from the initial  $q$ -dependence of  $S(q)$ :

$$S(q) = \left[ 1 + \frac{q^2 R_g^2}{3} \right]^{-1} \quad qR_g \leq 1 \quad (2)$$

The intensity autocorrelation function measured with DLS ( $g_2(t) = \langle I(0).I(t) \rangle / \langle I \rangle^2$ ) is related to the normalized electric field correlation function,  $g_1(t)$ , by the Siegert relation<sup>32</sup>.  $g_1(t)$  was analysed in terms of a distribution of relaxation times:

$$g_1(t) = \int A(\log \tau) \exp(-t / \tau) d \log \tau \quad (3)$$

$g_1(t)$  could be analyzed by the sum of a so-called generalized exponential (GEX) distribution:  $A(\tau) = k \cdot \tau^p \exp[-(\tau/\tau^*)^s]$ <sup>33</sup>, to describe the diffusion of the aggregates and a log-normal distribution to describe the diffusion of the residual native proteins. The relaxation time distribution represents a distribution of diffusion coefficients  $D = (\tau \cdot q^2)^{-1}$  and for dilute solutions may be transformed into a distribution of hydrodynamic radii ( $R_h$ ) if  $qR_h < 1$  using the Stokes-Einstein equation:

$$D = \frac{k \cdot T}{6 \cdot \pi \cdot \eta \cdot R_h} \quad (4)$$

with  $\eta$  the viscosity,  $k$  Boltzman's constant and  $T$  the absolute temperature.

**Confocal Laser Scanning Microscopy (CLSM)** was used in the fluorescence mode. Observations were made with a Leica TCS-SP2 (Leica Microsystems Heidelberg, Germany). A water immersion objective lens was used HCxPL APO 63x NA=1.2 with theoretical resolution of  $0.3 \mu\text{m}$  in the  $x$ - $y$  plane. A small fraction of  $\beta$ -lg was labelled with the fluorochrome rhodamine B isothiocyanate, by adding a small amount of a concentrated

rhodamine solution (5ppm) to the  $\beta$ -lg solutions before heat treatment. No effect of labelling on the kinetics of the aggregation or the structure of the systems was observed.

The images were analysed in terms of the pair correlation function of the fluorescence intensity fluctuations ( $g(r)$ ) as explained in <sup>34</sup>. We made sure that the fluorescence intensity was proportional to the protein concentration so that  $g(r)$  also represents the pair correlation function of the concentration fluctuations.

**Transmission electron microscopy.** The microstructure of heated protein dispersions was investigated by transmission electron microscopy (TEM) using the negative staining method. A drop of the protein dispersion diluted to 0.1wt% in Millipore water was deposited onto a formvar-carbon coated copper grid. The excess product was removed after 30 s using a filter paper. A droplet of 1% phosphotungstic acid at pH7.0 was added for 15 s, removing any excess. After drying the grid at room temperature for 5 min, observations were made with a FEI Tecnai G2 Spirit Biotwin transmission electron microscope operating at 120 kV (FEI company, The Netherlands). Images were recorded using a Quemesa camera (Olympus soft imaging solutions, Germany).

## Results and discussion

### 1. Effect of heating temperature and $\text{Ca}^{2+}$ concentration on the particle size and shape at steady state

In this section we discuss the system after heating  $\beta$ -lg solutions at  $C=40\text{g/L}$  and pH 7.0 for a sufficiently long time to reach steady state, i.e. when when all native proteins had reacted and the structure of the system no longer evolved. The time needed to reach steady state depended on the heating temperature and the salt concentration. It varied from less than 30min at  $85^\circ\text{C}$  to 3 days at  $62^\circ\text{C}$ . After heating, the protein solutions were sufficiently diluted ( $C<1\text{g/L}$ ) so that the mass and size of the aggregates could be determined using light scattering, as explained in the Materials and methods, without the effect of particles interactions.

The evolution of the z-average hydrodynamic radius ( $R_{hz}$ ) of the aggregates as a function of the molar ratio ( $R$ ) is shown in figure 1 for different heating temperatures ( $T$ ). Notice that  $R_{hz}$  represents the z-average over the total aggregate population. However, since the z-average gives a high weight to larger particles, the contribution of the larger

particles dominates even if its weight fraction is small. For  $T < 70^\circ\text{C}$ ,  $R_{\text{hz}}$  increased gradually with increasing  $R$ . Stable suspensions of large aggregates were formed for  $R=3$ , but the systems gelled at  $R=4$ . At  $T=85^\circ\text{C}$ ,  $R_{\text{hz}}$  increased sharply with increasing  $R$  between 1 and 1.5. A similar sharp increase occurred at  $T=75^\circ\text{C}$  between  $R=1.5$  and 2.0 and at  $T=70^\circ\text{C}$  between  $R=2.0$  and 2.5. At these temperatures gels were formed at  $R=3$ .

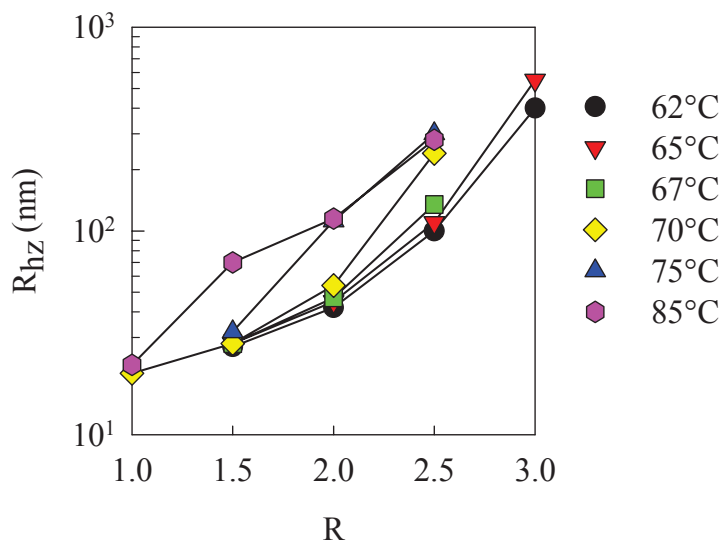
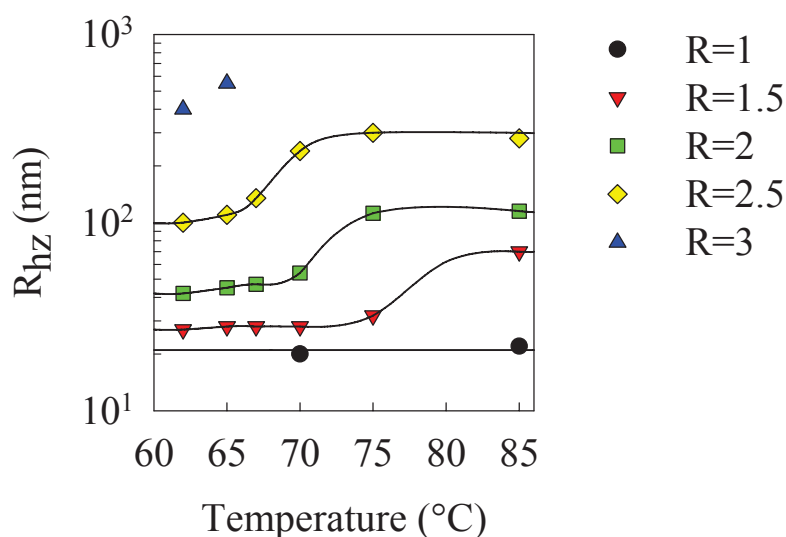


Figure 1. Evolution of  $R_{\text{hz}}$  as a function of  $R$  for  $\beta$ -lg aggregates formed by heating solutions of 40 g/L protein at pH 7.0 at different heating temperatures.

In figure 2 the same results are plotted as a function of  $T$  for different  $R$ . At  $R = 1$ ,  $R_{\text{hz}}$  was independent of  $T$  over the whole range investigated. At  $R = 1.5$ ,  $R_{\text{hz}}$  increased from 30 to 70 nm between  $T=75^\circ\text{C}$  and  $85^\circ\text{C}$ . For  $R = 2$  and 2.5, we observed an abrupt increase of  $R_{\text{hz}}$  between 70 and  $75^\circ\text{C}$  for  $R = 2$  from 50 to 100nm and between  $67^\circ\text{C}$  and  $70^\circ\text{C}$  for  $R = 2.5$  from 100 to 300nm. As mentioned above, at  $R = 3$  the system formed a gel at  $T > 65^\circ\text{C}$ , but stable suspensions of large aggregates at 62 and  $65^\circ\text{C}$ .



**Figure 2.**  $R_{hz}$  as a function of the heating temperature at different  $R$ . The lines are guides to the eye.

We investigated the shape of the aggregates by TEM. Figure 3 shows TEM images obtained by heating at 62°C, and 85°C for different ratios up  $R=2.5$ .

At 85°C only small strand-like aggregates are visible at  $R=1$ . At  $R=1.25$ , the majority of proteins still formed small strands, but a small amount of much larger spherical particles appeared. The fraction and the size of the spherical particles increased with increasing  $R$ . It appears that the sharp increase of  $R_{hz}$  between  $R=1$  and  $R=1.5$  (figure 1) corresponds to the formation of these spherical aggregates that can be considered as microgels. A similar transition between the formation of strands and microgels was observed at 75°C between  $R=1.5$  and 2 (not shown). We showed earlier that when both microgels and strands are formed the latter are formed at a later stage of the process<sup>18</sup>. We speculated that the reason is that when the microgels are formed they bind preferentially  $Ca^{2+}$  to neutralize the core of the microgels. When the amount of  $Ca^{2+}$  available for the residual native proteins drops below the critical value they will start forming strands.

At 62°C, strand-like aggregates were formed up to  $R=1$ . For  $R=2.5$  the aggregates appear more spherical. Similar aggregates were observed at  $R=3$  (not shown here). The spherical particles observed at higher  $R$  may be considered to be microgels. However, the transition between the formation of small strands at  $R=1$  and the microgels at  $R=2.5$  is not clear at this temperature. Neither do we observe both small strands and microgels. Similar observations were made at  $T=65^\circ C$  and  $T=70^\circ C$  (results not shown).

62°C

85°C

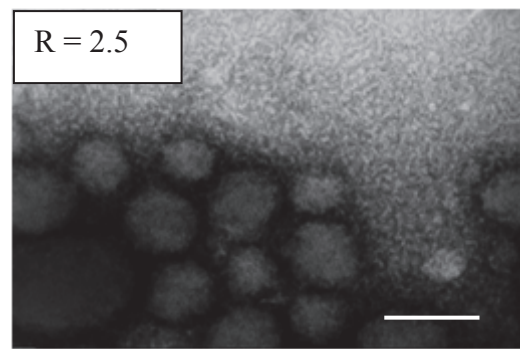
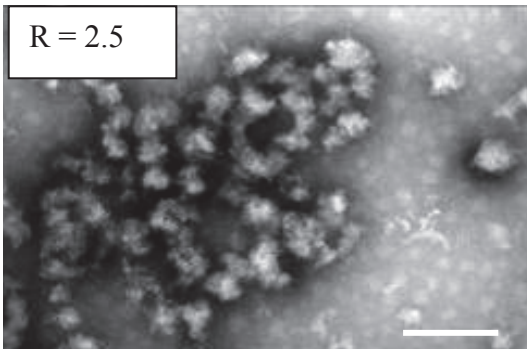
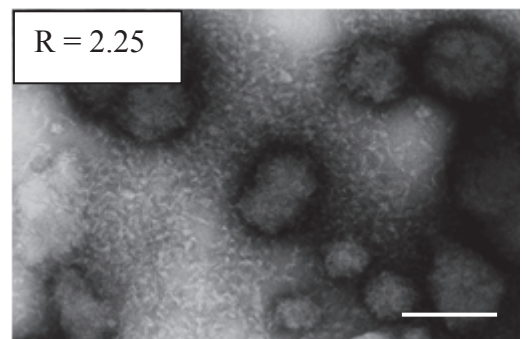
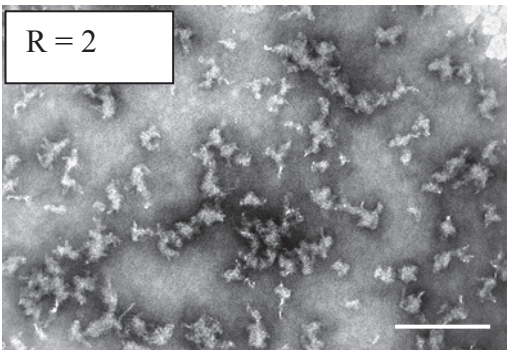
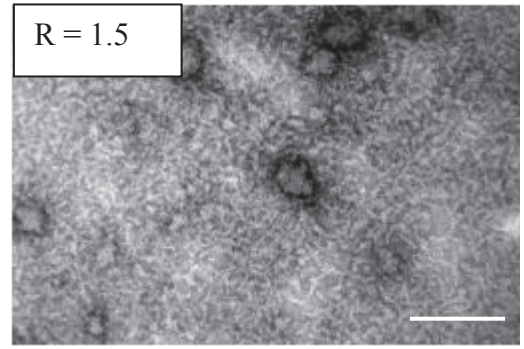
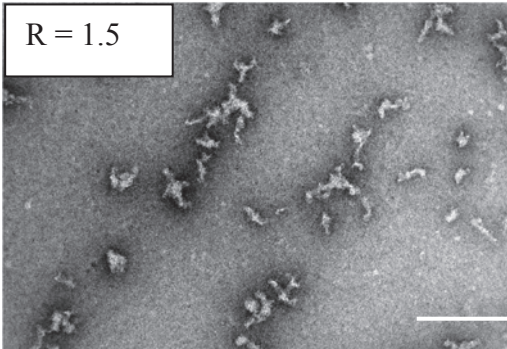
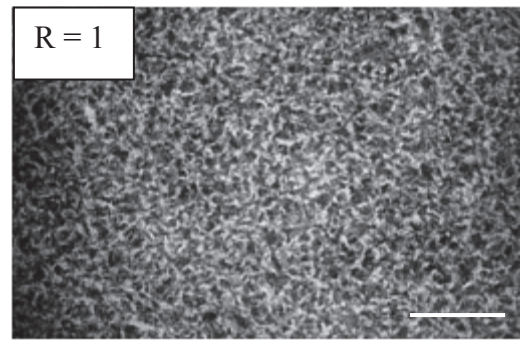
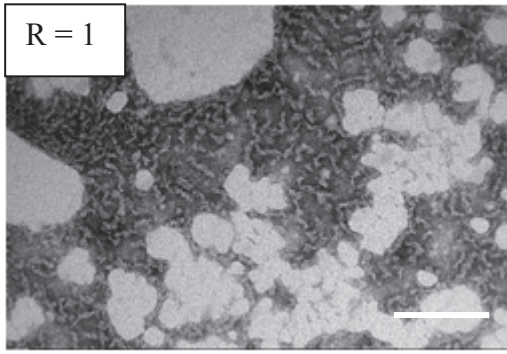


Figure 3. Negative staining TEM micrographs of stable microgel suspension of 40 g/L  $\beta$ -lg formed at different R indicated in the figure and heated at 62°C (left) or at 85°C (right). The bars represent 200 nm

The size of the microgels formed at 75°C and 85°C derived from the TEM images is consistent with the values of  $R_{hz}$  determined with DLS. However, the microgels formed at 62°C for R=2.5 appear significantly smaller on the TEM images ( $\approx$ 50nm) than the measured value of  $R_{hz}$  ( $\approx$ 100nm at R=2.5). Probably, the smaller microgels formed at 62°C are partially associated into larger clusters which sizes is measured by light scattering.

We showed elsewhere<sup>15</sup> that the microgels and strands formed at 85°C can be separated by centrifugation at  $5 \times 10^4 g$  for 1h, as the former precipitated and the latter remained in the supernatant. Figure 4 represents the fraction of microgels for solutions heated at 85°C as a function of R which confirms TEM observations that an increasing amount of microgels are formed for  $R > 1$ . However, when we analyzed in the same way aggregates formed at 62°C, we found that a large fraction precipitated at R=2 even though no microgels were visible in the TEM images. The reason is that the larger strand-like aggregates formed at T=62°C at R=1.5 and 2.0 also precipitate at these centrifugation conditions.

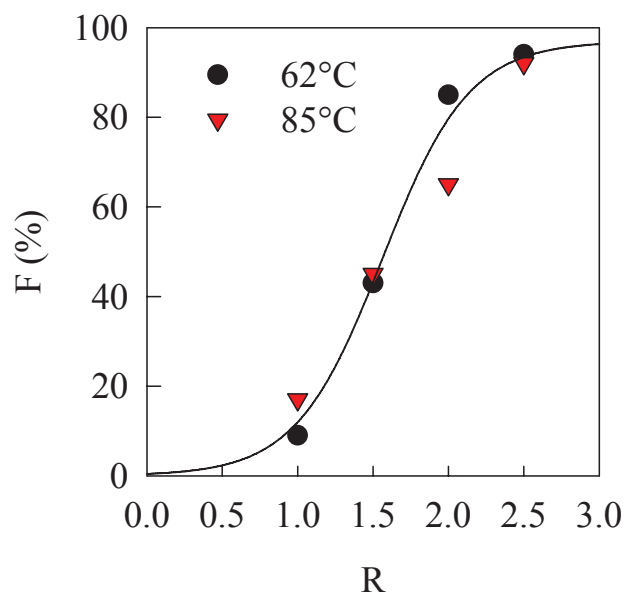


Figure 4: Fraction of proteins that precipitated after centrifugation at  $5 \times 10^4 g$  at C=40 g/L and pH 7.0 as a function of R at steady state after heating at different temperatures. The solid line is a guide to the eye.

We may conclude that when the protein solution is heated at temperatures between 75°-85°C, where aggregation is relatively fast, dispersions of well-defined microgels can be formed. The critical value of R above which they are formed decreases slightly with increasing temperature from between 1.5 and 2 at 75°C to between 1.0 and 1.5 at 85°C. The size of the microgels formed above the critical value of R increases with increasing Ca<sup>2+</sup> concentration. Preliminary measurements obtained after heating β-Ig (40g/L, pH7) at 85°C have shown that microgels are also formed in the presence of Fe<sup>2+</sup> (R> 2.5) and Mg<sup>2+</sup> (R>2.0). These results suggest that the transition between strands and microgels occurs in similar conditions for bivalent ions in general.

Comparing the present results with those obtained between pH 5.75 and pH 6.1 without added salt in the same range of heating temperatures<sup>15</sup>, it appears that the size range of the microgels is comparable (R<sub>hz</sub>=50-200nm). However, the internal structure of the microgels is modified by the presence of Ca<sup>2+</sup> as it was found that the density of the microgels increased with increasing Ca<sup>2+</sup> concentration<sup>18</sup>.

Spherical particles formed at 70°C and lower temperatures appear distinctly smaller than the microgels formed at higher temperatures in the TEM images and are formed only at R > 2 where we believe secondary aggregation takes place leading to larger particles. Remarkably, at pH 5.8 in the absence of salt the microgels formed at T<70°C were larger than those formed between 75°C and 85°C<sup>15</sup>. We will speculate below about the origin of this difference.

The size of the strands formed below the critical value of R also increased with increasing Ca<sup>2+</sup> from R<sub>hz</sub>≈15nm at R=0 to R<sub>hz</sub>≈40nm at R=2, but it was independent of the temperature over the whole range investigated. We note that the size of the strands formed in the absence of added salt was the same between pH 7 and pH 6.2<sup>15</sup> and was independent of the heating temperature.

## **2 Structure and composition during the aggregation process.**

In order to be able to investigate the structure of the aggregates at the earliest stages of the aggregation process, it was studied as function of time at 62°C where the aggregation is very slow. We will first discuss the rate at which native proteins are depleted from the solution and then the evolution of the aggregate size and composition as a function of heating time.

### a. Aggregation kinetics at 62°C

The fraction of residual native proteins ( $F_{\text{nat}}$ ) was determined by lowering the pH to 4.6 at which the aggregated proteins precipitate. In figure 5a,  $F_{\text{nat}}$  is plotted as a function of heating time for different  $R$  at  $C=40$  g/L. The data superimpose well after normalization of the heating time by the time at  $F_{\text{nat}}=0.5$  ( $t_h$ ).  $t_h$  decreased with increasing  $R$  from about 800 min at  $R=1$  to 250 min at  $R=3$ . The change in the kinetics appears especially marked between  $R=1.5$  and  $R=2.0$ , but the change in the aggregate size or shape is not particularly strong, see fig.3. The results could be well described by an apparent reaction order of 1.5. The same reaction order was found to describe the aggregation of  $\beta$ -lg in the presence of NaCl<sup>35</sup>. This observation suggests that the initial stage of the aggregation process is similar at different  $R$  and thus independent of the large scale aggregate structure.

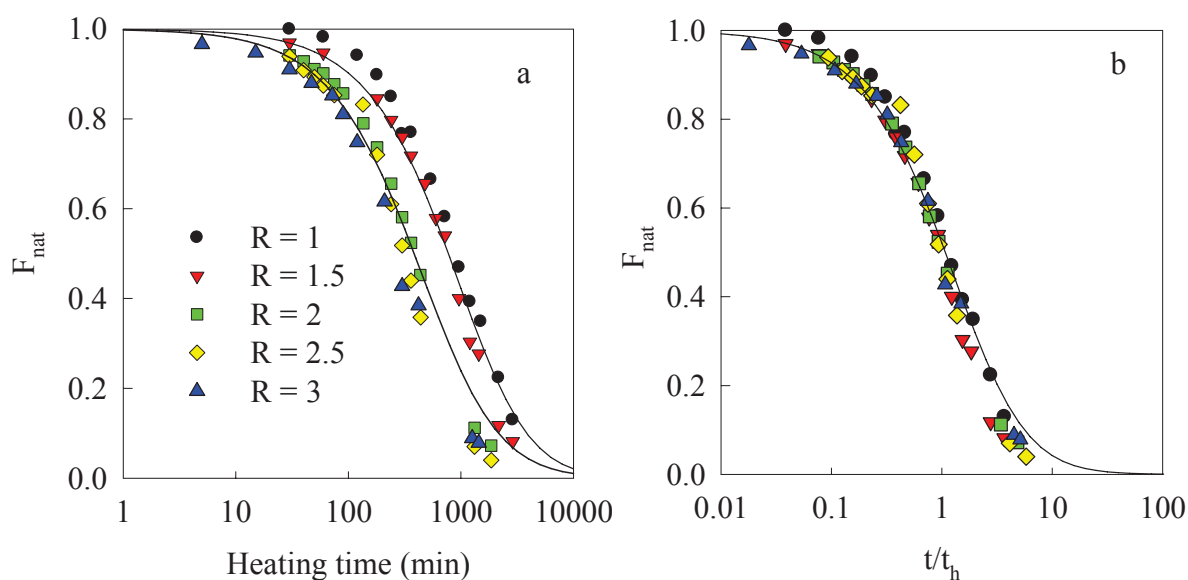


Figure 5a. Evolution of the fraction of native  $\beta$ -lg during heating at 62°C for different  $R$  indicated in the figure. The solid lines represent a reaction order of 1.5.

Figure 5b. Same data as in figure 5a plotted as a function of the heating time normalized by the time at  $F_{\text{nat}}=0.5$ . The solid lines represent a reaction order of 1.5.

### a. Size distribution of the aggregates as function of heating time at 62°C

The evolution of the size distribution of the aggregates during heating at 62°C was determined by dynamic light scattering. Aggregates are strongly weighted in DLS so that their size can be determined even if their weight fraction is very small. Aliquots were taken at chosen heating times and highly diluted in water at room temperature. DLS

measurements were done over a range of scattering angles, but at sufficiently low  $q$ -values the results were independent of  $q$ . Relaxation time distributions were obtained from the correlation functions at low- $q$  and transformed into distributions of the hydrodynamic radius, as described in the Materials and methods.

Fig. 6 shows particle size distributions as a function of heating time for  $R=2$ . At short times, the distributions contained 2 distinct peaks: a first one at  $R_h=3\text{nm}$  that can be attributed to residual native proteins<sup>36 3</sup> and a second one at  $R_h\approx 20\text{nm}$  attributed to small aggregates. With increasing heating time the area of the second peak increased, but did not shift. The implication is that initially more aggregates were formed with the same size. However, after about 2 h of heating, the second peak started to shift to larger values of  $R_h$  with increasing heating time, while the contribution of the first peak became negligible. After about 20h of heating, this second peak position stabilized at  $R_h \approx 80\text{nm}$ . We observed a similar evolution at other values of  $R$  between  $R=1$  where only strands were formed and  $R=3$  where mainly spherical particles were formed, see figure 3. On the basis of these measurements we suggest that the first stage of the aggregation process is the formation of nuclei corresponding to the second peak observed initially with  $R_h=20\text{nm}$  that subsequently grow. A similar nucleation and growth process was reported for aggregation in pure water at pH 7.0<sup>9</sup> and pH 5.8<sup>17 15</sup>. We stress that the suggested nucleation and growth process occurs at all conditions tested regardless whether it leads to spherical particles or to small strands.

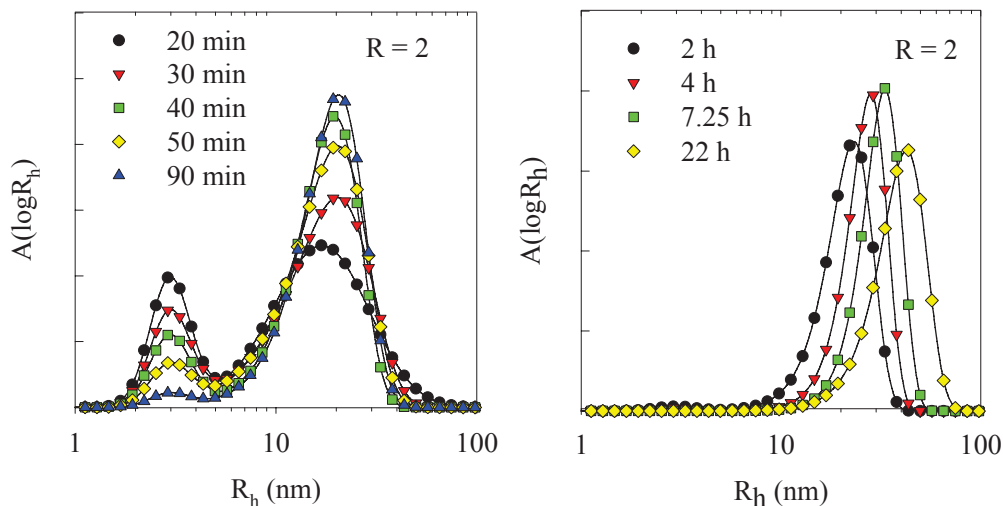


Figure 6. Amplitude of the light scattering signal at  $q=0.018\text{nm}^{-1}$  as a function of the hydrodynamic radius for  $\beta\text{-Ig}$  solutions at  $C = 40 \text{ g.L}^{-1}$  and  $R=2.0$  heated at  $62^\circ\text{C}$  for different times indicated in the figure.

The evolution of  $R_{hz}$  of the aggregates at different  $R$  are shown as a function of heating time and as a function of the fraction of aggregated proteins ( $F_{ag}=1-F_{nat}$ ) in figures 7a and 7b, respectively. Initially,  $R_{hz}$  remained almost constant for a duration that decreased with increasing  $R$  from about 100 min at  $R=1$  to about 10 min at  $R=3$ . This stage can be associated with the formation of nuclei. The size of the nuclei increased with increasing  $R$ :  $R_{hz}=11, 12, 20, 25$  and  $32$  nm for  $R=1, 1.5, 2, 2.5$  and  $3$ , respectively. After this nucleation period the aggregate size started to increase. The increase of  $R_{hz}$  was relatively weak for  $R=1, 1.5$  and  $2$  to  $R_{hz}= 20, 25$  and  $40$ nm, respectively. However, at  $R=2.5$  and  $3$  the increase was more important reaching  $R_{hz}= 100$  and  $400$ nm, respectively. The fraction of aggregated proteins were the nuclei started to grow decreased with increasing  $R$  from about 0.3 at  $R=1$  to less than 0.05 at  $R=3$ .

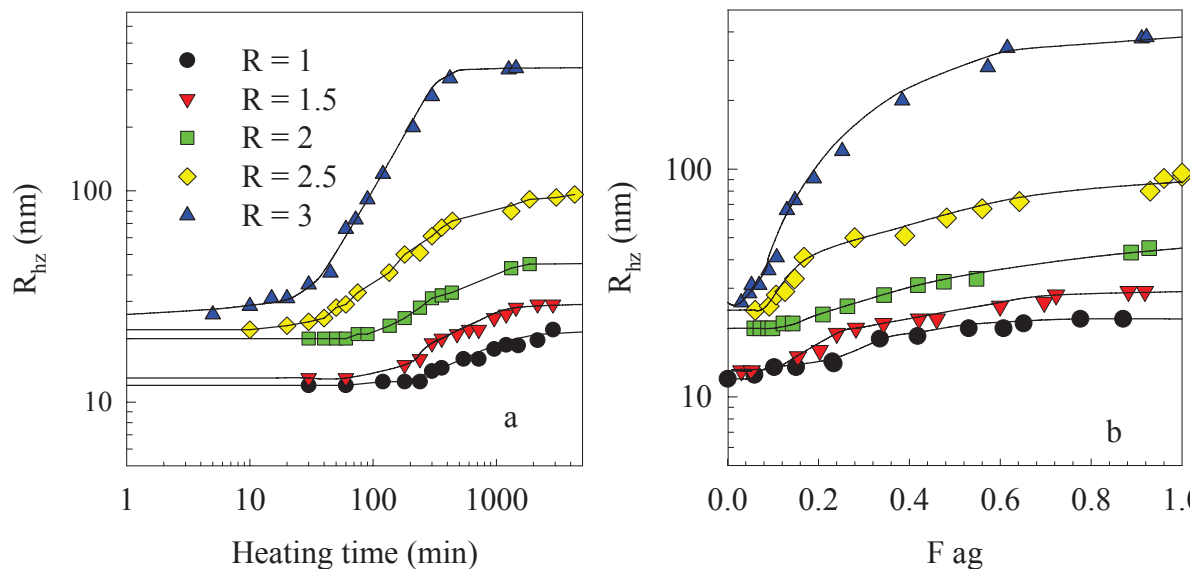


Figure 7. Z-average hydrodynamic radius of  $\beta$ -Ig aggregates as a function of heating time (a) and the fraction of aggregated proteins (b) after different heating times at  $62^{\circ}\text{C}$ . ( $\text{pH } 7.0, C = 40 \text{ g.L}^{-1}$ )

The molar concentration of aggregates ( $v$ ) can be calculated from their molar mass ( $M_w$ ):  $v = C.F_{ag}/M_w$ . In figure 8,  $v$  is plotted as a function of  $F_{ag}$  for different  $R$ . At low  $R$ ,  $v$  increased initially and then stabilized. The increase can be attributed to the increase of the concentration of nuclei. For  $R=2.5$  and  $3$ ,  $v$  decreased with increasing  $F_{ag}$ , which means that the nuclei and smaller aggregates associated into larger aggregates. We note that a decrease of  $v$  with increasing  $F_{ag}$  was also observed at  $\text{pH } 5.8$  without added salt. Thus at low  $R$  nucleation is faster than association of the nuclei, while at larger  $R$  and low  $\text{pH}$

association of the nuclei is faster. The growth of the nuclei is caused association, but also by binding newly denatured native proteins.

The fact that the aggregated nuclei form homogeneous spherical microgels suggests that the bonds between the aggregated nuclei are initially not permanent allowing restructuring. In this way small spherical particles can fuse and form a larger spherical particle. However, when the bonds have become permanent the spherical particles can no longer fuse and larger aggregates and the gel consist of randomly connected spherical particles. At pH 5.8 in the absence of added salt, large spherical particles were formed implying that the bonds became permanent only after fusion had occurred. At pH 7 the same process took place for  $T \geq 75^\circ\text{C}$ . We speculate that the microgels formed at pH 7 and  $R \geq 2.5$  are smaller for  $T \leq 70^\circ\text{C}$ , because the bonds within the microgels became permanent at an earlier stage of the growth process. We note that progressive reinforcement of the bonds in spherical particles formed by  $\beta$ -lg aggregates has been reported in the literature<sup>37</sup>.

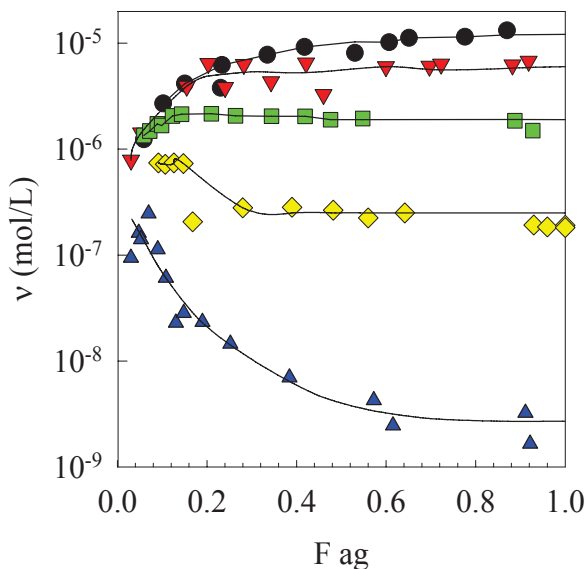


Figure 8. Number concentration of the aggregates as a function of the fraction of aggregated proteins in  $\beta$ -lg solutions that were heated for different times at  $62^\circ\text{C}$  and  $R = 1, 1.5, 2, 2.5$  or  $3$ . Symbols are as in figure 7.

### c Gelation

At  $R=4$  and higher, gels were formed at all heating temperatures tested. We have studied the aggregation and gelation by heating a  $\beta$ -lg solution at  $40\text{g/L}$  and  $R=4$ . A low heating temperature of  $60^\circ\text{C}$  was used so that even the earliest stages of the aggregation

could be easily characterized. Samples were taken at different heating times and diluted by a factor 100 in water. They were subsequently studied with CLSM and DLS.

Figure 9 shows the evolution of  $R_{hz}$  as function of heating time. Aggregates with a radius of about 100nm were formed already at the start of the process. The growth of the aggregates was relatively weak up to 150 min and then increased sharply until  $R_{hz}$  diverged at the gel point at  $t \approx 500$  min. Radii of gyration are 10-20% larger, which is expected for polydisperse spherical particles, because the  $R_{gz} = \langle R_g^2 \rangle^{0.5}$  gives stronger weight to the larger particles than  $R_{gh} = \langle R_h^{-1} \rangle^{-1}$ .

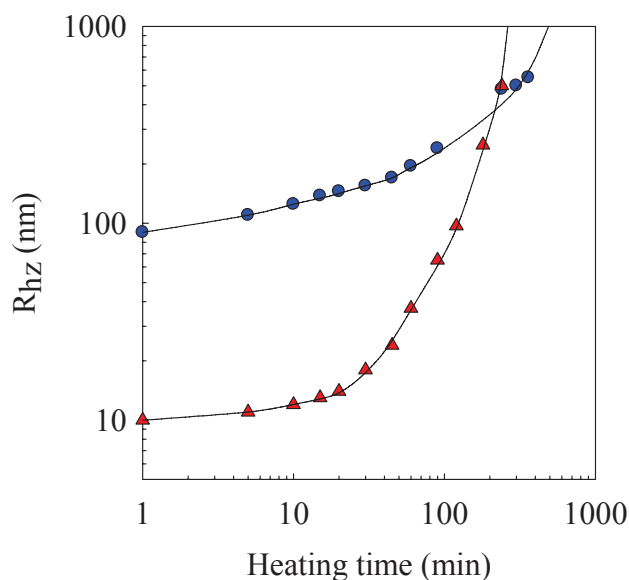


Figure 9. Evolution of  $R_{hz}$  as a function of heating time at 60°C for  $\beta$ -lg 40 g/L – pH 7.0 in the presence of 9 mM  $\text{CaCl}_2$  ( $R=4$ ) (circles) or in the presence 300 mM  $\text{NaCl}$  at 65°C (triangles). The gel times of the systems containing  $\text{CaCl}_2$  and  $\text{NaCl}$  are about 500 min and 330min, respectively. Solid lines are guides to the eye.

CLSM images taken at different stages show dispersed individual spherical aggregates at heating times up to about 100 min and clusters of these particles at longer times, see fig.10. At  $t=540$  min a weak gels had formed that broke up after dilution into small macroscopic bits. The image of one such bit shows network of randomly association spherical particles with a structure that is typical for so-called particulate gels.

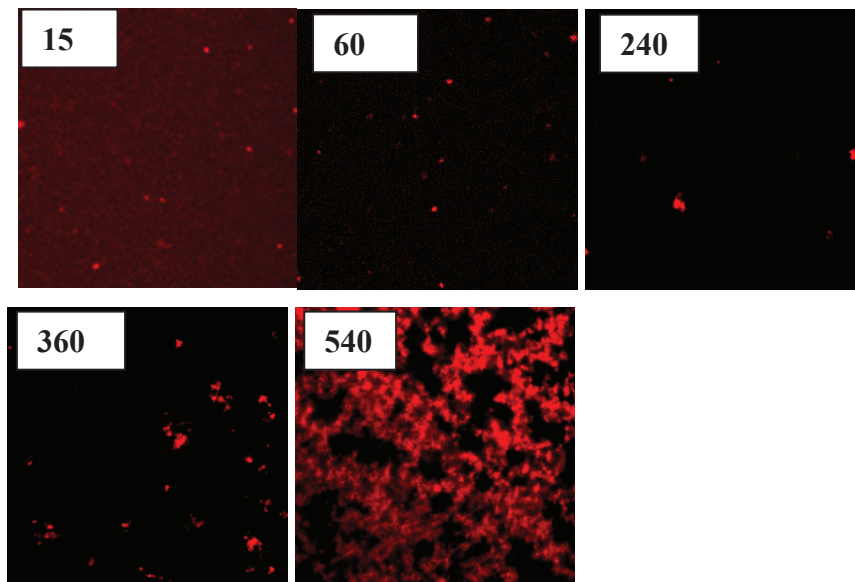


Figure 10. CLSM images of  $\beta$ -lg solutions at  $C = 40$  g/L and  $R = 4$  after heating at  $60^\circ\text{C}$  for different times indicated in minutes in the figures. The solutions were highly diluted (1g/L) in water before the images were taken. at  $t=540$  min a weak gel was formed that broke up into small macroscopic bits after dilution. The image of this sample was taken of one such bit. The images represent  $40 \times 40 \mu\text{m}$

### 3. Comparison with aggregation and gelation in NaCl.

As was mentioned in the introduction, the effect of adding NaCl on the aggregation and gelation of  $\beta$ -lg at pH 7 has already been studied in detail in the past. Figure 11 represents schematically the systems obtained at steady state as a function of the NaCl concentration for  $C=40$  g/L. At low protein concentrations, small strand-like aggregates are formed. The hydrodynamic radius of the strands increases with increasing NaCl concentration ( $[\text{NaCl}]$ ) from about 15nm in the absence of added salt to about 40nm at  $[\text{NaCl}]=50\text{mM NaCl}$  <sup>21</sup>.

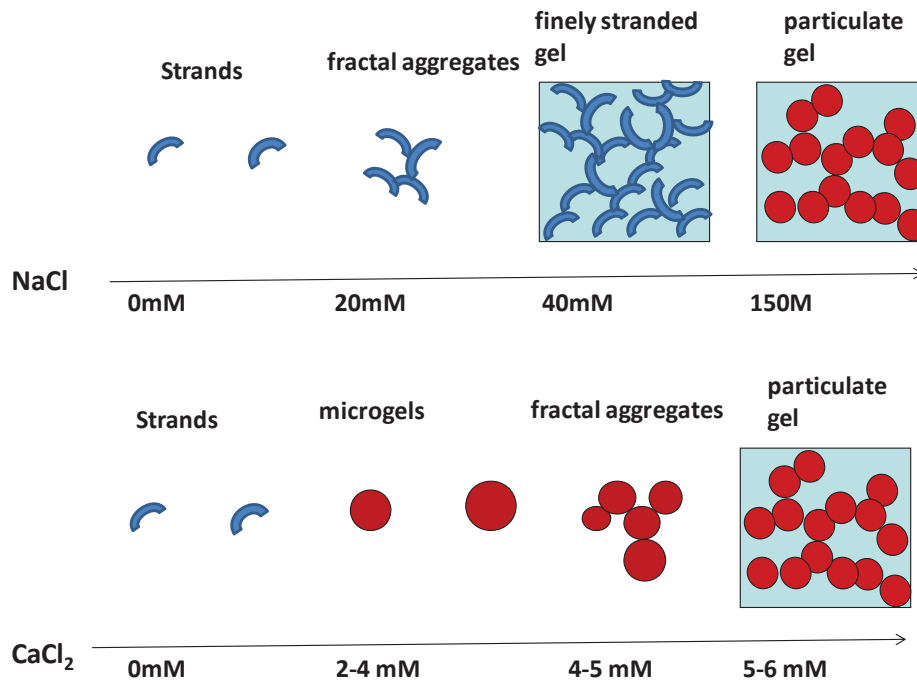


Fig. 11 Schematic representation of the effect of addition of NaCl or  $\text{CaCl}_2$  on the structure  $\beta$ -Ig solutions at pH7 and  $C=40$  g/L after heating (in the range tested 60-85°C) until steady state was reached. In pure water small strands are formed that increase in size with increasing NaCl or  $\text{CaCl}_2$  concentrations. Above 20mM NaCl secondary aggregation of the strands leads to the formation of large fractal aggregates leading eventually to the formation of finely stranded gels above 40mM NaCl and particulate gels above 150mM NaCl. Microgels are formed above a critical  $\text{CaCl}_2$  concentration. At higher  $\text{CaCl}_2$  concentrations the microgels associate into large fractal aggregates leading to particulate gels. The  $\text{CaCl}_2$  concentrations where these transitions occur increase weakly with decreasing temperature below 75°C.

The strands associate into larger fractal aggregates at higher protein concentrations for a given NaCl concentration or at higher NaCl concentrations for a given protein concentration. At  $C=40$ g/L secondary aggregation of the strands starts above about 10 mM NaCl. For  $[\text{NaCl}] \geq 100$ mM secondary aggregation starts at very low protein concentrations ( $<1$ g/L) and it is difficult to characterize the individual strands. However, small angle neutron scattering and cryo-TEM measurements showed that at all NaCl concentrations up to at least 400mM the large aggregates were formed by association of small strands<sup>38</sup>. The large scale structure of the aggregates could be described by eq.2 even for  $qR_g \gg 1$ , implying that aggregates were self-similar with a fractal dimension of 2<sup>21</sup>.

The secondary aggregation of the strands leads to gelation above a critical concentration ( $C_g$ ) that decreases with increasing NaCl concentration from about 95 g/L without added salt to about 1g/L at  $[\text{NaCl}]=400\text{mM}$ <sup>21</sup>. At a fixed protein concentration gelation occurs above a critical NaCl concentration which is about 40mM at  $C=40\text{g/L}$ . The heating temperature was found to have only an effect on the aggregation rate, but not on the structure of the aggregates.

These literature results show that microgels cannot be formed at pH 7 by screening the electrostatic repulsion with  $\text{Na}^+$ . This means that the screening of the electrostatic repulsion is not sufficient to generate microgels. Remarkably, above about 150mM NaCl, nevertheless, particulate gels are formed, consisting of randomly associated of spherical particles with very similar structures as gels formed in the presence of  $\text{CaCl}_2$ . We have shown here that spherical particles are formed already at the start of the aggregation process in the presence of  $\text{Ca}^{2+}$ , but this appears not to be case in the presence of  $\text{Na}^+$ . It has been suggested that the aggregates formed at higher NaCl concentrations micro phase separate into spherical particles that subsequently randomly associate to form a gel<sup>22</sup>.

So far, the aggregation process at high NaCl concentrations, where it leads to the formation of particulate gels, has not yet been studied as a function of time. Therefore we investigated the evolution of a  $\beta$ -lg solution at  $C=40\text{g/L}$  at  $65^\circ\text{C}$  in the presence of 300mM NaCl. At this heating temperature a gel is formed after about 330 min. The evolution of  $R_{\text{hz}}$  is compared with that in the presence of 9mM  $\text{CaCl}_2$  in fig.9. We stress that NaCl at the same ionic strength as 9mM  $\text{CaCl}_2$  the system does not gel.

It is clear that whereas at 9mM  $\text{CaCl}_2$  relatively large aggregates with  $R_{\text{hz}} = 100\text{nm}$  were formed already very early on in the reaction, at 300mM NaCl small aggregates with  $R_{\text{hz}}= 10\text{nm}$  were formed initially. The size of the latter is close to that of the small strands formed at low NaCl concentrations. After about 20min heating, the aggregates in NaCl started to grow sharply, while the growth of the aggregates in  $\text{CaCl}_2$  was more progressive until very close to the gelpoint. The structure factor of the larger aggregates formed at 0.3M NaCl could be fitted to eq.2, indicating that they were formed by random association of the small strands, see fig.12.

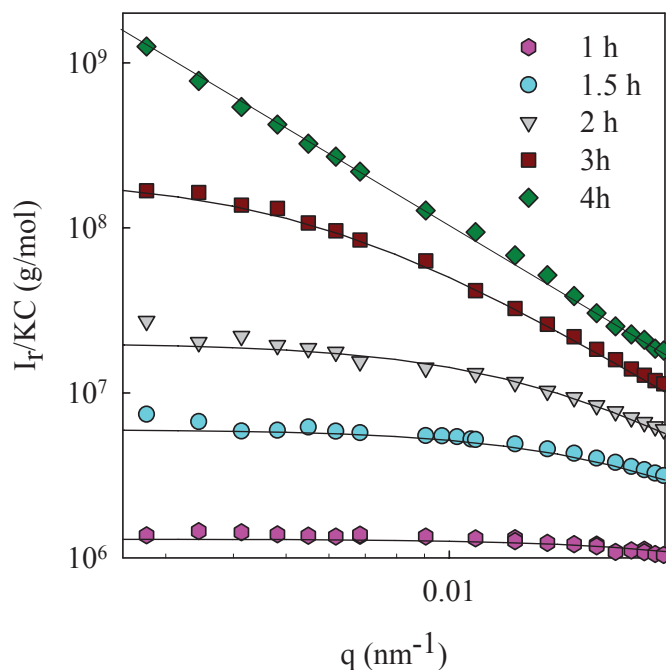


**Figure 12. a.** Scattering wave vector ( $q$ ) dependence of the relative excess intensity of light scattered ( $I_r$ ) by dilute solutions of  $\beta$ -lg aggregates formed at  $C=40$  g/L and pH 7.0 in 300mM NaCl after different heating times at  $65^\circ\text{C}$ . The solid lines represent  $I_r/KC = M_w / (1 + q^2 \cdot R_{gz}^2 / 3)$ .

In order to observe the formation of the more heterogeneous gels at high NaCl concentrations, we made CLSM images of the undiluted system at different heating times and compared them with the system in 9 mM  $\text{CaCl}_2$  ( $R=4$ ), see figure 13. As was already shown in fig. 10, in  $\text{CaCl}_2$  distinct protein particles are visible from the start of the aggregation process. However, no features could be observed during the first few hours in the presence of NaCl even though also in this case the aggregates became larger than 100nm. The reason is that the aggregates are polydisperse and have a low density due to their fractal structure so that they have less contrast and can overlap. After about 2 hours an increasingly more heterogeneous structure developed similar to the structure observed in 9mM  $\text{CaCl}_2$  that can be described as particulate gels.

$\text{CaCl}_2$                       30 min                      2h                      4h                      7h

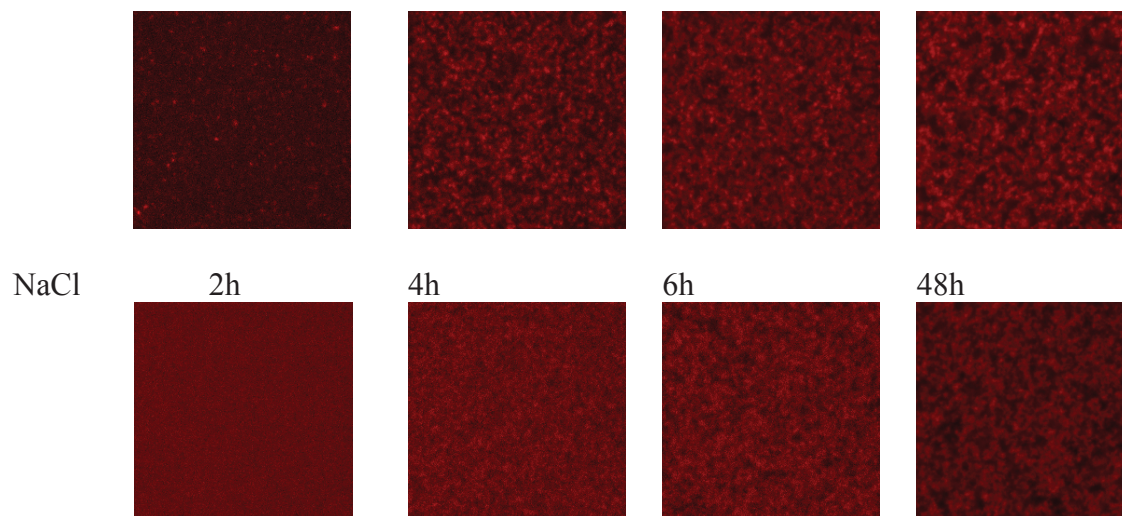
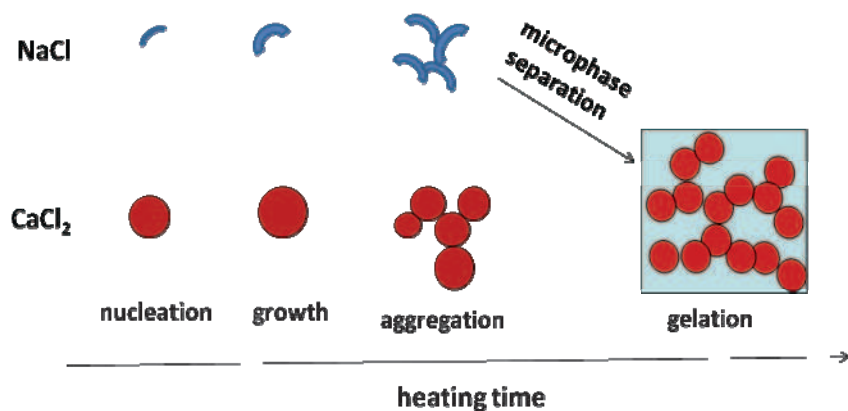


Figure 13. CLSM images of undiluted solutions and gels of  $\beta$ -lg at  $C=40$  g/L and pH 7.0 in the presence of 9mM  $\text{CaCl}_2$  ( $R = 4$ ) during heating at  $60^\circ\text{C}$  or in the presence of 0.3M NaCl during heating at  $65^\circ\text{C}$ . The images represent  $40 \times 40 \mu\text{m}$ .

These results clearly show that microgels are not a first step of the formation of particulate gels at high NaCl concentrations. Instead, small strands are formed that randomly associate into self-similar aggregates and only at a late stage of the process reorganize into a more heterogeneous particulate gel. Possibly, this occurs because the larger aggregates are not soluble in high NaCl concentrations and phase separate into dense spherical domains<sup>22</sup>. These domains resemble the microgels that are formed already in the early stages of the aggregation process in presence of  $\text{CaCl}_2$  or in pure water when the pH is close to pI.

Figure 14 shows schematically the different mechanisms by which particulate gels are formed during heating in presence of NaCl and in  $\text{CaCl}_2$ . In order to form particulate gels with  $\text{CaCl}_2$  one needs to exceed a critical number of  $\text{Ca}^{2+}$  per protein ( $R>3$ ), which means that the critical  $\text{CaCl}_2$  concentration increases with increasing protein concentration, To form particulate gels with NaCl one needs to exceed a critical NaCl concentration ( $>150\text{mM}$ ) that only weakly depends on the protein concentration. Here we have supposed that the nuclei of the strand-like and the spherical particles are themselves strand-like and spherical. Detailed investigation of the aggregates as a function of heating time using small angle X-ray or neutron scattering will be necessary to confirm this hypothesis.



*Fig.14 Schematic representation of the formation of particulate gels of  $\beta$ -lg at pH 7 and  $C=40$  g/L in 300mM NaCl or 9mM  $CaCl_2$  during heating at 85°C. In NaCl small strands are nucleated that grow and subsequently associate into increasingly larger fractal aggregates. Close to gelation microphase separation occurs leading to the formation dense domains that associate into a particulate gel. In  $CaCl_2$  microgels are nucleated that grow and subsequently associate into increasingly larger fractal aggregates until they percolate into a particulate gel*

## Conclusion

The present work has shown the impact of  $Ca^{2+}$  and  $Na^+$  on the heat-induced formation of protein particles and gels for the case of  $\beta$ -lg at  $C=40$ g/L after prolonged heating at temperature between 60-85°C at pH7.

Small curved strand-like aggregates are formed in the presence of  $Na^+$  and below a critical molar ratio between  $Ca^{2+}$  and  $\beta$ -lg. At higher ratios mainly larger spherical particles are formed. The critical ratio needed increases weakly with decreasing heating temperature from 1-1.5 at 85°C to 2- 2.5 at 70°C. At  $T > 70^\circ C$  the spherical particles are comparable in terms of shape and size to the microgels formed between pH 5.75 and 6.2 in absence of salt at pH5.8. Below 70°C stable suspensions of individual microgels could not be formed.

From the study of the structure formed as function of heating time, it appears that formation of strands and microgels occurs via a nucleation and growth process. The growth involves addition of newly denatured proteins, but also fusion of smaller aggregates. The latter suggest that not all bonds within the nuclei are permanent at an early stage of the reaction allowing restructuring and fusion the nuclei. The size of the aggregates at steady

state increases with increasing  $\text{CaCl}_2$  concentration. The size of the microgels is independent of the heating temperature for  $T > 70^\circ\text{C}$ . At higher  $\text{CaCl}_2$  concentrations, or higher protein concentrations, the microgels randomly associate leading above a critical value to the formation of a particulate gel. At  $T = 62^\circ\text{C}$  approximately spherical particles are formed at  $R = 2.5$  and  $3.0$ , but some secondary aggregation occurs in these cases. The transition between the formation of small strands and microgels is more gradual at this temperature, where the aggregation is very slow.

In the presence of  $\text{NaCl}$  only small strands are formed that at higher salt or protein concentrations randomly associate to form larger self-similar aggregates leading above a critical concentration to gelation. Homogeneous, so-called finely stranded, gels are formed at lower  $\text{NaCl}$  concentrations, but more heterogeneous particulate gels are formed at higher  $\text{NaCl}$  concentrations ( $> 200\text{mM}$ ). The structure of these gels is similar to the gels formed in pure water close to the isoelectric point or at  $\text{pH } 7$  in presence of  $\text{CaCl}_2$ , but the mechanism by which they are formed is different. Whereas the latter gels are formed by random association of microgels, the former are formed by micro phase separation of the self similar aggregates at a later stage of the gelation process.

## References

1. Nicolai, T.; Britten, M.; Schmitt, C., beta-Lactoglobulin and WPI aggregates: Formation, structure and applications. *Food Hydrocolloids* **2011**, *25*, (8), 1945-1962.
2. Hambling, S. G.; Mc Alpine, A. S.; Sawyer, L.,  $\beta$ -lactoglobulin. In *Advanced Dairy Chemistry - 1: Proteins*, Fox, P. F., Ed. Elsevier Applied Science: London, 1992; pp 141 - 190.
3. Aymard, P.; Nicolai, T.; Durand, D.; Clark, A., Static and dynamic scattering of beta-lactoglobulin aggregates formed after heat-induced denaturation at  $\text{pH } 2$ . *Macromolecules* **1999**, *32*, (8), 2542-2552.
4. Veerman, C.; Ruis, H.; Sagis, L. M. C.; van der Linden, E., Effect of Electrostatic Interactions on the Percolation Concentration of Fibrillar  $\beta$ -Lactoglobulin Gels. *Biomacromolecules* **2002**, *3*, (4), 869-873.
5. Arnaudov, L. N.; de Vries, R.; Ippel, H.; van Mierlo, C. P. M., Multiple Steps during the Formation of  $\beta$ -Lactoglobulin Fibrils. *Biomacromolecules* **2003**, *4* (6), 1614-1622
6. Gosal, W. S.; Clark, A. H.; Ross-Murphy, S. B., Fibrillar  $\beta$ -Lactoglobulin Gels: Part 1. Fibril Formation and Structure. *Biomacromolecules* **2004**, *5*, (6), 2408-2419.
7. Krebs, M. R.; Domike, K. R.; Donald, A. M., Protein aggregation: more than just fibrils. *Biochemical Society transactions* **2009**, *37*, (4), 682-685.
8. Adamcik, J.; Jung, J.-M.; Flakowski, J.; De Los Rios, P.; Dietler, G.; Mezzenga, R., Understanding amyloid aggregation by statistical analysis of atomic force microscopy images. *Nature Nanotechnology* **2010**, *5*, 423-428.

9. Aymard, P.; Gimel, J. C.; Nicolai, T.; Durand, D., Experimental evidence for a two-step process in the aggregation of beta-lactoglobulin at pH 7. *Journal De Chimie Physique Et De Physico-Chimie Biologique* **1996**, 93, (5), 987-997.
10. Mehalebi, S.; Nicolai, T.; Durand, D., Light scattering study of heat-denatured globular protein aggregates. *International Journal of Biological Macromolecules* **2008**, 43, (2), 129-135.
11. Jung, J. M.; Savin, G.; Pouzot, M.; Schmitt, C.; Mezzenga, R., Structure of heat-induced beta-lactoglobulin aggregates and their complexes with sodium-dodecyl sulfate. *Biomacromolecules* **2008**, 9, (9), 2477-2486.
12. Donato, L.; Schmitt, C.; Bovetto, L.; Rouvet, M., Mechanism of formation of stable heat-induced beta-lactoglobulin microgels. *International Dairy Journal* **2009**, 19, (5), 295-306.
13. Schmitt, C.; Bovay, C.; Vuilliomenet, A. M.; Rouvet, M.; Bovetto, L.; Barbar, R.; Sanchez, C., Multiscale Characterization of Individualized beta-Lactoglobulin Microgels Formed upon Heat Treatment under Narrow pH Range Conditions. *Langmuir* **2009**, 25, (14), 7899-7909.
14. Moitzi, C.; Donato, L.; Schmitt, C.; Bovetto, L.; Gillies, G.; Stradner, A., Structure of beta-lactoglobulin microgels formed during heating as revealed by small-angle X-ray scattering and light scattering. *Food Hydrocolloids* **2011**, 25, (7), 1766-1774.
15. Phan-Xuan, T.; Nicolai, T.; Durand, D.; Schmitt, C.; Donato, L.; Bovetto, L., On the crucial importance of the pH for the formation and self-stabilisation of protein microgels and strands. *Langmuir* **2011**, 15092-15101.
16. Schmitt, C.; Moitzi, C.; Bovay, C.; Rouvet, M.; Bovetto, L.; Donato, L.; Leser, M. E.; Schurtenberger, P.; Stradner, A., Internal structure and colloidal behaviour of covalent whey protein microgels obtained by heat treatment. *Soft Matter* **2010**, 6, (19), 4876-4884.
17. Bromley, E. H. C.; Krebs, M. R. H.; Donald, A. M., Mechanisms of structure formation in particulate gels of beta-lactoglobulin formed near the isoelectric point. *European Physical Journal E* **2006**, 21, (2), 145-152.
18. Phan-Xuan, T.; Durand, D.; Nicolai, T.; Donato, L.; C., S.; Bovetto, L., Heat induced formation of beta-lactoglobulin microgels driven by addition of calcium ions. *Food Hydrocolloids* **2012**, DOI 10.1016/j.foodhyd.2012.09.008
19. Zittle, C. A.; Della Monica, E. S.; Rudd, R. K.; Custer, J. H., The Binding of Calcium Ions by b-Lactoglobulin Both before and after Aggregation by Heating in the Presence of Calcium Ions. *Contribution from the eastern regional research laboratory* **1957**, 79, 4661-4666.
20. Renard, D.; Lefebvre, J.; Griffin, M. C. A.; Griffin, W. G., Effects of pH and salt environment on the association of b-lactoglobulin revealed by intrinsic fluorescence studies. *International Journal of Biological Macromolecules* **1998**, (22), 41-49.
21. Baussay, K.; Le Bon, C.; Nicolai, T.; Durand, D.; Busnel, J. P., Influence of the ionic strength on the heat-induced aggregation of the globular protein beta-lactoglobulin at pH 7. *International Journal of Biological Macromolecules* **2004**, (34), 21-28.
22. Ako, K.; Nicolai, T.; Durand, D.; Brotons, G., Micro-phase separation explains the abrupt structural change of denatured globular protein gels on varying the ionic strength or the pH. *Soft Matter* **2009**, 5, (20), 4033-4041.
23. Langton, M.; Hermasson, A. M., Fine-stranded and particulate gels of  $\beta$ -lactoglobulin and whey protein at varying pH. *Food Hydrocolloids* **1992**, 5, 523-540.
24. Lefevre, T.; Subirade, M., Molecular differences in the formation and structure of fine-stranded and particulate beta-lactoglobulin gels. *Biopolymers* **2000**, 54, (7), 578-586.

25. Barbut, S., Effects of Calcium Level on the Structure of Pre-heated Whey Protein Isolate Gels. *Lebensmittel-Wissenschaft & Technologie* **1995**, 28, 598-603.
26. Hagiwara, T.; Kumagai, H.; Matsunaga, T., Fractal analysis of the elasticity of BSA and b-lactoglobulin gels. *Journal of Agricultural and Food Chemistry*, **1997**, 45, 3807–3812.
27. Roefs, S. P. F. M.; Peppelman, H. A., Aggregation and gelation of whey proteins: Specific effect of divalent cations? In *Food Colloids Fundamentals of Formulation*, Dickinson, E.; Miller, R., Eds. The Royal Society of Chemistry: Cambridge, 2001.
28. Foegeding, E. A.; Davis, J. P.; Doucet, D.; McGuffey, M. K., Advances in modifying and understanding whey protein functionality. *Trends in Food Science & Technology* **2002**, 13, (5), 151-159.
29. Sherwin, C. P.; Foegeding, E. A., The effects of CaCl<sub>2</sub> on aggregation of whey proteins. *Milchwissenschaft-Milk Science International* **1997**, 52, (2), 93-96.
30. Nicolai, T., Food structure characterisation using scattering methods. In *Understanding and controlling the microstructure of complex foods*, McClements, D. J., Ed. Woodhead: Cambridge: 2007; pp 288– 310.
31. Brown, W., *Light Scattering: Principles and development*. Clarendon Press: Oxford: 1996.
32. Berne, B. J.; Pecora, R., *Dynamic Light Scattering*. Oxford University Press: 1993.
33. Nicolai, T.; Gimel, J. C.; Johnsen, R., Analysis of relaxation functions characterized by a broad monomodal relaxation time distribution. *Journal De Physique II* **1996**, 6, (5), 695-711.
34. Ako, K.; Durand, D.; Nicolai, T.; Becu, L., Quantitative analysis of confocal laser scanning microscopy images of heat-set globular protein gels. *Food Hydrocolloids* **2009**, 23, (4), 1111-1119.
35. Le Bon, C.; Nicolai, T.; Durand, D., Kinetics of Aggregation and Gelation of Globular Proteins after Heat-Induced Denaturation. *Macromolecules* **1999**, 32, (19), 6120–6127.
36. Griffin, W. G.; Griffin, M. C. A.; Martin, S. R.; Price, J., Molecular-Basis of Thermal Aggregation of Bovine Beta-Lactoglobulin-A. *Journal of the Chemical Society-Faraday Transactions* **1993**, 89, (18), 3395-3406.
37. Baussay, K.; Nicolai, T.; Durand, D., Effect of the cluster size on the micro phase separation in mixtures of beta-lactoglobulin clusters and kappa-carrageenan. *Biomacromolecules* **2006**, 7, (1), 304-309.
38. Pouzot, M.; Nicolai, T.; Visschers, R. W.; Weijers, M., X-ray and light scattering study of the structure of large protein aggregates at neutral pH. *Food Hydrocolloids* **2005**, 19, (2), 231-238.